

A global view on stratospheric ice clouds: assessment of processes related to their occurrence based on satellite observations

Ling Zou¹, Sabine Griessbach¹, Lars Hoffmann¹, and Reinhold Spang²

¹Jülich Supercomputing Centre (JSC), Forschungszentrum Jülich, Jülich, Germany

²Institute of Energy and Climate Research (IEK-7), Forschungszentrum Jülich, Jülich, Germany

Correspondence: Ling Zou (l.zou@fz-juelich.de; cheryl_zou@whu.edu.cn)

Abstract.

Ice clouds play an important role in regulating [the](#) water vapor and influencing the radiative budget in the atmosphere. ~~In this study, This study investigates~~ stratospheric ice clouds (SICs) ~~and stratospheric aerosols from based on~~ the Cloud-Aerosol Lidar and Infrared Pathfinder Satellite Observations (CALIPSO), ~~deep convection and gravity waves from Atmospheric Infrared~~
5 ~~Sounder (AIRS) observations and tropopause temperature from ERA5 are~~, [Tropopause temperature, double tropopauses, clouds in the upper troposphere and lower stratosphere \(UTLS\), gravity waves and stratospheric aerosols, were](#) analyzed to investigate their ~~long-term variation and processes potentially related to the formation of SICs on the global scale~~ [relationships with the occurrence and variability of SICs in the tropics and at midlatitudes.](#)

[We found that](#) SICs with cloud top heights [of](#) 0.25 km above the first [lapse rate](#) tropopause are mainly detected [in the tropics.](#)
10 [Monthly time series of SICs from 2007 to 2019 show that high frequencies of SICs follow the Intertropical Convergence Zone \(ITCZ\) over time in the tropics and that SICs vary inter-annually at different latitudes. Results show that SICs associated with double tropopauses, which are related to poleward isentropic transport, are mostly found at midlatitudes. More than 80 % of the SICs around 30° N/S are associated with double tropopauses.](#) ~~over the tropical continents. SICs associated with the double tropopause events, where the cloud top is between the first and second thermal tropopause, are mostly located in midlatitudes~~
15 ~~(between 25°–60°). The seasonal cycle and the inter-annual variability of SIC frequencies from 2007 to 2019 show that high SIC frequencies are mainly observed south of the equator from November to March, and at 10° N–20° N from July to September. At mid- and high latitudes, more SICs are observed from December to May in the northern hemisphere and in the southern hemisphere during May to October.~~

[Correlation coefficient and long-term anomaly analyses of SICs and all the other processes indicate that the occurrence](#)
20 [and variability of SICs are mainly associated with the tropopause temperature in the tropics. UTLS clouds have the highest correlations with SICs in the monsoon regions and the central United States. Tropopause temperature and gravity waves are mostly related to SICs at midlatitudes, especially over Patagonia and the Drake Passage. However, besides the highest correlation coefficients, the cold tropopause temperature, the occurrence of double tropopauses, high stratospheric aerosol loading, frequent UTLS clouds and gravity waves all have high correlations with the SICs. The occurrence and variability](#)
25 [of SICs demonstrate a strong dependence on various processes, both locally and temporally.](#) ~~Relations between SICs and first tropopause temperature, deep convection, gravity waves, and stratospheric aerosol were analyzed, respectively, on a~~

global scale. Positive correlations between SIC frequencies and deep convection, gravity waves, and stratospheric aerosol and an inverse correlation between SIC frequency and tropopause temperature were observed worldwide. Overlaps of high correlations/anti-correlations were detected over tropical continents, i. e., tropical South America, equatorial Africa, and western Pacific, suggesting a combined effect of tropopause temperature, deep convection, gravity waves, and stratospheric aerosol on SIC occurrence in these regions. Over Central America, North America, the Asian Monsoon, and mid- and high latitudes deep convection and gravity waves present a strong correlation with the occurrence of SICs, individually or interdependently.

The overlapping and similar correlation coefficients between SICs and all processes indicate strong associations between all processes themselves. Due to their high inherent correlations, it is challenging to disentangle and evaluate their contributions to the occurrence of SICs on a global scale. However, the correlation coefficient analyses between SICs and all processes and high associations between all processes observed in this study help us better understand the sources of SICs on a global scale. Regional analyses demonstrated specific relations of tropopause temperature, deep convection, gravity waves, and stratospheric aerosol with SICs at a finer scale. Low tropopause temperature and high occurrence frequency of stratospheric aerosol show strong correlations with high frequencies of SICs over the Indo-Pacific Warm Pool, tropical South America, and equatorial Africa. Deep convection and gravity waves have the strongest correlation with occurrence frequency of SICs over the Asian Monsoon and the North American Monsoon. Gravity waves and tropopause temperature are highly correlated with SIC occurrence over South America and the northern Atlantic. Moreover, the El Niño phenomenon in 2009-2010 and 2015-2016 coincides with low SIC occurrences over the Indo-Pacific Warm Pool. High stratospheric aerosol loads related to volcanic eruptions (Puyehue-Cordón Caulle and Nabro in 2011) and wildfires (over the United States and Canada in 2017) are closely related to high occurrence frequencies of SICs.

We investigated the global distribution and long-term variation of SICs and present a global view of relations between SIC occurrence and tropopause temperature, deep convection, gravity wave activity, and stratospheric aerosol. This work provides a better understanding of the physical processes and climate variability of SICs.

1 Introduction

Stratospheric ice clouds (SICs) play an important role in regulating the water vapor in the upper troposphere and lower stratosphere (UTLS), i. e., ice cloud formation and sedimentation may dehydrate the UTLS (Jensen and Pfister, 2004; Schoeberl and Dessler, 2011; Schoeberl et al., 2019), while injection of convective clouds and sublimation of ice in the lower stratosphere would hydrate the stratosphere (Dinh et al., 2012; Jain et al., 2013; Avery et al., 2017). Thin ice clouds in the UTLS region produce net radiative heating by trapping outgoing longwave radiation, while thick ice clouds cause radiative cooling in the atmosphere (Zhou et al., 2014; Lolli et al., 2018). SICs are also important indicators for better understanding the vertical temperature structure in the UTLS, transport between the troposphere and stratosphere, and the intensity and dynamics of deep convection (Liou, 1986; Corti et al., 2006; Mace et al., 2006; Jensen et al., 2011; Kärcher, 2017). Therefore, understanding the microphysical and macrophysical properties of SICs is of importance for global atmospheric modeling and future climate prediction.

Global occurrence of ~~high-altitude ice clouds~~ ice clouds in the UTLS is about 20–40 % over the world (Liou, 1986; Wylie et al., 1994, 2005). The earliest discoveries of stratospheric ice clouds were reported in Murgatroyd and Goldsmith (1956) and Clodman (1957) from in-situ observations. Since then, more and more studies ~~have~~ demonstrated the existence of SICs from in-situ measurements, satellite measurements and ground-based lidar observations (~~Wang et al., 1996; Keckhut et al., 2005~~) (~~De Reus et al., 2009; Dessler, 2009; Spang et al., 2015; Bartolome Garcia et al., 2021~~). For example, 7 % of observations with

~~the cloud top above the first tropopause were detected from lidar observations over the Site Instrumental de Recherche par Télédétection Atmosphérique (SIRTA) between 2002 and 2006 (Noël and Haeffelin, 2007). Six encounters in total 90 encounters with ice clouds in the tropical lower stratosphere were observed from Forward Scattering Spectrometer Probe (FSSP-100) and Cloud Imaging Probe (CIP) measurements (De Reus et al., 2009). 5-day lasting SICs at 18.6 km on March 2014 were found over Gadanki from the ground-based Mie lidar observations and space-borne observations (Sandhya et al., 2015).~~

~~Several cases of ice clouds were discovered above convective anvils reaching up to the lower stratosphere from the Geostationary Operational Environmental Satellite (GOES) and the Next-Generation Weather Radar (NEXRAD) program Weather Surveillance Radar-1988 Doppler (WSR-88D) network (Homeyer et al., 2017).~~

(Wang et al., 1996; Keckhut et al., 2005; De Reus et al., 2009; Dessler, 2009; Bartolome Garcia et al., 2021). On a global scale, the worldwide distribution of SICs is detected from ~~the~~ Cloud-Aerosol Lidar and Infrared Pathfinder Satellite Observations (CALIPSO) measurements (Pan and Munchak, 2011; Zou et al., 2020). More SICs are observed over the tropics than ~~mid- and high latitudes~~ at midlatitudes. The SICs are more often distributed over tropical continents with frequencies as ~~high~~ large as 24 % to 36 %. ~~With increasing evidence for the existence and occurrence of SICs, potential driving forces for the formation~~ It is critical to have a better understanding of the potential formation mechanisms and maintenance of ice clouds in the UTLS ~~attract more attention.~~

~~Atmospheric thermodynamics, dynamics, and aerosol properties are critical features for stimulating~~ Temperature, atmospheric aerosol particles and water vapor are important factors for the formation of ice clouds ~~and inducing a change of ice cloud~~ (Haag and Kärcher, 2004). Ice cloud formation in the UTLS shows a significant dependence on cold ambient temperature (Holton and Gettelman, 2001), direct injection or outflow from deep convection (Jensen et al., 1996; Massie et al., 2002), large-scale upwelling of moist air parcels (Brewer, 1949; Pfister et al., 2001), and temperature perturbations induced by atmospheric

~~(Holton and Gettelman, 2001; Pruppacher and Klett; Cziczo et al., 2013). The variability of vertical velocities caused by convective systems and gravity waves, which could induce temperature fluctuation and transport atmospheric aerosols, also play a crucial role in affecting the formation and distribution of ice clouds (Massie et al., 2002; Kärcher and Ström, 2003; Podglajen et al., 2018)~~

Cold temperatures, as well as temperature fluctuations caused by gravity waves and wave breaking (~~Boehm and Verlinde, 2000~~) (~~Podglajen et al., 2018~~)

~~Nucleation of ice crystals is in favor of cold temperatures in the UTLS. For example,~~ have a significant impact on the occurrence of ice clouds (Schoeberl et al., 2015; Jensen et al., 2016; Wang et al., 2016). 5-day lasting SICs observed at 18.6 km over Gadanki ~~on in~~ March 2014 were ~~attributed to a~~ found to be produced by wave-induced cold ~~temperature anomaly~~ (Sandhya et al., 2015). ~~A large-scale cirrus cloud on 27–29 January 2009~~ temperatures (Sandhya et al., 2015). Over the tropics, approximately 80 % of the cirrus clouds at an altitude above 14.5 km were detected in the cold phase of gravity waves and a

95 wave-induced air parcel cooling process (Chang and L'Ecuyer, 2020). Another study showed that low temperatures excited by an extra-tropical intrusion also produced a large-scale cirrus cloud over the Eastern Pacific observed by CALIPSO was caused by the lower temperature induced by an extratropical intrusion (Taylor et al., 2011). The temperature controls the formation and variability of ice clouds (Tseng and Fu, 2017). (Taylor et al., 2011).

Deep convection leads to ice clouds formation Convective systems form ice clouds directly from ice injection, and anvil out-
 100 flow, and indirectly from radiative and dynamic cooling associated with updrafts and waves (Homeyer et al., 2017). Tropopause-
 penetrating convection and large convection-related UTLS winds are more closely associated with the detection of SICs
 (Homeyer et al., 2017), as well as indirectly from updrafts and wave-induced cooling (Homeyer et al., 2017). Deep convection was responsible for 47 % cirrus clouds were of the cirrus clouds observed at 10-15 km on Manus Island, Papua New Guinea, in
 1999 initiated from deep convection based on ground-based (millimeter cloud radar (MMCR) and Geosynchronous Meteorological
 105 Satellite (GMS)) data (Mace et al., 2006). A close association of cirrus clouds and deep convection activities in the TTL was
 found based on a 2-year dataset from CALIPSO and CloudSat satellites, as high deep convection frequency are detected
 together with high cirrus cloud frequency (Sassen et al., 2009). (Mace et al., 2006). During the Deep Convective Clouds and
 Chemistry (DC3) experiment, stratospheric cirrus were cirrus observed at altitudes of 1–2 km above the tropopause on
May–June 2012 over the continental United States evolved from enhanced deep convection (Homeyer et al., 2014), which
 110 is facilitated by double tropopause events (Peevey et al., 2012, 2014). over the continental United States in May–June 2012
(Homeyer et al., 2014).

Perturbations of the temperature fields induced by gravity waves and wave breaking have substantial impacts on the occurrence
 of ice clouds (Schoeberl et al., 2015; Jensen et al., 2016; Dinh et al., 2016; Wang et al., 2016). Atmospheric waves significantly
 modulate the occurrence and maintenance of ice clouds in the tropical tropopause layer (TTL) at an altitude range of 14–18 km
 115 over the Pacific based on observations from the Global Hawk aircraft in the Airborne Tropical Tropopause EXperiment
 (ATTREX) (Kim et al., 2016). Wave-induced cooling of air parcels has a strong influence on the cirrus cloud occurrence.
 Similar results have been presented by Chang and L'Ecuyer (2020), with about 80 % of the cirrus clouds detected in the
 cold phase of gravity waves and wave-induced air parcel cooling process at altitude above 14.5 km over tropics during
 January 2007 to December 2013 from CALIPSO and 2C-ICE measurements. By using a cloud model – Wisconsin Dynamic
 and Microphysical Model (WISCDYMM), Wang et al. (2016) found that internal gravity wave breaking is the source of
 120 stratospheric cirrus layers on 23 December 2009 in Argentina in CALIPSO measurement.

Uplifted aerosol particles, such as sulfate aerosol, organic aerosol, and dust from volcanic eruptions or biomass burning, are
 effective ice nuclei for cirrus cloud formation and variation (Lohmann et al., 2003; Lee and Penner, 2010; Jensen et al., 2010)
 (Froyd et al., 2010; Cziczo et al., 2013). Cirrus cloud formation and a five times enhanced ice crystal concentration was demonstrated
 125 by microphysical simulations assuming volcanic aerosol at temperatures below about (Lee and Penner, 2010; Jensen et al., 2010)
(Froyd et al., 2010; Cziczo et al., 2013). For example, the ice crystal numbers were found to increase maximally by 50°C
 (Jensen and Toon, 1992). The stratospheric sulfur aerosol and cirrus reflectance show a strong inverse correlation in 2001–2011
 from Moderate Resolution Imaging Spectroradiometer (MODIS) observations (Friberg et al., 2015). From MOSAiC (Multidisciplinary
 drifting Observatory for the Study of Arctic Climate), Ohnaiser et al. (2021) observed % in the tropics after the Mount Pinatubo

130 ~~eruption by the ECHAM4 general circulation model in a scenario of aerosol number concentrations rising by 10-25 cm³ (Lohmann et al., 2003). Major wildfire events in July and August 2019 were the origin of 30 km-high aerosol and cloud layers over high altitudes in the northern hemisphere from October 2019 to May 2020 and found out that those cloud layers were generated by the major wildfire events in July and August 2019. Atmospheric aerosol show an impact on the occurrence and variability of ice clouds, while the influence of aerosol on their microphysical properties remains highly uncertain. km high~~
135 ~~cloud and aerosol layers at Northern Hemisphere (Ohneiser et al., 2021).~~

~~The large-scale atmospheric disturbances, e. g., El Niño–Southern Oscillation (ENSO), Madden-Julian Oscillation (MJO), and the stratospheric quasi-biennial oscillation (QBO) affect the occurrence of ice cloud in the UTLS (Collimore et al., 2003) (Eleftheratos et al., 2007; Inai et al., 2012; Liess and Geller, 2012). In the warm phase of ENSO (the El Niño condition), a cold tropopause and more ice clouds were found in the UTLS over the mid-Pacific, whereas a warm tropopause and less ice clouds~~
140 ~~were found over the western Pacific and Indonesia (Massie et al., 2000; Avery et al., 2017). The MJO also plays an important role in influencing the occurrence of ice clouds at altitudes of ~15–18 km (Inai et al., 2012). Virts and Wallace (2010) investigated the relation of ice clouds in TTL with MJO and ENSO. They found that MJO-related deep convection modulates ice cloud frequency in the TTL, i. e., higher frequencies of ice clouds are observed over equatorial continents when convection over the Pacific is enhanced. Phases of ENSO regulate the zonal shift of peak frequency of ice clouds in the tropics that~~
145 ~~more ice clouds can be found over the central Pacific region in the warm ENSO phase (El Niño) and more detected over the Maritime Continent in the cold phase (La Niña). Eleftheratos et al. (2011) explored the contribution of ENSO and QBO on the interannual variability of cirrus clouds from 1985–2005 over the tropical Pacific Ocean from the International Satellite Cloud Climatology Project (ISCCP) data. They found that the largest impact on cirrus cloud variability over the eastern and western Pacific is generated by ENSO. Moreover, the flow of moist air from the tropical upper troposphere to the extra-tropical strato-~~
150 ~~sphere along at isentropic levels is also important for the occurrence of SICs. The Based on Cryogenic Infrared Spectrometers and Telescopes for the Atmosphere (CRISTA) measurements in August 1997, the quasi-isentropic transport of high humidity air was found to be a source for the occurrence of SICs over northern middle and high latitudes (Spang et al., 2015) based on the Cryogenic Infrared Spectrometers and Telescopes for the Atmosphere (CRISTA) measurements in August 1997.~~

~~The occurrence and maintenance of ice clouds shows a significant dependence on atmospheric dynamics and thermal~~
155 ~~structure. The regional and global occurrence and distribution of SICs have been examined in previous works individual and combined effects of the above-stated factors and processes, i. e., atmospheric temperature, atmospheric aerosols, atmospheric processes including convection systems, gravity waves, and isentropic transport are significantly influencing the formation and evolution of ice clouds (Haag and Kärcher, 2004; Homeyer et al., 2017; Schoeberl et al., 2015; Jensen et al., 2016). However, studies on the potential formation mechanisms of high-altitude ice clouds have typically been limited constrained by short-term~~
160 ~~observations with specific factors particular focus and mainly over small regions. To or in specific cases. Global-scale research of the relationships between the occurrence of SICs and those factors and processes will help to better understand the ice clouds detected in the lower stratosphere, we used 13 years (2007–2019) cloud data from CALIPSO to revisit the global formation and variability of SICs.~~

The objectives of this study are to 1) examine the distribution and long-term variation of stratospheric ice clouds and explore their relations with tropopause temperature, deep convection, gravity waves, and stratospheric aerosol. In addition, regions of SIC hotspots were selected and analyzed in combination with the above factors and ENSO and QBO indices to investigate potential mechanisms of occurrence of SICs. Information on data-2) investigate potential effects of atmospheric temperature, stratospheric aerosols, UTLS clouds, and gravity waves on the occurrence and distribution of SICs on a global scale. The individual relationships between SICs and processes were evaluated globally. In Section 2, we give information on data sources and detection methods for SICs, stratospheric aerosol, deep convection UTLS clouds, and gravity waves are presented in Section 2. Global SIC occurrences. Section 3.1 presents the global distribution and long-term variation of SICs. Section 3.2 highlights the location of SICs associated with double tropopauses. 3.3-3.6 show individual relationship analyses between SICs and tropopause temperature, deep convection UTLS clouds, gravity waves, stratospheric aerosol, and their relations and stratospheric aerosols. Regional analyses are presented in Section 3. The Sect. 3.7. Section 4 discusses the data uncertainties and relation-relationship uncertainties between SICs and all parameters are discussed in Section 4. processes. Conclusions are presented in Section 5. Sect. 5.

2 Data and method

2.1 Tropopause data from the ERA5 reanalysis

~~The first tropopause (1st-TP) is defined~~

The first lapse rate tropopause (LRT1) is determined based on the World Meteorological Organization definition (WMO, 1957) as the lowest level at which the lapse rate decreases to 2° C/km or less, provided the average lapse rate between this level and all higher levels within 2 km does not exceed 2° C/km based on World Meteorological Organization definition (WMO, 1957). If the average lapse rate at any level and at all higher levels within one kilometer exceeds 3° C/km above the 1st-TP LRT1, the second tropopause (2nd-TP LRT2) is defined by the same criteria as the first tropopause. The cold-point tropopause (CP-TP) is defined as the minimum in the vertical temperature profiles (Highwood and Hoskins, 1998). Unlike the CP-TP, which is more related to atmospheric activities mainly over tropics (Munchak and Pan, 2014; Pan et al., 2018), the first thermal tropopause is a globally applicable tropopause definition to identify the transition between the troposphere and stratosphere (Munchak and Pan, 2014; Xian and Homeyer, 2019). Therefore, thermal tropopause (1st-TP and 2nd-TP LRT1 and LRT2) are analyzed in this work to conduct the identify stratospheric ice clouds on a global scale.

Tropopause heights are derived from the fifth generation European Centre for Medium-Range Weather Forecasts' (ECMWF's) reanalysis - ERA5, which is produced using 4D-Var data assimilation and model forecasts in CY41R2 of the ECMWF Integrated Forecast System (IFS) (Hersbach et al., 2020). ERA5 provides hourly high-resolution data from 1979 to present with a horizontal grid resolution of 0.25° and 0.3° and 137 hybrid sigma/pressure levels vertically from the surface to 0.01 hPa. The vertical resolution of ERA5 data is about 300 -360- 360 m around the first tropopause level at the altitude range from 9 to 188 to 17 km. In our study, the vertical resolution of tropopause height is improved after heights is improved by interpolating the ERA5 data to a much finer vertical grid with a cubic spline interpolation method (Hoffmann, 2021a)(Hoffmann and Spang, 2022).

In previous studies, e.g. Tegtmeier et al. (2020a) found that LRT1 height differences between ERA5 and Global Navigation Satellite System-Radio Occultation observations are less than 200 g., Homeyer et al. (2010); Pan and Munchak (2011); Zou et al., (2020) used a tropopause threshold of 500 m to identify stratospheric clouds. Because of the higher vertical resolution m in the tropics. Based on US High Vertical Resolution Radiosonde Data (HVRRD) data and coarser-resolution Global Positioning System (GPS) data, (Hoffmann and Spang, 2022) also showed that the uncertainty of the LRT1 heights of ERA5, which is improved by a factor of 2 compared with ERA-Interim, is in the range of ± 200 m at different latitudes. Therefore, a height difference of 250 m is employed as a valid tropopause with respect to the tropopause is used as threshold for ERA5 to extract data to identify stratospheric ice clouds in this study. One should keep in mind that gravity waves and deep convection are generally important factors influencing the height and variability of the tropopause (Sherwood et al., 2003; de la TORRE et al., 2004) (Hoffmann and Spang, 2022).

2.2 CALIPSO observations of stratospheric Stratospheric ice clouds and stratospheric aerosols from CALIPSO observations

The Cloud-Aerosol Lidar with Orthogonal Polarization (CALIOP), which is a dual-wavelength polarization-sensitive lidar instrument loaded on the CALIPSO satellite, probes high-resolution vertical structure structures and properties of thin clouds and aerosols on a near-global scale since June 2006 (Winker et al., 2007, 2009). CALIPSO equatorial crossing times are at 01:30 local time (LT) for the descending orbit and 13:30 LT for ascending orbit sections. The vertical resolution of CALIPSO observations varies as a function of altitude, which. It is 60 m at a in the altitude range from 8.2 to 20.2 km. In the horizontal the profiles are averaged over 1 km along track distance between 8.2 km and 20.2 km of altitude.

Ice cloud clouds and aerosol are extracted from the Vertical Feature Mask data (CAL_LID_L2_VFMStandardV4) in this study. According to the cloud and aerosol subtype classifications determined by the CALIPSO's cloud-aerosol discrimination (CAD) algorithm and the International Satellite Cloud Climatology Project (ISCCP) definitions, ice clouds in this work include both cirrus clouds and deep convective clouds. Aerosols are Aerosol includes dust, contaminated dust, and volcanic ash. Samples marked with high feature type quality are used to ensure high reliability of data. Considering that aerosols in the lower stratosphere are relatively long-lived and can contribute to the production of ice clouds, both day and nighttime aerosols are included. As for ice clouds, only nighttime Only nighttime data are investigated due to their higher signal-to-noise ratios and detection sensitivity with extinction coefficients down to 10^{-3} km^{-1} (Getzewich et al., 2018; Gasparini et al., 2018).

The highest sample of cloud and aerosol in each samples of clouds and aerosols in each vertical profile are extracted to identify stratospheric ice clouds and aerosols. Only those with clouds/aerosols top heights (CTHs/ATHs) (SICs) and stratospheric aerosols (SAs) whose top heights are at least 250 m above the 1st-TP are defined as stratospheric ice clouds (SICs) and stratospheric aerosols (SAs). The LRT1 in ERA5. The occurrence frequency of SICs and SAs is defined as the ratio of SIC/SA detections to total profile numbers in a specific region. A filter criterion for polar stratospheric clouds (PSC) (Sassen et al., 2008), i. e., data are excluded if CTHs are higher than 12.0 km in areas with local winter latitude $\geq 60^\circ$ N and 60° S, are is utilized here to avoid possible miscounting of PSC. This filter criterion doesn't apply to some However, this filter criterion may not catch all low altitude PSCs. Due to large uncertainties of data over polar region, SICs detected at high latitudes will not be

discussed in detail in this work. The occurrence frequency of SICs and SAs is defined as the ratio of SIC/SA detection numbers to total profile numbers in a given region. Therefore, we limited our analyses to the latitude range of $\pm 60^\circ$.

2.3 AIRS observations of deep convection UTLS clouds, gravity waves and SO₂ in AIRS

The Atmospheric Infrared

235 The Atmospheric InfraRed Sounder (AIRS) (Aumann et al., 2003; Chahine et al., 2006) is carried by NASA's Aqua satellite. AIRS has the same equatorial crossing time as CALIPSO at 01:30 LT for the descending orbit and at 13:30 LT for ascending orbit. It as CALIPSO. AIRS measures the thermal emissions of atmospheric constituents in the nadir and sublimb viewing geometry. There are It has a total of 2378 spectral channels in total for AIRS infrared spectrometer with a spectral coverage covering the spectral ranges of 3.74 to 4.61 μm , 6.20 to 8.22 μm and 8.8 to 15.4 μm . Over the full dynamic range from 190 K to 325 K, the The absolute accuracy of each spectral channel is better than 3 % over the full dynamic range from 190 K to 325 K and noise is less than 0.2 K at 250 K scene temperature (Aumann et al., 2000).

Deep convection, gravity waves and sulfur dioxide (SO₂) emissions from volcanic eruptions can be retrieved from AIRS in wavebands.

2.3.1 UTLS clouds

245 Aumann et al. (2006) and Aumann et al. (2011) retrieved deep convective clouds from AIRS at 8.1 μm , 4.3 (the 1231 μm and 7.3 μm , respectively (Aumann et al., 2003, 2006; Hoffmann and Alexander, 2010; Hoffmann et al., 2013, 2014a,b, 2016) Since a constant cm^{-1} atmospheric window channel) in the tropics. The term "deep convective clouds" in their studies refers to clouds tops of thunderstorms in non-polar regions with a brightness temperature (BT) threshold for deep convection detection may lead to of less than 210 K. When the top of anvil of thunderstorms has a brightness temperature of less than 210 K, the deep convective clouds are considered to reach the tropopause region in the tropics (Aumann et al., 2006). However, the threshold of 210 K is too low for midlatitude convective events (Hoffmann and Alexander, 2010), and a constant brightness temperature threshold for convective event detection may produce ambiguous results at different latitudes and seasons (Hoffmann et al., 2013).

255 In this study, temperature differences between AIRS brightness temperatures (BT_{AIRS}) at 1231 cm^{-1} (8.1 μm) and tropopause temperatures (T_{TP}) from ERA5 are used to detect deep convection events (Zou et al., 2021). An offset employed to detect high altitude clouds in the tropics and at midlatitudes. A threshold of +7 K on top of the above T_{TP} was set as the threshold to include all possible deep convection events with cloud tops near or above the tropopause,

$$BT_{AIRS} - T_{TP} \leq 7 \text{ K}.$$

~

$$260 \quad BT_{AIRS} - T_{TP} \leq 7 \text{ K}, \quad (1)$$

was chosen to identify possible high altitude clouds with tops in the upper troposphere and lower stratosphere, also referred to as UTLS clouds (Zou et al., 2021). In the tropics, most tropopause-reaching clouds with large optical thickness could be related to a deep convection origin (Gettelman et al., 2002; Tzella and Legras, 2011). At midlatitudes, high altitude clouds could also be related to frontal systems (warm front uplifting), mesoscale convective systems and mesoscale convective complexes, jet stream, mountain wave and contrails (Field and Wood, 2007; Trier and Sharman, 2016; Trier et al., 2020). UTLS clouds are considered here as a proxy for deep convection in the tropics and other high altitude ice cloud sources at midlatitudes.

The choice of the temperature threshold determines strongly influences the absolute values of the occurrence frequencies of the deep convection events, but it does not fundamentally affect UTLS clouds, but has no fundamental effect on the spatial and temporal patterns of deep convection (Zou et al., 2021). The term “deep convection” here includes convection from storm systems and fronts, mesoscale convective systems, and mesoscale convective complexes. UTLS clouds events (Zou et al., 2021). Similar to Hoffmann et al. (2013), monthly mean brightness temperatures at mid- and high latitudes midlatitudes are applied to filter cases with low surface temperatures, which make it particularly difficult to detect convection. Observations are removed if monthly mean brightness temperatures are below 250 K over regions with latitude $> 25^\circ$ N/S.

As the occurrence (coverage) of SICs associated with deep convection depends on the intensity, spatial extent, and duration of the deep convection, detection numbers of SICs and deep convection may not be the best indicator to elucidate their relations (Zou et al., 2021). Therefore, to effectively investigate the relation of SICs and deep convection, Next to the occurrence frequencies, the event frequency is defined in this work as the ratio of number of days in which deep convection UTLS clouds or SICs (≥ 1 detection) occurs occur to the total number of days in a given time period over a given region. This event frequency evaluates how frequently deep convection and SICs occur rather than their coverage, and it is largely independent of intensity, spatial extent or the duration of the deep convection. The event frequency helps overcome some of the limitations related to cloud geometries for UTLS clouds and SICs. The occurrence frequency of UTLS clouds, which is the ratio of profiles with UTLS clouds to the total profile number in a specific grid box (Appendix B), are not discussed in detail in this work.

The mean variance of

2.3.2 Gravity waves

In this study, mean variances of detrended brightness temperatures in the $4.3 \mu\text{m}$ waveband and is carbon dioxide waveband are used to identify stratospheric gravity wave signals waves from AIRS observations (Hoffmann and Alexander, 2010; Hoffmann et al., 2013). Measurements of 42 AIRS channels from 2322.6 to 2345.9 cm^{-1} and 2352.5 to 2366.9 cm^{-1} are averaged to reduce noise and improve the detection sensitivity of the AIRS gravity wave observations. This detrended and noise-corrected mean BT variance has the Even though the AIRS observations have the highest sensitivity at an altitude range of 30 – 40 km (Hoffmann and Alexander, 2010; Hoffmann et al., 2013, 2018). However, it can also provide information on gravity waves in, the averaged BT variance can provide gravity wave information for the lower stratosphere because as gravity waves typically propagate upward from the tropospheric sources into the stratosphere. Instead of setting a variance threshold to identify gravity wave events (Hoffmann and Alexander, 2010; Zou et al., 2021), here we use mean BT variances directly as a measure of gravity wave activity. A higher mean BT variance indicates a larger amplitude of the It is also important to keep in mind that like most

satellite instruments, AIRS is only capable of observing a specific part of the full wavelength spectrum of gravity waves. ~~Note that the~~ AIRS is most sensitive to short horizontal and long vertical wavelength waves (Ern et al., 2017; Meyer et al., 2018).

The observed BT variance is strongly dependent on both, the gravity wave sources and the background winds in the stratosphere, and ~~its observation is as events are highly~~ intermittent in time, ~~i.e.,~~ monthly or seasonal mean values can smooth ~~its~~ characteristics. ~~It is also important to keep in mind that like most satellite instruments, AIRS is only capable of observing a~~ specific part of the full stratospheric spectrum of the statistics. Instead of setting a variance threshold to identify gravity wave events (Hoffmann and Alexander, 2010; Zou et al., 2021), here we use mean BT variances directly as a proxy for gravity wave activity. A higher mean BT variance indicates a larger amplitude of the gravity waves. ~~Being a nadir instrument, AIRS is most~~ However, it is important to note that BT variances should not be confused with atmospheric temperature variances. The AIRS nadir observation geometry significantly reduces the sensitivity of the BT measurements compared to real atmospheric temperature fluctuations for short vertical wavelength waves. For the BT variances, the response to atmospheric temperature variances is near zero below 30 km of vertical wavelength and increases to about 50% at 65 km of vertical wavelength (Hoffmann et al. (2014a)). With these measurement characteristics, AIRS is mostly sensitive to short horizontal and long vertical ~~wavelength waves~~(Ern et al., 2017; Meyer et al., 2018). ~~wavelengths waves, which are expected to propagate from the tropopause to the upper stratosphere within less than 1–2 h and horizontal propagation distances less than a few hundred~~ kilometers. The AIRS BT measurements should be seen as a proxy of gravity wave activity.

2.3.3 Sulfur dioxide (SO₂)

As brightness temperature differences are an effective method to detect volcanic SO₂ from AIRS observations (Hoffmann et al., 2014b, 2016), spectral features of SO₂ at 1407.2 cm^{-1} and 1371.5 cm^{-1} are used to calculate the SO₂ Index (SI),

$$SI = BT(1407.2\text{ cm}^{-1}) - BT(1371.5\text{ cm}^{-1}). \quad (2)$$

The SI represents the SO₂ column density from the mid troposphere to the stratosphere, where a high SI indicates a high SO₂ column density. The SI is most sensitive to SO₂ layers at an altitude range from 8 to 13 km and an SI > 4 K is most likely related to volcanic emissions (Hoffmann et al., 2014b). In this work, an SI threshold of 10 K is applied to ~~identify relatively strong volcanic eruptions whose emissions may affect the lower stratosphere~~ detect strong explosive volcanic eruptions with injections into the UTLS region.

3 Results

3.1 Global ~~lower~~ stratospheric ice clouds

~~Ice clouds with cloud top heights at least 250 m above the first tropopause were defined as stratospheric ice clouds (SICs).~~

Figure 1 a-d ~~present~~ presents the global distribution and mean occurrence frequency of SICs from 2007 to 2019 in December-January-February (DJF), March-April-May (MAM), June-July-August (JJA) and September-October-November (SON). ~~Seasonally averaged occurrence frequencies of ice clouds as a function of altitude are shown in Fig. 1 e-h.~~ Similar to the results of previous

studies (Pan and Munchak, 2011; Zou et al., 2020; Dauhut et al., 2020), ~~enhanced-increased~~ occurrences of SICs are observed ~~at-over~~ the tropical continents. The highest SIC frequencies over the tropics are detected in boreal winter (DJF) (~ 0.36) with the regional mean of ~ 0.15 . The ~~weakest-signal-lowest frequency~~ of SICs over the tropics occurs in boreal summer (JJA), when the hotspots of SICs are shifted to the north of the equator over the Asian Monsoon and North American Monsoon. ~~In-the-At~~ midlatitudes, more SICs are observed in the ~~northern-hemisphere-Northern Hemisphere (NH)~~ over the northern Atlantic and Europe in DJF. In JJA, only the region over central North America presents relatively high SIC frequencies (0.08-0.12). ~~In-the-southern-hemisphere-At Southern Hemisphere (SH),~~ SICs are observed continuously along ~~mid-and-high-latitude-midlatitude~~ belts in JJA. MAM and SON have similar features as DJF and JJA. In the vertical, ice clouds are mostly found ~~at-in~~ the tropopause region (± 500 m around the tropopause). Seasonally averaged occurrence frequencies of ice clouds as a function of altitude are shown in Fig. 1 e-h. Most ice clouds are observed around the tropopause in the tropics and at midlatitudes. In the tropics, about 1 % of ice clouds have cloud tops 1 km above the tropopause in DJF, MAM, and SON. But very few ice clouds are found at midlatitudes with cloud tops 1 km above the tropopause.

~~As defined in Section 2, the occurrence frequency is the ratio of ice cloud detections to the total number of profiles in a given region. As the occurrence (coverage) of SICs associated with deep convection depends not only on spatial extent but also on the intensity and duration of the deep convection, the event frequency is proposed in this work as the ratio of days with SIC or deep convection detection to the total number of days in a given time period to effectively investigate the relation between SICs and deep convection. The global mean event frequencies of SICs by season are presented in Appendix A. Generally, the mean event frequencies show similarities with the occurrence frequency of SICs in Figure 1.~~

~~To investigate spatial and temporal variations of SICs, monthly averaged occurrence frequencies of SICs in the-altitude range from -4-5° latitude bands from 2007 to 4km with respect to 2019 are shown in Fig. 2. Seasonal cycles and inter-annual variability of SICs are observed in the tropics and at midlatitudes. SICs in the tropics follow the Intertropical Convergence Zone (ITCZ) over time, i.e., high SIC frequencies in the first thermal tropopause (e-h) in DJF, MAM, JJA and SON. The data are shown as zonal averages, globally, for the tropics (latitude range of 20° S-20° N move from south to north from boreal winter to summer and north to south from boreal summer to winter. The correlation with the ITCZ suggests that there is a strong correlation with deep convection. Most SICs are observed between 15° 20S-5° N)-and-midlatitudes (40N, which show higher SIC occurrence frequencies (> 0.24) and longer occurrence times (November to March of the following year). The SIC frequencies are stronger in the SH tropics, whereas SICs extend to higher latitudes in the Northern Hemisphere. Some SICs are identified at 25° -60N-30°)N from June to August, which are absent in the Southern Hemisphere, which would relate to the uplift of the Tibetan Plateau and the Asian Monsoon region.~~

~~At midlatitudes, the frequencies of SICs at midlatitudes are at least twice as low as in the tropics. However, we can still notice an inter-annual variation of SICs at midlatitudes, where SICs are more often observed in winters/early springs. It suggests other sources for the occurrence of SICs at midlatitudes besides deep convection. Therefore, we investigate the correlation of different processes with respect to SIC occurrences in the following sections, including tropopause temperature, double tropopauses, UTLS clouds, gravity waves, and stratospheric aerosol, which are expected to have an impact on cloud formation.~~

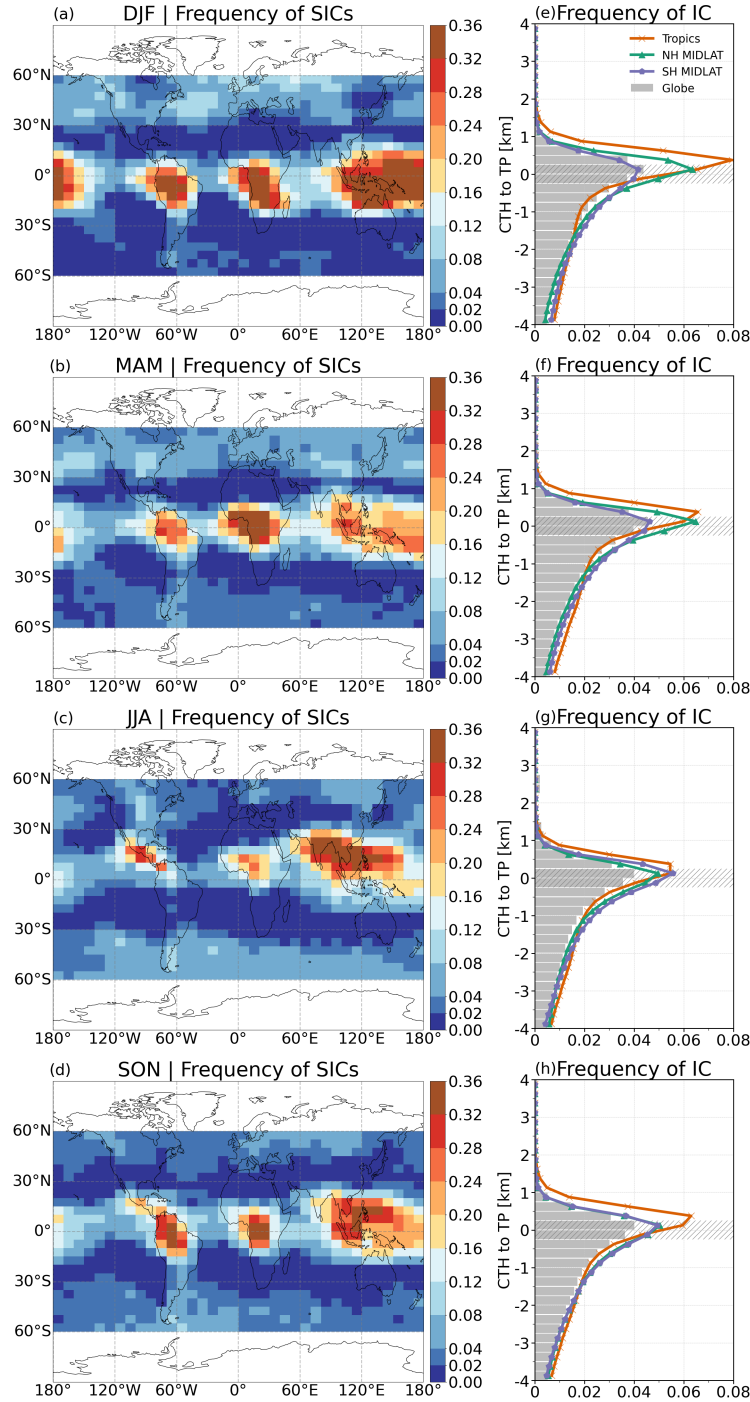


Figure 1. Occurrence frequencies of SICs on a $5^\circ \times 10^\circ$ (latitude \times longitude) grid (a-d) and occurrence frequencies of ice clouds in the altitude range from -4 to 4 km with respect to the first thermal tropopause (e-h) in DJF, MAM, JJA and SON. The data are shown as zonal averages, globally, for the tropics (20°S - 20°N) and midlatitudes (40° - 60°).

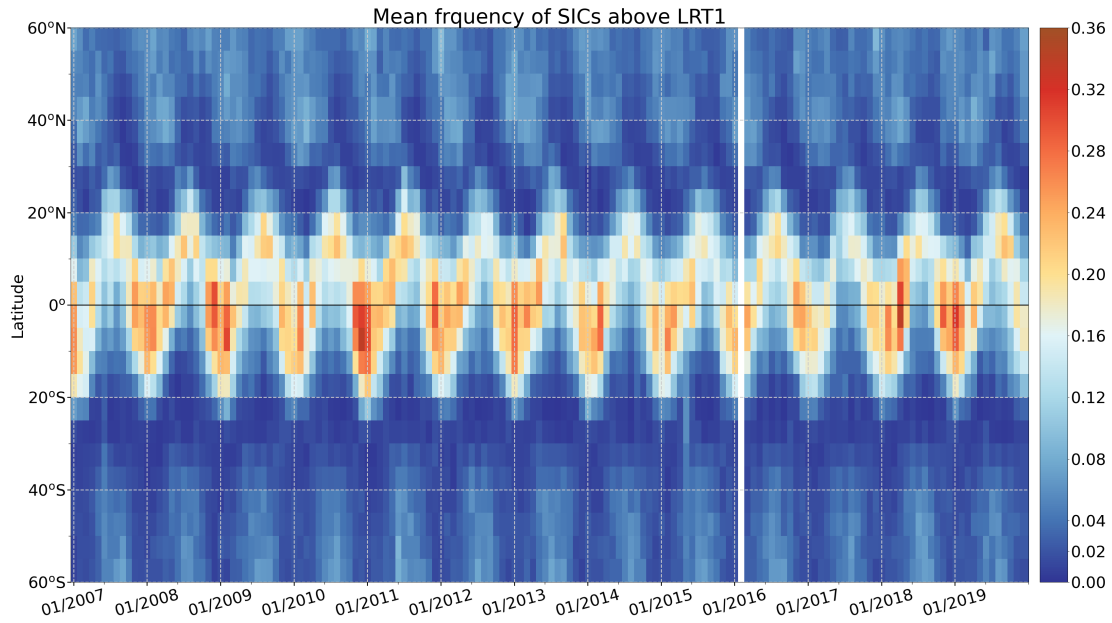


Figure 2. Monthly mean occurrence frequencies of SICs in latitudes band of 5° from 2007 to 2019.

360 3.2 Double tropopauses and SICs

Following the definition of the WMO, a second tropopause is identified if the average lapse rate at any level and at all higher levels within one kilometer exceeds 3° C/km above the first tropopause. The existence of a second tropopause indicates a less stable temperature structure ~~and double tropopauses may enhance deep convection to the lower stratosphere~~ (Homeyer et al., 2014). ~~The frequencies of~~ in the UTLS region (Homeyer et al., 2014). Randel et al. (2007) discovered that the ~~double tropopause indicates a region of enhanced transport from the tropics to higher latitudes. Thin ice clouds observed in the low stratosphere over the northern middle and high latitudes in August 1997 originated from tropical high-humidity air~~ (Spang et al., 2015). Therefore, SICs detected in the vicinity of double tropopauses are probably related to quasi-isentropic transport of humid air from the tropics to the extratropics.

SICs with cloud top heights ~~more than~~ 0.25 m above the first tropopause but below the second tropopause are shown in Fig. 3 a-d. SICs ~~coinciding associated~~ with double tropopauses are mostly observed ~~in at~~ midlatitudes, e. g., over the northern Pacific Ocean, northern Atlantic near the United States, and Tibetan Plateau in DJF and MAM, over central North America and southern South America in JJA and SON. In the tropics, there are about 2 ~~—~~ 4 % of the SICs associated with double tropopauses, mainly located over the Maritime Continent in DJF, equatorial Africa in MAM, and the northeastern Indian Ocean in JJA and SON. The ~~occurrence of double tropopauses in general greatly impacts the SICs' occurrences associated with double tropopauses. The~~ patterns of SICs associated with double tropopauses in Fig. 3 a-d resemble the patterns of ~~occurrence frequencies of double tropopauses~~ double tropopauses occurrence in Peevey et al. (2012) and Schwartz et al. (2015). ~~The~~

~~presence of double tropopauses is associated with the subtropical jet stream, which enhances transport from the tropics to higher latitudes (Randel et al., 2007).~~

In addition, Fig. 3 e-h show the fraction of SICs associated with double tropopauses to the total ~~occurrence frequency of~~ SICs. Up to 80-100 % of all SICs around a latitude band of 30° in both hemispheres during local winter and autumn are associated with double tropopauses. However, the highest correlations are found in regions with low SIC frequencies. In the tropics over the Maritime Continent in DJF, equatorial Africa in MAM and northeastern Indian Ocean in SON less than 40 % of the SICs coincide with double tropopauses. Only over the northwestern Indian Ocean in JJA up to 60 % of the SICs are associated with double tropopauses. ~~This indicates that double tropopauses~~The double tropopauses, which enhance convective overshooting
(Homeyer et al., 2014) and isentropic transport (Randel et al., 2007), have a non-negligible impact on the occurrence of SICs at midlatitudes, especially in and around the subtropical jet stream. ~~SICs associated with double tropopauses in the polar region may be due to misclassified PSCs and larger uncertainties in the thermal tropopause due to the relatively constant temperature profile in the polar winter UTLS. In this work, we focus our analyses mainly on the tropics and midlatitudes.~~

To investigate spatial and temporal variations of SICs, monthly averaged occurrence frequencies of SICs in 5° latitude bands from 2007 to 2019 are shown in Fig. 2. Seasonal cycles and inter-annual variability of SICs are observed in all latitude belts. In the tropics, the high SIC occurrence frequency varies with the seasonal motion of the Sun, with the highest frequency generally occurring at 20° S in boreal winter, then gradually moving to 20° N in boreal summer. High frequencies of SICs (>0.20) are found in 15° S - 5° N in November to March while relatively low values (0.16 - 0.24) are found at latitudes 10° N - 20° N in July to September. In mid- and high latitudes, SICs are more often observed from December to May in the northern hemisphere and from May to October in the southern hemisphere. In the tropics there are several pronounced high SIC occurrence frequencies in December 2008 to February 2009, November 2010 to January 2011, December 2011, January 2013, February 2018 to April 2018, and November 2018 to January 2019. Some relatively low occurrence frequencies between 10° N - 20° N are visible in boreal summer in 2012, 2014 to 2017. There is a consistency in the spatial distribution of SICs over time, i. e., SICs in the tropics follow the Intertropical Convergence Zone (ITCZ) and also follow an annual pattern in the midlatitudes. However, interannual changes are also evident. In the following we investigate possible explanations for the SICs' global patterns and their temporal variability.

~~Monthly mean occurrence frequencies of SICs in latitudes band of 5° from 2007 to 2019.~~

3.3 Tropopause temperature and SICs

~~Tropopause~~

The tropopause temperature plays a vital role in influencing ice clouds and regulating water vapor in the lower stratosphere. Low temperatures and cooling processes are more favorable for ice formation, and temperature normally has ~~negative relation a~~ negative relationship with cirrus cloud frequency (Eguchi and Shiotani, 2004; Kim et al., 2016). To better understand the effects of tropopause temperature on the global distribution and occurrence of SICs, seasonal mean ~~first tropopause temperature and~~ SICs-LRT1 temperature (LRT1-T) and frequencies are presented in Fig. 4. Low tropopause ~~temperature are characteristic in~~ temperatures are characteristic of the tropics, where large-scale updrafts, convection, and waves cause its cooling. As already

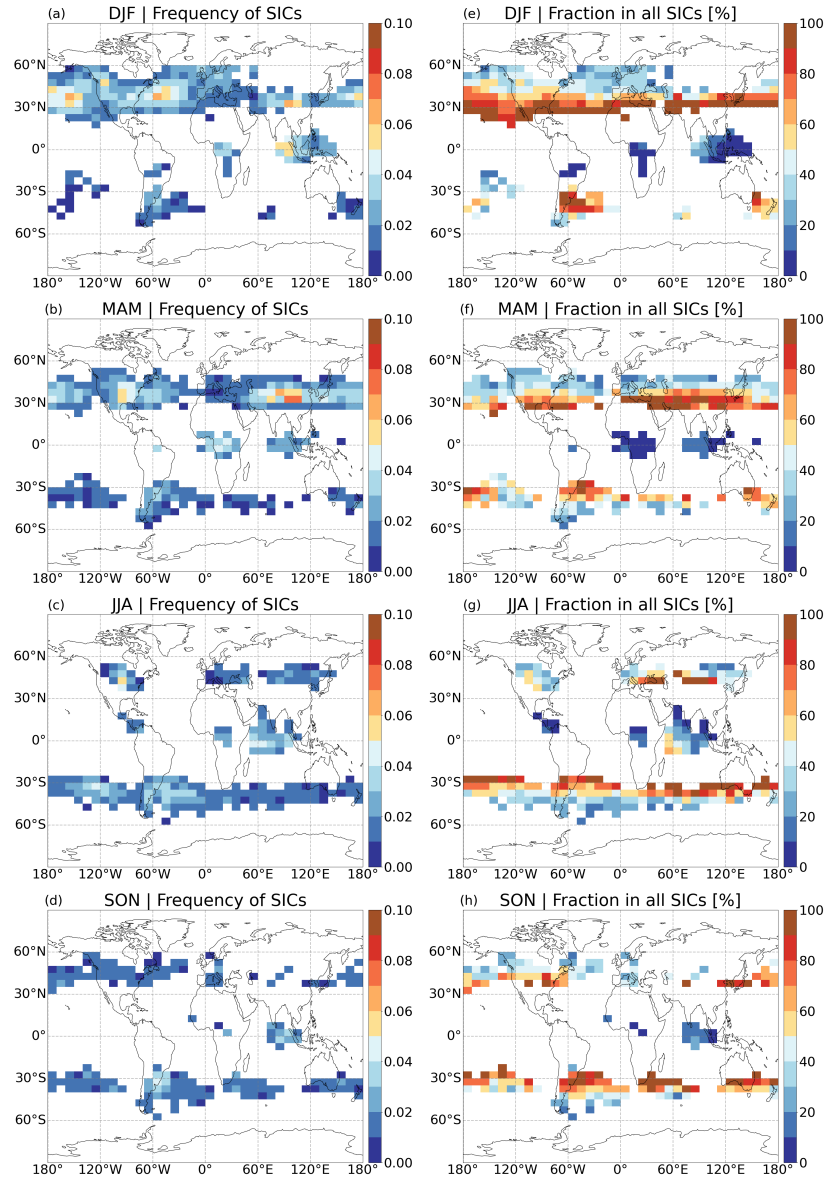


Figure 3. The occurrence frequencies of SICs associated with the double tropopauses with respect to all profiles (a-d) where the cloud-top heights are 0.25 km above the first tropopause and below the second tropopause. e-h) are the fraction of SICs associated with double tropopauses to total SICs (e-h).

noted by Chae and Sherwood (2007) ~~that,~~ tropopause temperatures over ~~the~~ tropics are colder in boreal winter than ~~summer,~~ ~~in~~ ~~summer,~~ and we can find higher occurrence frequencies of SICs over ~~the~~ tropics in DJF than in JJA (Fig. 4). In general, regions with low tropopause ~~temperature~~ ~~temperatures~~ are co-located with ~~a high occurrence frequency~~ ~~high occurrence frequencies~~ of SICs.

415 To further investigate their relation, Spearman correlation coefficients between monthly averaged tropopause temperatures, and occurrence frequencies of SICs from 2007 to 2019 for each grid-cell (in 5° latitude \times 10° longitude) are shown in Fig. 10a. Only grid-boxes with SIC frequencies larger than 0.02, with more than 80 (156 months in total) data points in each grid-box and correlation coefficients significance at 99 % level are presented here. The tropopause temperature is negatively correlated with SIC frequency, especially in the SIC hotspots in the tropics, where r -values are generally < -0.6 and even reach up to
420 < -0.8 in several grid-boxes in tropical South America, at the western coast of equatorial Africa, and northern Australia. Negative correlations are also observed over mid- and high-latitudes ($> 40^\circ$). r -values < -0.6 are detected over Greenland, Iceland, and northwestern Europe. However, positive correlation coefficients are observed in several grid-boxes in the North American Monsoon, North African Monsoon, Indian Monsoon, and Western North Pacific Monsoon. The occurrence of SICs over tropical continents shows a significant dependence on tropopause temperature.

425 Seasonal mean first tropopause temperature derived from ERA5 (color boxes) and occurrence frequencies of SICs derived from CALIPSO (contour lines with the interval of 0.12).

The Spearman correlation coefficients of SIC frequency with the first tropopause temperature, deep convection frequency, gravity waves, and stratospheric aerosol frequency. Only grid-boxes with SIC frequency > 0.02 , ≥ 80 (in 156 months) total data points in each grid-box, and at 99 % significance level are presented.

430 Time-series of monthly anomalies of SIC frequencies and tropopause temperatures at different latitude-bands (5° for each band) are shown in Fig. ??a and b. The monthly anomalies of SIC frequency and mean temperature for each grid-box were computed as the difference between the monthly zonal mean values and ~~However, at midlatitudes, regions with SIC frequency larger than 0.06 are found for warmer tropopause temperatures than in the tropics. The differences with respect to tropopause temperatures in the interannual mean of the monthly zonal mean values,~~

435 For $\theta_i \in [\theta - 5^\circ, \theta]$, where $\theta = [-80^\circ, -75^\circ, \dots, 80^\circ, 85^\circ]$;

For $m \in \text{month} [1, 2, 3, \dots, 10, 11, 12]$;

$$D_T(\theta_i, m, y) = D(\theta_i, m, y) - \frac{1}{N} \sum_{y=2007}^{2019} D(\theta_i, m, y)$$

where θ_i is the latitude-band, $y \in \text{year } 2007, 2008, \dots, 2018, 2019$, N is the number of years, which is 13; $D(\theta_i, m, y)$ is data of SIC frequency or tropopause temperature, and $D_T(\theta_i, m, y)$ is the anomaly value.

440 As stated above, SIC frequencies and tropopause temperatures are generally negatively correlated. We expected anomalies of SIC frequencies and tropopause temperature to have opposite features in time series. Significant anomalies of SIC frequency are visible over ~~tropics and at midlatitudes suggest that the processes leading to SIC formation are inherently different in~~

the tropics (Fig. ??a). Anomalies of SIC frequencies and tropopause temperature overall show contrary features, such as February 2007 to July 2007, January 2008 to Jun 2008, October 2012 to Jun 2013, and July 2016 to Jun 2017. However, some remarkable positive anomalies of SIC frequencies between November 2010 to January 2011 coincide with positive temperature anomalies. Exceptions like these may be due to enhanced stratospheric aerosols (Noh et al., 2017; Chouza et al., 2020) or downward propagating of QBO (Feng and Lin, 2019; Tegtmeier et al., 2020b). Overall, tropopause temperatures are negatively correlated with the occurrence of SICs spatially and temporally, especially over tropical continents. In comparison, some positive correlations over monsoon regions and in the tropics at certain times need further investigation (deep convection) and at midlatitudes (e.g. isentropic transport through double tropopauses, gravity waves, mesoscale convective systems, frontal systems).

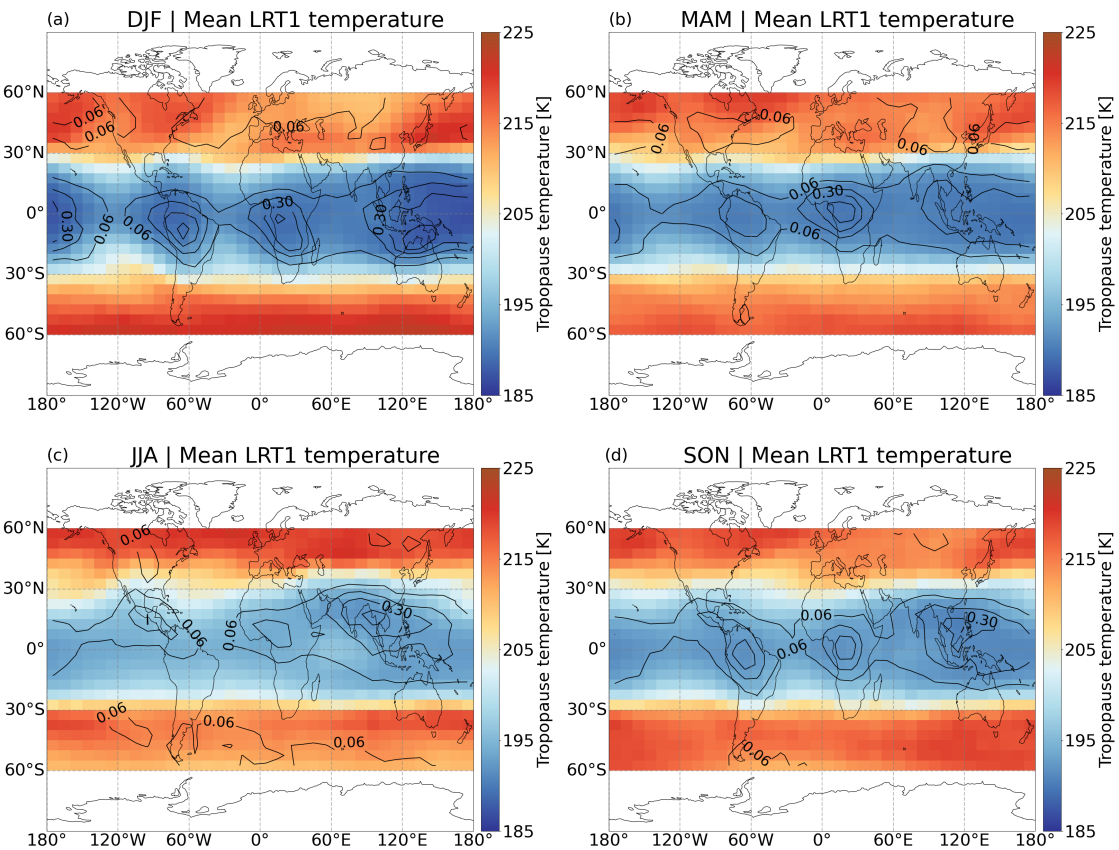


Figure 4. Monthly anomalies of SIC frequency derived from CALIPSO and the Seasonal mean first tropopause temperature derived from ERA5 (color boxes) and occurrence frequencies of SICs from 2007 to 2019. CALIPSO (contour lines with an interval of 0.12).

3.4 ~~Deep convection~~ UTLS clouds and SICs~~Deep convection, which~~

Deep convection can inject water vapor and ice particles into the lower stratosphere and hence provides a source of humidity for in-situ nucleation above anvil tops ~~, is closely related to the occurrence of SICs. As deep convection is the primary factor related to the occurrence of SICs over the Great Plains in storm season (Zou et al., 2021), here we investigate the correlation~~
455 ~~between deep convection and SICs on a global scale. To remove possible uncertainties related to the intensity, spatial extent and duration of deep convection, the event frequency of nighttime deep convection is investigated in this work (Cooney et al., 2018).~~
~~. This study uses UTLS clouds retrieved from AIRS as a proxy for deep convection in the tropics and other high altitude cloud sources at midlatitudes Compared to the occurrence frequency of UTLS clouds (Fig. 5). As stated in Sect. 2, B1), similar patterns are observed for~~ the event frequency ~~is the ratio of the number of days with deep convection to the total number of~~
460 ~~days in one month, whereas the occurrence frequency is the ratio of profiles with deep convection to the total profile number in a specific grid box. The occurrence frequency of deep convection is shown in Appendix B. The patterns of event frequency and occurrence frequency are similar for deep convection in of UTLS clouds in Fig. 5 and Fig. B1 and the seasonal patterns of event frequency are overall similar to results shown in Hoffmann et al. (2013).~~ However, event frequencies are much higher than the occurrence frequencies and the results in Hoffmann et al. (2013). ~~This is~~ due to different ~~computing analysis~~ methods
465 and detection thresholds. In the tropics, the highest event frequencies follow the ITCZ and are ~~the~~ strongest over the continents and southeastern Asia. ~~In the~~ At midlatitudes, the highest event frequencies are found over the oceans and southern South America in DJF and the highest frequencies are observed over the continents in JJA (Fig. 5).

~~Correlation coefficients between monthly averaged event frequency of SIC and deep convection from 2007 to 2019 are shown in Fig. 10 b. The SIC event frequencies are generally positively correlated with deep convection. High correlations are found over Central America, tropical South America, southern Asia, maritime continent and northern Australia, southern Africa and Madagascar with the highest coefficient > 0.8 , which demonstrates that the occurrence of SICs over those regions is highly correlated with the occurrence of deep convection. As a colder tropopause aligns with the higher frequency of tropopause-penetrating convection over the tropics (Gettelman et al., 2002), we conclude that the interaction between tropopause temperature and deep convection both associate with the occurrence of SICs based on the co-location of large correlation~~
475 ~~coefficients in Fig. 10 a and b.~~

To ~~further~~ investigate the effects of ~~deep convection~~ UTLS clouds, we analyzed the fraction of SICs related to ~~deep convection~~ UTLS clouds (Fig. 6), which is defined as the ratio of the number of days with co-occurrence of SICs and ~~deep convection~~ UTLS clouds ($N_{(SICs \cap DC)}$) UTLS clouds to the number of days with occurrence of SICs ($N_{(SICs)}$) in each grid box. Observations at the same local time (LT) for SICs and ~~deep convection~~ UTLS clouds, which is named as 0 local time difference (0 LTD), are
480 presented in Fig. 6. In DJF (Fig. 6 a) more than 50 % of the SICs are correlated with ~~deep convection~~ UTLS clouds over Argentina and southern Brazil, the eastern Tibetan Plateau (with maximum fraction of 80-90 %), the northern Pacific Ocean (maximally 70-80 %) and the maritime continent. In JJA (Fig. 6 c), the highest correlations between SIC and ~~deep convection~~ UTLS clouds are observed over the Great Plains (maximally 70-80 %), Central America (with the highest fraction of 90-100 %), central Africa (about 50-60 %), eastern and southern Asia, Europe and Western Pacific Ocean, and over a latitudinal

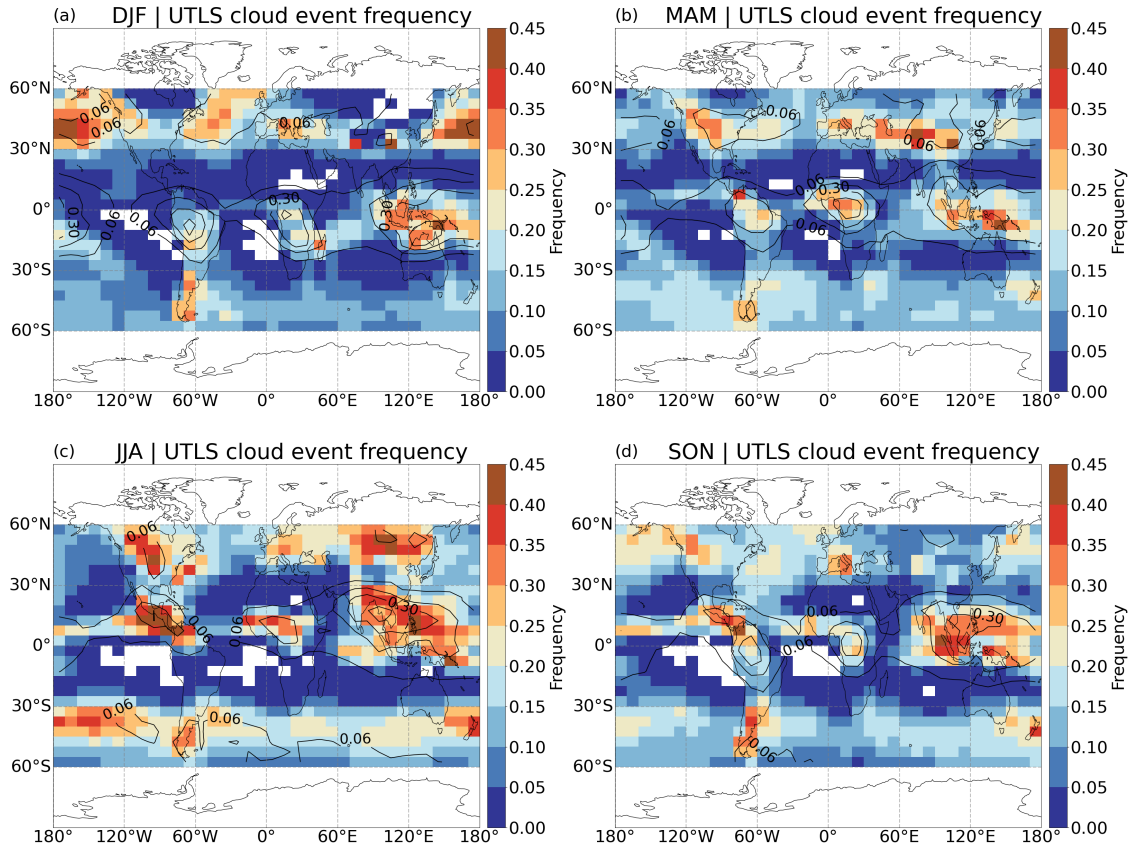


Figure 5. Seasonal event frequency of ~~deep-convection (DC)~~ UTLS clouds derived from AIRS during 2007-2019. Occurrence frequencies of SICs are shown in black contours with the interval of 0.12.

band along 30°S-45°S (40-80 %). During boreal summer, more than 40 % of SICs over the ~~northern hemisphere continents and southern hemisphere~~ NH midlatitudes continents and SH midlatitudes oceans are correlated with ~~deep-convection~~ UTLS clouds. In MAM (Fig. 6 b), regions with the largest correlations are similar to JJA but with lower statistics. In SON, regions with the highest correlations between SICs and ~~deep-convection~~ UTLS clouds are similar to JJA and DJF (Fig. 6 d). The pattern of ~~a high fraction~~ high fractions is similar to patterns of positive vertical velocity within cirrus clouds for corresponding months in Barahona et al. (2017, Fig.06) Barahona et al. (2017, Fig. 6). Overall, the influence of ~~deep-convection~~ UTLS clouds on the occurrence of SICs follows the ITCZ in the tropics. ~~Most high values are observed in JJA. SICs detected~~ SICs detected in the tropics, over the Great Plains, the North American Monsoon and the Asian Monsoon ~~in JJA and over northern Pacific in DJF regions in JJA~~ are mainly attributed to ~~deep-convection~~.

As the lifetime of TTL cirrus may be as long as 12-24 h (Jensen et al., 2011), we also analyzed the correlation with deep convection observed by AIRS measurements 12 hours (-12h LTD) and 24 hours (-24h LTD) before (Appendix. C). The left column of Fig. C1 shows fractions of SICs related to deep convection, which are detected at 0 LTD and -12h LTD (DC at

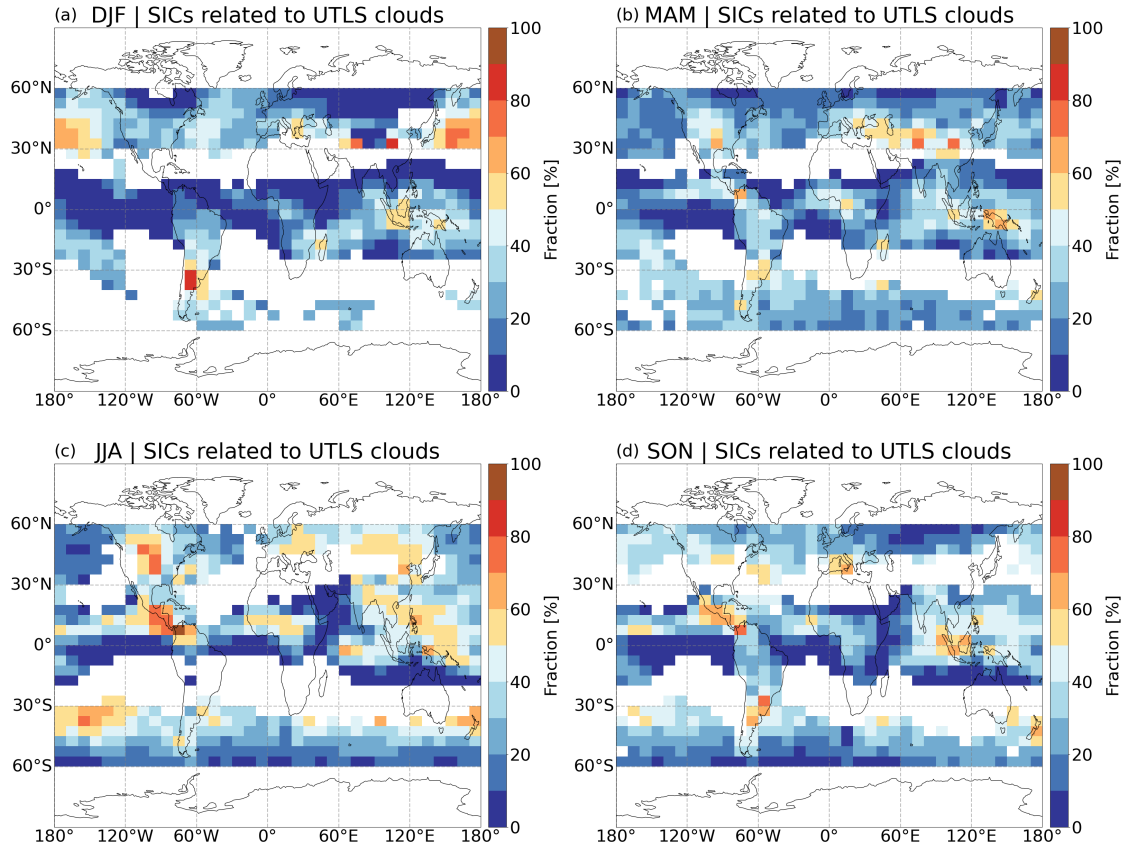


Figure 6. The fraction of SICs associated with UTLS clouds at the same local time (0 LTD).

-12h \cup 0h LTD) to SICs, and the right column (Fig. C1) are fractions of SICs UTLS clouds which are mainly related to deep convection detected at 0 LTD, -12h LTD and -24h LTD (DC at -24h \cup -12h \cup 0 LTD) in different seasons. We find that fractions of SICs related to deep convection generally increase by 10% when one more time detection is included. Therefore, more SIC occurrence can be traced back to deep convection if the lifetime of SICs is taken into account. However, since the lifetime of SICs is unavailable in our dataset, we mainly focus on the deep convection detected simultaneously with SICs origin. The high fractions in the northern Pacific and southern South America in DJF and in the southern Pacific in JJA are associated with other UTLS cloud sources.

The fraction of SICs associated with deep convection at same local time (0 LTD) (color box). Occurrence frequency of SICs are shown in red contours with the interval of 0.12.

3.5 Gravity waves and SICs

Gravity waves are crucial factors locally affecting the pressure, temperature, and vertical velocity of an air parcel. As the cold phase and cooling effects of gravity waves have a significant influence on cirrus cloud occurrence (Chang and L'Ecuyer,

2020; Ansmann et al., 2018), it is essential to investigate the relation between gravity waves and the occurrence of SICs. Mean
510 variances of brightness temperatures (BT) at $4.3\ \mu\text{m}$ from AIRS observations are applied to identify gravity wave ~~amplitudes.~~
~~Due events. Note that due~~ to the wind filtering and visibility effects, gravity waves ~~in AIRS measurements~~ are not significantly
observed in ~~tropics (Hoffmann et al., 2013).~~ the tropics in AIRS (Hoffmann et al., 2013).

In JJA, hotspots of large amplitude waves (mean BT variance $> 0.1\ \text{K}^2$) are observed at ~~mid- and high latitudes in the~~
~~southern hemisphere~~ midlatitudes in the Southern Hemisphere, especially over Patagonia ~~, Drake Passage, and the Antarctic~~
515 ~~Peninsula and the Drake Passage~~. In the Northern Hemisphere, high variance is found over ~~southern-south~~ and southeastern
Asia, the Great Plains, Florida, and northern Africa in Fig. 7c. In DJF (Fig. 7 a), high variance ($> 0.1\ \text{K}^2$) is observed over the
northern Atlantic, eastern Canada and the United States ~~, Europe and the~~ and Europe. The mean variances of all regions north of
 40°N , except for the ~~northern-north~~ Pacific Ocean, are greater than $> 0.03\ \text{K}^2$. In the southern ~~Hemisphere~~ hemisphere, several
gravity wave hotspots ~~are have been~~ detected over southern Africa and Madagascar, northern Australia and ~~coral-sea~~ the Coral
520 ~~Sea~~, and southern Brazil. In MAM, gravity waves are observed mainly over the ~~southern hemisphere~~ Southern Hemisphere,
with a similar pattern to that in JJA, but with weaker signals ~~, and southern Greenland~~ (Fig. 7 b). Similar patterns with weaker
signals to DJF are observed in SON over the ~~northern hemisphere~~ Northern Hemisphere, and an intense center is detected over
Patagonia ~~, Drake Passage and the Antarctic Peninsula in~~ and the Drake Passage at this time (Fig. 7 d). ~~Regions with high mean~~
~~BT variance for each season are in agreement with hotspots of SICs (Fig. 1) and deep convection (Fig. 5).~~

525 ~~The mean brightness temperature variance at $4.3\ \mu\text{m}$ from AIRS measurements, which indicates the amplitude of gravity~~
~~waves. Occurrence frequency of SICs are shown in blue contours with the interval of 0.12.~~

~~The correlation coefficients between the monthly averaged frequency of SICs and mean BT variance are shown in Fig. 10c.~~
~~Positive correlation coefficients are discovered in most regions of the world. High correlations with correlation coefficients~~
 ~~> 0.8 are found over southern Asia, northern Australia, southern Africa and Madagascar, central Pacific Ocean, and Central~~
530 ~~America. This indicates that the amplitude of gravity waves has a significant impact on the~~ At midlatitudes, SICs are co-located
with high BT variance in DJF and JJA suggesting an important role of gravity waves in the formation and occurrence of SICs.
~~In addition, high correlation regions of~~ However, in the tropics, regions with high mean BT variance ~~overlapped with high~~
correlations with deep convection over Central America, tropical South America, southern Asia, southern Africa, and northern
~~Australia are in agreement with low LRT1 temperature~~ (Fig. 10b and c), which provides information for high correlation of
535 deep convection and gravity waves. ~~However, positive correlation of SICs and gravity waves and negative correlations of SICs~~
~~and deep convection are found in high latitudes, which indicates the important role of gravity waves on the occurrence of SICs~~
~~in high latitudes. All in all, we conclude that gravity waves~~ 4) and deep convection are important factors influencing UTLS
clouds (Fig. 5). Those overlaps suggest strong correlations between tropopause temperature, UTLS clouds, gravity waves, and
the occurrence of SICs, ~~interactively and respectively.~~

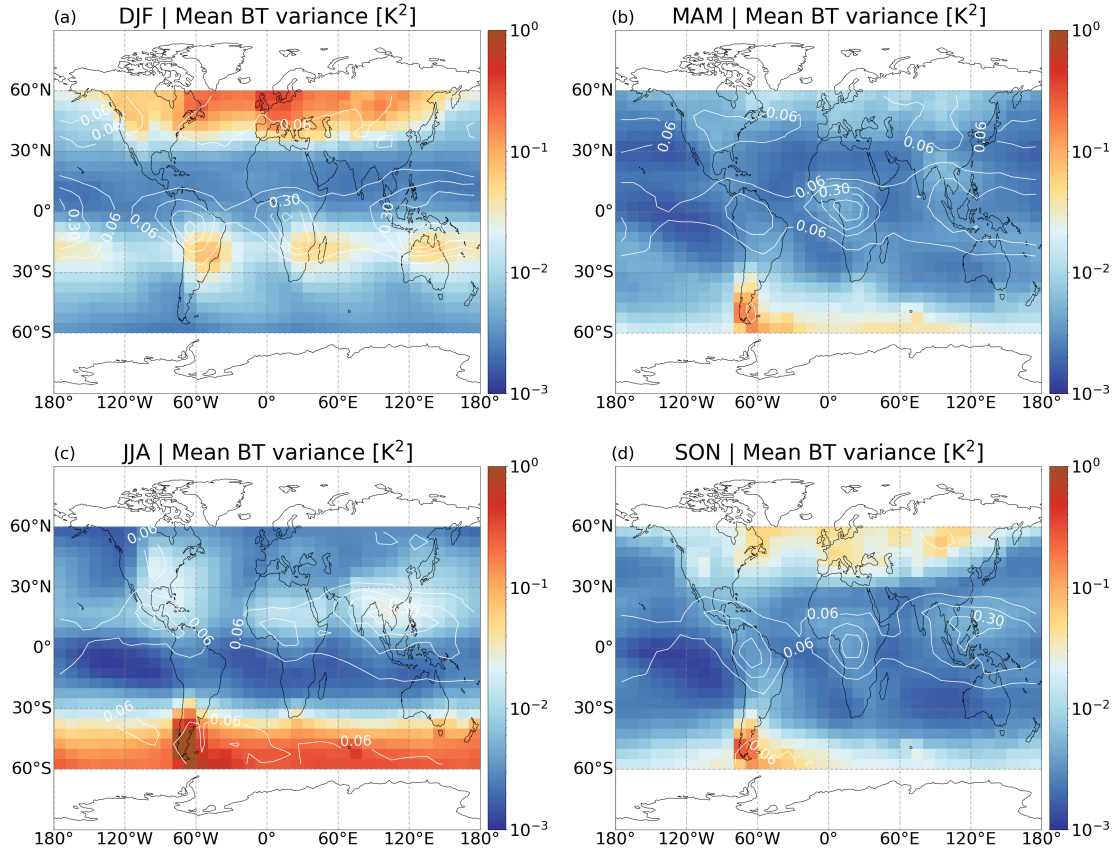


Figure 7. Mean brightness temperature variance at $4.3 \mu\text{m}$ from AIRS measurements, which correlates with the amplitude of gravity waves. The occurrence frequencies of SICs are shown in blue contours with an interval of 0.12.

540 3.6 Stratospheric aerosols and SICs

The time-series of SIC frequency anomalies (Fig. 12a) and stratospheric aerosol anomalies (Fig. 12b) are presented together with significant volcanic eruptions derived from AIRS SO_2 measurements, where occurrences of SO_2 Index (SI) > 0.5 are marked as triangles. As aerosol particles provide cloud condensation nuclei and ice nuclei, the occurrence of SICs is expected to correlate with aerosols (Lohmann and Feichter, 2005). In Fig. 10 K are marked as triangles. The largest positive anomalies of SICs are found in the tropics at 0° – 20° S in November 2010 to January 2011, 5° N – 20° N in June and July 2011, 5° S – 5° N in June and July 2015, 15° S – 20° N in April and May 2018, and 5° N – 25° N in September to November 2019. No reasonable explanation could be obtained from relation analyses of SIC frequency with deep convection, tropopause temperature and gravity waves. However, we noticed that those high SIC frequencies coincide with volcanic eruptions of Merapi (7.5° S) in November 2010, Nabro (13° N) in June 2011, Wolf (0°) in May 2015, Ambae (15.4° S) in April 2018, and Ulawun (5° S) in August 2019, respectively (Global Volcanism Program, 2013; Hoffmann, 2021b). At mid-latitudes the most pronounced positive anomalies

in SIC frequency correlate with the ash-rich volcanic eruptions of Kasatochi (August 2008, 52° N), Puyehue-Cordón-Caulle (June 2011, 41° S) Calbuco in April/May 2015 (41° S) and Raikoke (June 2019, 48° N) compare with AIRS ash and SO₂ index (Hoffmann, 2021b). High SIC anomalies coincide to a large extent with volcanic eruptions and hence, suggest a potential influence of aerosol on the CALIPSO ice cloud product.

Daily frequencies of SAs and frequency anomalies of SICs over tropics and midlatitudes in different years are selected as examples to demonstrate their relations in Fig. 8. In Figure 8a, high SA frequency and high SIC frequency anomalies are found on day-days 160-180 in 2011 at southern midlatitudes, where an SI>10 K was found approximately 10-20 days before. Similar patterns were found between days 90 to and 120 in the tropics in 2018 (Fig. 8c) and between day-days 170 and 210 at northern midlatitudes in 2019 (Fig. 8d). In these cases, stratospheric aerosol injected by volcanic eruptions, such as Puyehue-Cordón Caulle in 2011 (Klüser et al., 2013), Ambae in 2018 (Malinina et al., 2021), and Raikoke in 2019 (Kloss et al., 2021), show strong relationships with large positive SIC frequency anomalies. The enhanced SA and SIC frequency anomaly between days 220 and 240 in 2017 at northern midlatitudes (Fig. 8b) is related to wildfires over the United States and Canada in August and September 2017 that greatly increased stratospheric aerosol load (Ansmann et al., 2018; Selimovic et al., 2019). The examples above demonstrate the high correlations between stratospheric aerosols and SICs.

Long-term correlations between monthly mean frequency of SICs and stratospheric aerosol Seasonal occurrence and distribution of SAs in CALIPSO are presented in Fig. 10d. Positive correlations are generally observed over the world. High coefficients (≥ 0.9). Significantly higher SA frequencies are found at northern midlatitudes and over South America, which are associated with strong volcanic eruptions such as Kasatochi (August 2008, 52° N) are located over southern Asia, northern Australia, southern Africa and Madagascar, the central Pacific Ocean, and Central America (N). Redoubt (March 2009, 60° N), and Raikoke (June 2019, 48° N) at northern midlatitudes and Puyehue-Cordón Caulle (June 2011, 41° S), and Calbuco (April/May 2015, 41° S) in South America where high frequencies can be affected by the South Atlantic Anomaly (SSA) (Noel et al., 2014). No significant correlation can be seen with the long-term averaged SIC frequencies in those regions. However, high frequencies of SICs are consistent with SAs in all seasons over continents in the tropic in DJF, MAM and SON and over the North American Monsoon, Asian Monsoon regions and equatorial Africa in JJA. Those are known regions with large-scale upwelling and tropopause-penetrating convection, which may lead to the vertical transport of aerosol from the troposphere to the stratosphere. The likely cloud seeding by Kasatochi volcanic aerosols (Campbell et al., 2012) demonstrate a close relation of atmospheric aerosols and occurrence of cirrus clouds. Whereas, strong inverse correlations were observed between stratospheric sulfur aerosol and cirrus cloud reflectance in Friberg et al. (2015). The positive correlations would also be affected by the classification method for ice and aerosol in CALIOP and the possible misclassification of them (Reverdy et al., 2012). that indicate interconnections between the occurrence of SAs, UTLS clouds and gravity waves.

Daily frequency of stratospheric aerosols (SA) and daily anomaly of SIC frequency over tropic and midlatitudes from CALIPSO measurements in a) 2011, b) 2017, c) 2018, d) 2019. Volcanic eruptions (SI > 10 K from AIRS measurements) are shown as green triangles. Blanks are missing data or filtered abnormal data that are three times greater than the standard deviation of regional mean frequency at that day.

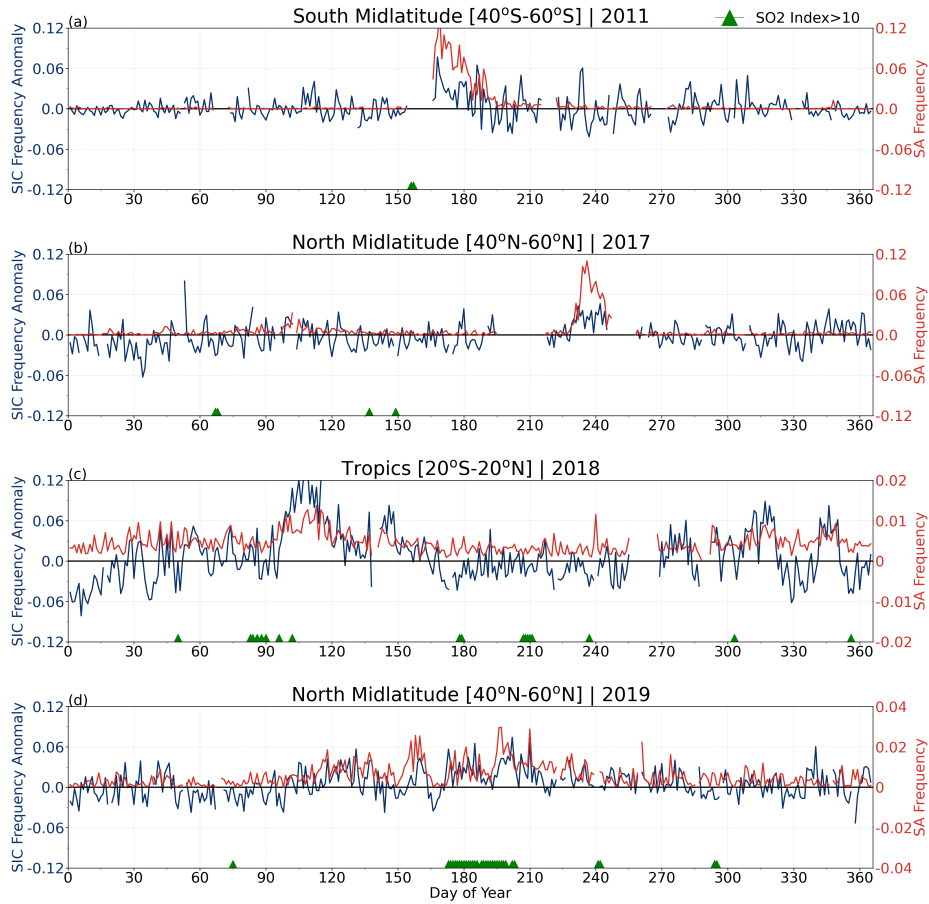


Figure 8. Daily frequency of stratospheric aerosols (SA) and daily anomaly of SIC frequency over the tropics and at midlatitudes from CALIPSO measurements in a) 2011, b) 2017, c) 2018, d) 2019. Volcanic eruptions (SI > 10 K from AIRS measurements) are shown as green triangles. Blanks are missing data or filtered abnormal data that is three times greater than the standard deviation of regional mean frequency on that day.

585 3.7 Assessment of processes related to SIC occurrence Regional analyses

Relations between Individual relationships between the occurrence of SICs and tropopause temperature, deep convection UTLS clouds, gravity waves, stratospheric aerosol on a global scale were investigated above. All factors play important roles in the occurrence and stratospheric aerosols were analyzed in the above sections. To better understand the global distribution of SICs, but the importance varies seasonally from region to region. Therefore, in this section selected regions are studied in detail. The regions shown in Fig. 9 were selected based on hotspots of SIC frequencies, i.e., Spearman correlation coefficients were calculated. Figure 10 presents the correlation coefficients between monthly averaged tropopause temperatures, UTLS clouds, gravity waves, stratospheric aerosols and SICs from 2007 to 2019 for each grid cell (in 5° latitude × 10° longitude). Only

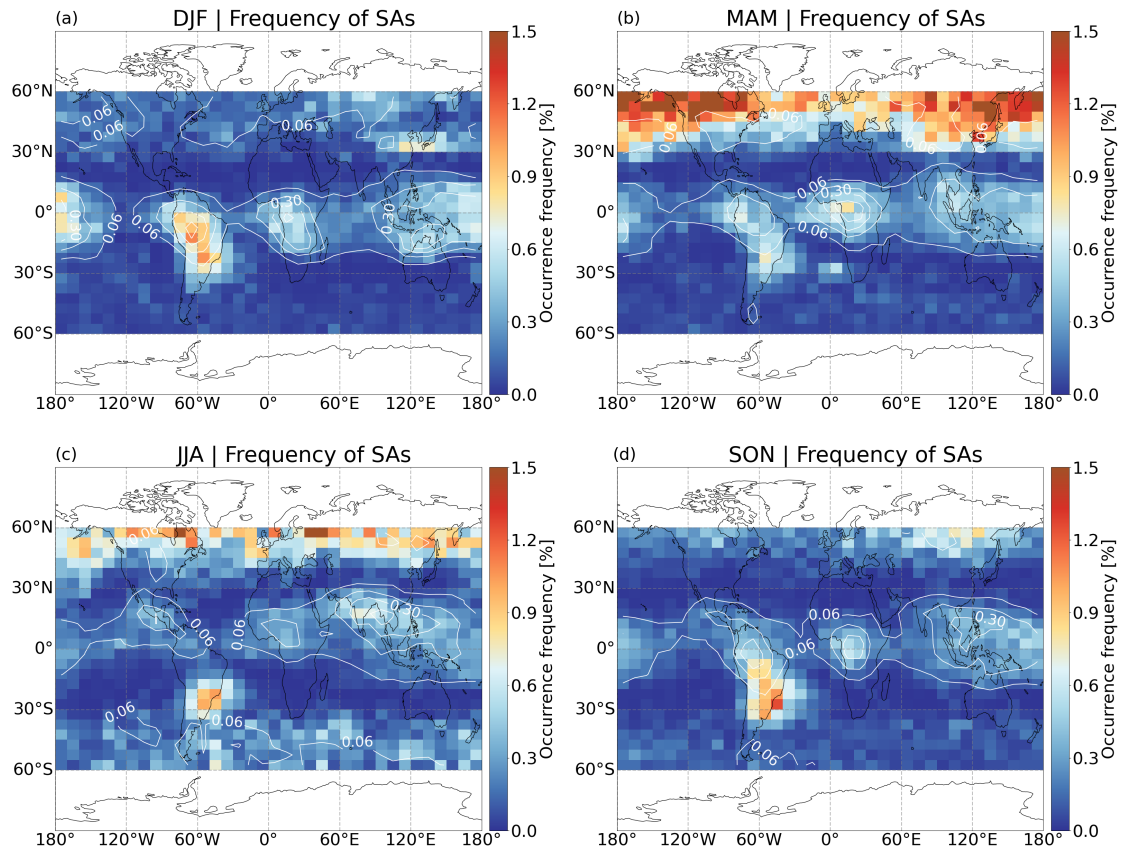


Figure 9. Monthly anomalies of SIC Seasonal frequency and of stratospheric aerosol frequency-aerosols from CALIPSO observations from 2007 to 2019. Blue triangles indicate volcanic events, identified by an SI > 10 K derived from AIRS observations during 2007-2019. Occurrence frequency of SICs are shown in white contours with the interval of 0.12.

grid boxes with SIC frequencies greater than 0.02 with more than 80 data points (156 months in total) in each grid box and correlation coefficient significance at the 99 e. , Indo-Pacific Warm Pool (IPWP, 15°S-15°N, 90°E-180°E), Asian Monsoon (AM, 5°N-35°N, 50°E-120°E), southern South America (SSA, 30°S-60°S, 10°W-80°W), % level are presented here.

The occurrence of SICs has a general negative correlation with tropopause temperature, while SICs have positive correlations with UTLS clouds, gravity waves and stratospheric aerosols. The highest negative and positive correlations are mostly observed over the tropical continents and the western Pacific with correlation coefficients of < -0.8 between SICs and LRT1-T and > 0.8 between SICs and UTLS clouds, gravity waves, and stratospheric aerosols. High positive correlations are also found over the Asian Monsoon and the North American Monsoon regions between SICs and UTLS clouds, gravity waves, and aerosol. While the LRT1 shows a general negative correlation, there are strong positive correlations over central America and the Caribbean Sea, Philippines and South Chinese Sea, and the Tibetan Plateau to the Caspian Sea. The highest correlation coefficients are as large as 0.8-1.0 in the North American Monsoon (NAM, 0°-30°N, 60°W-120°W), tropical South America

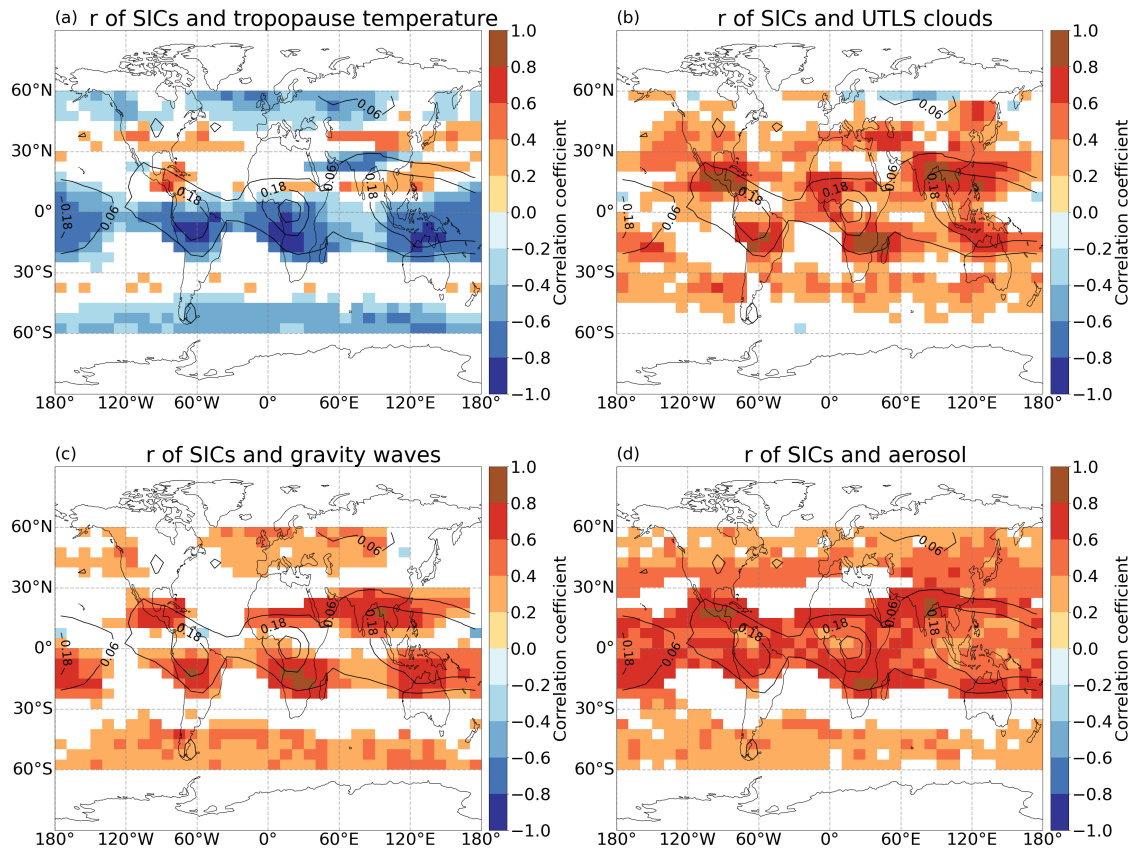


Figure 10. Spearman correlation coefficients of SIC frequency and the first tropopause temperature, UTLS cloud frequency, gravity waves, and stratospheric aerosol frequency. Only grid boxes with SIC frequency > 0.02 and > 80 data points in each grid box and at 99 % significance level are presented. Occurrence frequency of SICs are shown in black contours with an interval of 0.12.

(TSA, 20°S-10°N, 40°W-100°W), equatorial Africa (EA, region, even for LRT1-T. In the Asian Monsoon region, negative correlations are detected over the Tibetan plateau, but positive correlations are seen over southern Asia and India between SICs and LRT1-T. High correlation coefficients imply the important role of tropopause temperature, UTLS clouds, gravity waves and stratospheric aerosols for the occurrence of SICs. However, overlapping high correlation coefficients indicate also strong connections between the tropopause temperature, UTLS clouds, gravity waves, and stratospheric aerosols themselves.

To further investigate the source of SICs, the highest and second-highest correlation coefficients between SICs and all processes for each grid box are shown in Fig 11. Over the tropical continents, the highest correlation coefficients of SICs relate to tropopause temperature. The highest correlation coefficients are found between UTLS clouds and SICs in the monsoon domains in the latitude range between 15° S-15 and 30°N-10, e.g., the North American Monsoon, the Asian Monsoon, the South African Monsoon regions and the La Plata basin. In the central United States, tropopause temperature and UTLS clouds have the highest correlations with SICs. Over Patagonia and the Drake Passage, tropopause temperature and gravity waves have

the highest correlation with the occurrence of SICs. In the latitude range between 45° W-40and 60°E) and northern Atlantic (NA, 40°N-75°N, 50°W-30°E), the strongest correlations are found between SICs and tropopause temperature and gravity waves. However, the second-highest correlation coefficients of SICs are related to stratospheric aerosols, UTLS clouds, and gravity waves over the tropical continents, the North American Monsoon and the Asian Monsoon regions. The rather similar correlation coefficients of SICs with all processes indicate high correlations between all processes themselves.

For all processes, increased tropopause-penetrating convection may result in a cooler tropopause across the tropics (Gettelman et al., 2002). Gravity waves and wave breaking will locally cause a colder temperature in the atmosphere and air cooling (Dinh et al., 2016). High correlations were found between deep convection and gravity waves (Hoffmann et al., 2013), and vertical motion of air will transport aerosols into the stratosphere (Bourassa et al., 2012). The inherent correlations between all processes may help to explain the positive correlations between SICs and LRT1-T in the North American Monsoon and the Asian Monsoon regions. Even if the tropopause temperature is warm, UTLS clouds, gravity waves, and stratospheric aerosol could all contribute to the high occurrence frequency of SICs. For example, Fu et al. (2006) discovered that deep convection in the Asian Monsoon injected more ice and water vapor into the stratosphere with warmer tropopause temperatures. However, their strong correlation also makes it challenging to disentangle all processes' effects on the occurrence of SICs.

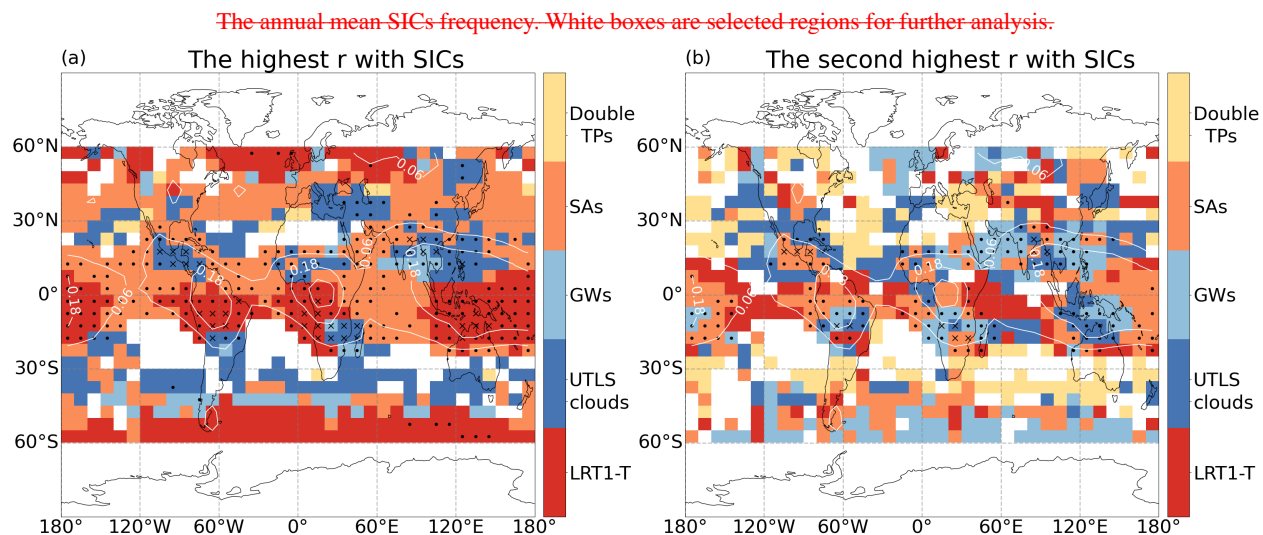


Figure 11. The highest and second-highest correlation coefficients between SIC frequency and all processes (LRT1-T, UTLS clouds, gravity waves (GWs), stratospheric aerosols (SAs) and double tropopauses (Double TPs)). Only grid boxes with absolute $r \geq 0.3$ are presented, and grid boxes filled with ' ' means $0.6 < \text{absolute } r < 0.8$, 'x' means $0.8 < \text{absolute } r < 1.0$. Occurrence frequency of SICs are shown in white contours with an interval of 0.12.

Monthly first tropopause temperature (1st-TPT), stratospheric aerosol frequency (SAs), gravity waves (GW, mean BT variance), monthly mean zonal wind over Singapore (1° N, 104° E) at a pressure level of 70 hPa, representing the Quasi-Biennial Oscillation (QBO) of the winds in the equatorial stratosphere (QBO-70hPa) and sea surface temperature over Niño 3.4 region (

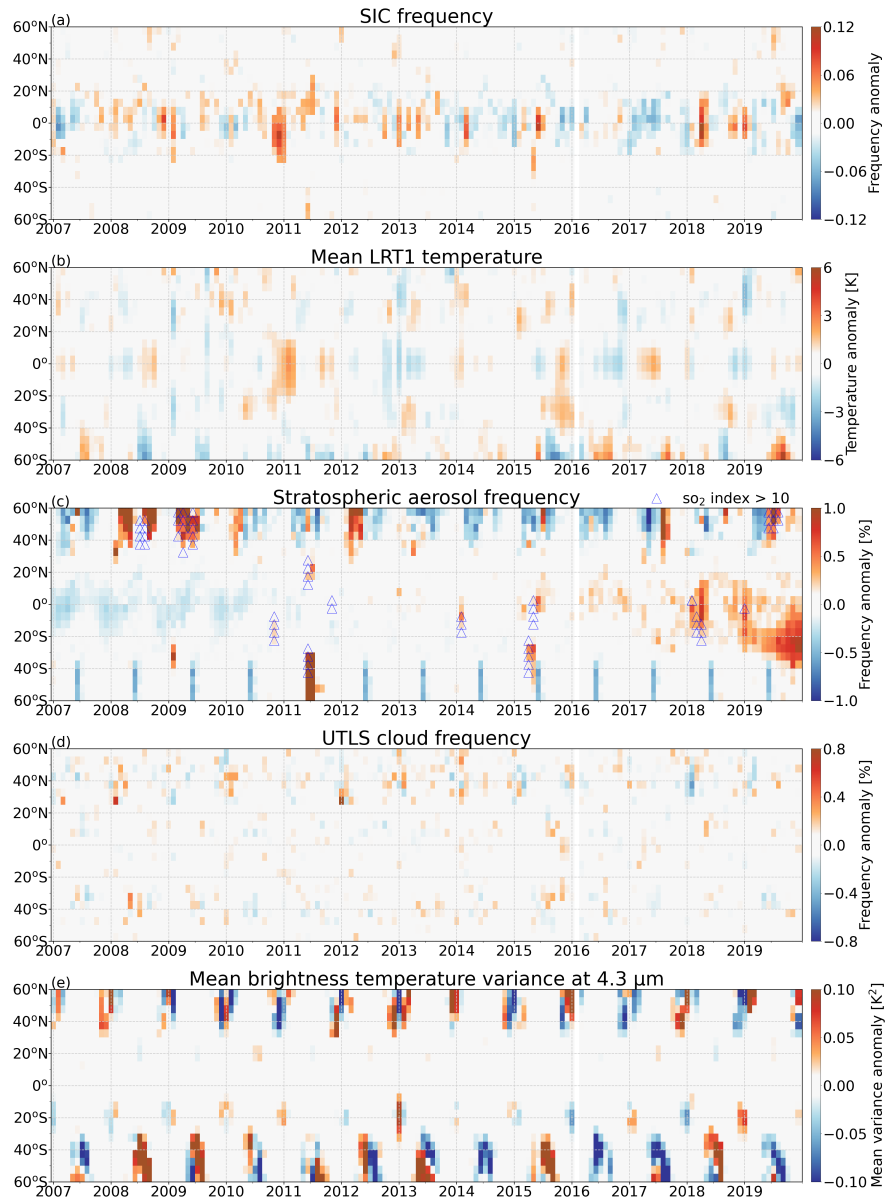


Figure 12. Monthly anomalies of SIC frequency, LRT1 temperature, stratospheric aerosol frequency, UTLS clouds and gravity waves from 2007 to 2019. Blue triangles indicate high SIC frequency related to strong volcanic events, identified by an SI > 10 K derived from AIRS observations.

To explain the tempo-spatial variation of SICs, monthly SIC frequencies and all processes at different latitude bands (5° N- 5° S, 170° W- 120° W) (Niño3.4 SST) were analyzed along with anomalies of SIC frequency as well as anomalies of SIC and DC event frequencies over different regions. Correlation coefficients between SIC frequency and all other parameters are listed in Tab. ?? . Averaged Spearman correlation coefficients were obtained by re-sampling all data 50 times using the Bootstrap method (Efron and Tibshirani, 1985). Three regions of monthly anomalies of all parameters are selected and for each band) from 2007 to 2019 are presented in Fig. ?? Fig. ?? . The anomalies were calculated by subtracting all month-averaged data from monthly values. All data in February 2016 were excluded due to the absence of CALIPSO measurements.

Mean correlation coefficients of SIC frequency with first tropopause temperature (1st-TPT), event frequency of deep convection frequency (eDC), stratospheric aerosol frequency (SAs), mean BT variance (GW), QBO 70hPa, Niño3.4 SST and their standard deviations from a bootstrapping analysis: Regions 1st-TPT eDC SAs GW QBO 70hPa Niño3.4 SST **IPWP** (15° S- 15° N, 90° E- 180° E) -0.67 ± 0.05 0.40 ± 0.07 0.54 ± 0.05 0.37 ± 0.09 -0.21 ± 0.06 -0.50 ± 0.06 TSA (12. The monthly anomalies for each band were computed as the difference between the monthly zonal mean values and the inter-annual mean of the monthly zonal mean values, which excludes seasonal cycles of parameters. The regionally averaged monthly anomalies of SIC frequencies and all processes with seasonal cycles over the tropics (20° S- 10° S- 20° N N), northern midlatitudes (40° W- 100° N- 60° W) -0.81 ± 0.04 0.18 ± 0.09 0.60 ± 0.05 0.47 ± 0.06 -0.06 ± 0.09 -0.20 ± 0.08 EA (15 N) and southern midlatitude (40° S- 15° N, 10° W- 40° E) -0.71 ± 0.05 0.22 ± 0.08 0.62 ± 0.05 0.06 ± 0.08 -0.09 ± 0.08 -0.12 ± 0.08 AM (5° N- 35° N, 50° E- 120° E) -0.55 ± 0.06 0.92 ± 0.01 0.52 ± 0.05 0.71 ± 0.04 -0.04 ± 0.07 0.11 ± 0.07 NAM (0° - 30° N, 60° W- 120° W) 0.15 ± 0.09 0.89 ± 0.02 0.51 ± 0.07 0.54 ± 0.05 0.00 ± 0.07 0.01 ± 0.08 SSA (30° S- 60° S, 10° W- 80° W) -0.78 ± 0.04 0.61 ± 0.05 -0.08 ± 0.08 0.74 ± 0.03 0.04 ± 0.08 0.11 ± 0.07 NA (40° N- 75° N, 50° W- 30° E) -0.83 ± 0.04 0.60 ± 0.05 0.04 ± 0.08 0.66 ± 0.05 0.06 ± 0.08 -0.10 ± 0.09 S) can be found in Appendix. D.

Over Indo-Pacific Warm Pool (IPWP), the variation of SICs is strongly correlated with the 1st-TPT (-0.67 For global-scale anomalies excluding the effect of seasonal cycles, significant anomalies in SIC frequency can be observed in the tropics. Anomalies of SIC frequencies at ± 0.05), SAs (0.54 ± 0.05) and Niño3.4 SST (-0.50 ± 0.06) (Tab. ??). From Fig. ??, we find SIC frequencies are higher in winter and spring (NDJF) and lower in summer and autumn (JJAS), following the ITCZ. Seasonal fluctuations in SIC frequencies are similar to SA frequencies and gravity waves, but are inversely correlated with 1st-TPT. Some high frequencies of SICs are found in November to next year February 20° are generally demonstrating contrary features to the LRT1 temperature. For instance, negative anomalies of SICs in February 2007, 2008, to July 2007, November 2009, 2018 and December 2011, to January 2010, October 2013 to June 2014 (excluding March 2014), and October 2015 to January 2016, January-August 2017, November-December 2019 are compatible with positive LRT1 temperature anomalies. And positive SIC anomalies in January-June 2008, January 2013. Cold tropopause, high loading of stratospheric aerosols, large gravity wave amplitude all show high relationships with those high SICs, i. e., the coldest tropopause and cold phase of ENSO in November 2007 to the following February, peak gravity wave in January 2013, high SA frequencies in November June-July 2015, June-December 2016, October 2018 to the following February. During November 2009 and 2015 to the following February, low SIC frequencies coincide with the warm phase of ENSO, when tropopause is warm and less convective cloud-ice is produced over the Western Pacific (Avery et al., 2017). Fluctuations of tropopause temperature February 2019 are

critical factors in the seasonal cycle of SIC frequency, while SA, GW and atmospheric turbulence all affect variations of SICs over IPWP co-located with negative LRT1 temperature anomalies. During those periods, tropopause temperature variations are important for the anomalous variability of SICs in the tropics.

Over the Asian Monsoon region, anomalies of SIC frequencies are high in JJA and low in DJF. Seasonal cycles of SIC and deep convection event frequencies coincide well in time (Fig. ??b), following the ITCZ, with a correlation coefficient of 0.92 ± 0.01 indicating the crucial role of deep convection on the occurrence of SICs over the Asian Monsoon. Similar to temporal variation of SIC and deep convection frequency, gravity waves also show a high correlation with the occurrence of SICs ($r = 0.71 \pm 0.04$). In the summers of 2007, However, tropopause temperatures cannot explain some remarkable positive anomalies in SIC frequencies. For example, high SICs in November 2010 to January 2011, December 2011, March 2014, and April-May 2018 over the equator and high SIC anomalies in April-July 2011 at 5°N - 20°N . We need to note that the cold temperature as well as the cooling of the atmosphere (Kim et al., 2016) are important for the variation of SICs. And the uplifting motions, 2012-2014, 2017 and 2019, high SIC frequencies are influenced by deep convection and gravity waves. The peak SIC frequency in July 2011 correlates with enhanced stratospheric aerosol after the volcanic eruption of Nabro in June 2011. Two highest SIC frequency anomalies in June-September 2010, the El Niño-Southern Oscillation (ENSO) and 2013 are related to QBO's easterly phase, La Niña phenomenon, enhanced deep convection and gravity waves. Deep convection and gravity waves are two main factors related to the occurrence and variability of SICs over the Asian Monsoon region. quasi-biennial oscillation (QBO) and potentially other effects would all impact the temperature and temperature variations (Abhik et al., 2019; Feng and Lin, 2019; Tegtmeier et al., 2020b) associated with SIC variability.

Over southern South America, positive anomalies of SIC frequencies are detected in JJA along with a cold tropopause (Fig. ??). Tropopause temperature is an important factor influencing the frequency of SICs with the correlation of -0.78 ± 0.04 . Gravity wave events and deep convection have a consistent seasonal cycle with SIC frequency with correlations of 0.74 ± 0.03 . Stratospheric aerosols, UTLS clouds and 0.61 ± 0.05 , respectively. The effect of stratospheric aerosols is limited in gravity waves are further analyzed to understand those anomalous SICs. Enhanced stratospheric aerosols due to volcanic eruptions coincide with the high SIC frequencies at 25°S - 10°N in November 2010 to January 2011 and 2019. High SAs frequencies are probably related to the (Merapi volcano), 5°N - 20°N in April-July 2011 (Nabro volcano), 15°S - 10°N in March 2014 (Mt. Kelud volcano), 15°S - 20°N in April-May 2018 (Ambae volcano) (Global Volcanism Program, 2013; Hoffmann, 2021b). In the extra-tropics, the most pronounced positive anomalies in SIC frequency correlate with the ash rich volcanic eruptions of Kasatochi (August 2008, 52°N), Puyehue-Cordón Caulle (June 2011), Ulawun (June-August 2019) and Ubina (July 2019). Orographically generated gravity waves (Hoffmann et al., 2013) and gravity wave induced temperature perturbations may regulate the occurrence of SICs over southern South America, i.e., high SIC frequencies are highly correlated with high wave amplitude in 2010S), Calbuco in April-May 2015 (41°S), and Raikoke (June 2019, 48°N) (compare with AIRS ash and SO_2 index) (Hoffmann, 2021b). High SIC frequencies around 40°N in January-March 2011 and from December 2012, 2014, 2015, 2017 and 2018 and relatively low SIC frequencies are consistent with relatively low BT variance in 2009, 2013 to January 2013 are co-occurring with high anomalies of UTLS clouds and 2016.

According to Tab. ??, variations of SIC frequencies over tropical South America and equatorial Africa have high correlations with tropopause temperature and stratospheric aerosols, which is similar to IPWP. The highest correlations of SIC frequencies with deep convection and gravity waves are observed over the Asian Monsoon and the North American Monsoon. Over the northern Atlantic, The tempo-spatial analyses of LRT1 temperature, UTLS clouds, gravity waves and tropopause temperatures show the strongest correlation with the variability of SIC frequencies, which is similar to southern South Africa. As the highest correlations of processes with SIC frequencies over the regions of tropical South America and equatorial Africa, North America Monsoon and northern Atlantic are similar to the above analyzed three regions, the detailed information on those four regions are presented in Sect. ??.

On the whole, tropopause temperature, deep convection, gravity wave, stratospheric aerosol and atmospheric turbulence are all important factors related to the stratospheric aerosols provide explicit awareness of processes on the occurrence and variability of SICs. However, leading factors differ over regions at different latitude bands and time ranges.

Monthly anomalies of SIC frequency, tropopause temperature(1st-TPT), event frequencies of SIC and deep convection, stratospheric aerosol frequency, gravity waves, QBO at 70hPa and Niño3.4 SST over Indo-Pacific Warm Pool (IPWP-15° S-15° N, 90° E-180°) from 2007 to 2019.

Monthly anomalies of SIC frequency, tropopause temperature(1st-TPT), event frequencies of SIC and deep convection, stratospheric aerosol frequency, gravity waves, QBO at 70hPa and Niño3.4 SST over Asian Monsoon (5° N-35° N, 50° E-120° E) from 2007 to 2019.

Monthly anomalies of SIC frequency, tropopause temperature(1st-TPT), event frequencies of SIC and deep convection, stratospheric aerosol frequency, and gravity waves over southern South America (30° S-60° S, 40° W-80° W) from 2007 to 2019.

4 Discussion

4.1 Tropopause threshold and SICs identification In this work and tropopause uncertainty

In this study, a tropopause threshold of 250 m is was applied to identify stratospheric ice clouds and stratospheric aerosols (As mentioned in Sect. 2.1). While 500 m is an acceptable threshold for tropopause uncertainty (Homeyer et al., 2010; Pan and Munchak, 2011), and it is solidly applied to ERA-Interim data (Zou et al., 2020, 2021), 250 m is a reasonable tropopause threshold for the vertical resolution of tropopause heights in ERA5 data due to its two times higher vertical resolution than in ERA-Interim. Moreover, the lapse rate tropopause height difference between was improved by applying a cubic spline interpolation method (Hoffmann and Spang, 2022). When compared to radiosonde and GPS data, the height uncertainty for the LRT1 in ERA5 and radiosonde data (Global Navigation Satellite System-Radio Occultation) of is less than 200 m in the tropics (Fig. 08)(Tegtmeier et al., 2020a) further supports the 250 m uncertainty of ERA5 tropopauses (Tegtmeier et al., 2020a; Hoffmann and Spang, 2022). In the tropics, the SIC occurrence frequencies using ERA5 tropopauses with a threshold of 250 m above the tropopause is identical with the SIC occurrence frequency we found using are very similar to the SIC occurrence frequencies using the ERA-interim reanalyses and reanalysis with a threshold of 500 m above the tropopause (Zou et al., 2020). Although one would expect a

higher SIC occurrence frequency when using a smaller distance to the tropopause, the results remain ~~identical~~similar. The major reason for this finding is that the ERA5 tropopauses in the tropics are ~~in on~~ average 100 to 150 m higher than the ERA-interim tropopauses (~~Hoffmann and Spang, 2021, Fig6a, at 0 °~~) (Hoffmann and Spang, 2022, Fig. 6a, at 0 °) and hence, compensate most of the effect of a lower distance to the tropopause. At midlatitudes, however, about three times more SICs are detected in this study using ERA5 tropopauses (Fig. 1) compared to Zou et al. (2020, Fig.3) using ERA-interim tropopauses. The statistical analysis of ERA-interim and ERA5 tropopause heights shows that ~~depending on season and hemisphere,~~ the mean midlatitude tropopause in ERA5 is between 100 m lower ~~to and~~ 80 m higher than the ERA-interim tropopause (~~Hoffmann and Spang, 2021, Fig6a, at 45 °~~) (depending on season and hemisphere (Hoffmann and Spang, 2022, Fig. 6a, at 45 °)). Hence, the ERA5 tropopause at midlatitudes remains ~~the approximately same, lowering of~~ approximately the same as in ERA-Interim, and lowering the threshold distance to the tropopause results in more cloud detections, as one would expect.

4.2 Deep convection frequency uncertainties

~~Clouds are labeled as deep convection if the cloud top brightness temperature is close to the tropopause temperature with an offset of 7 K from the. As for the possible impacts of gravity waves and deep convection on the tropopause temperature. The temperature threshold plays an important role in defining deep convection (Zou et al., 2021). A high threshold will include more tropospheric clouds, and a low threshold may miss some deep overshooting. Even though the numbers of deep convection detection may vary slightly, the global pattern of deep convection is robust across different temperature thresholds.~~ Hoffmann and Spang (2022) found much more pronounced effects of gravity waves on the variability of tropopause heights and temperatures for ERA5 than ERA-Interim. However, convection-associated tropopause uplifts are not commonly represented, even in ERA5, due to the limited horizontal resolution of the reanalyses data sets. Since we used the same tropopause data set as Hoffmann and Spang (2022), tropopause uncertainties related to unresolved deep convection would exist in our study.

~~The occurrence frequency of deep convection is usually defined as the coverage of~~

4.2 UTLS clouds and SICs uncertainties

~~UTLS clouds observed in AIRS are used here as a proxy for deep convection in a region, which is the ratio of deep convection detections to total observations. However, limitations of occurrence frequency will stick out when we investigate its relation with the occurrence of SICs since the intensity, spatial extent and duration of deep convection are important features affecting the occurrence of SICs. Therefore, event frequency is proposed the tropics. At midlatitudes they represent high altitude clouds from mesoscale convective and storm sources when the cloud top brightness temperatures are close to the tropopause temperature with an offset of 7 K. Event frequency is used in this work to investigate their relations, which is defined as the number of days with deep convection/SIC detection to the total number of days in a specific time period and grid box.~~

~~The event frequency can effectively demonstrate the relations of SICs and deep convection demonstrate the relationships between SICs and UTLS clouds, which can help eliminate the morphological effects of UTLS clouds. Even though there are large quantitative differences are observed between event frequency and the occurrence frequency of deep convection UTLS clouds, the global patterns of event frequency and occurrence frequency are matched comparable (Fig. 5 and Fig. B1). The~~

event frequencies are ~~larger~~ greater than 40 % over ~~Northern~~ the northern Pacific in DJF, ~~and~~ over Central America, the Great Plains, Maritime continent in JJA, but the occurrence frequencies are only about 3 %. ~~Event frequency can get rid of~~ The event frequency can reduce the effects of the intensity, spatial extent and duration of ~~deep convection~~ UTLS clouds. For example, ~~signals of occurrence frequency~~ the occurrence frequencies (Fig. B1) over the tropics are much weaker than ~~that in event frequency~~ the event frequencies (Fig. 5). It means ~~deep convection over tropics happens as frequent as in midlatitudes on time scale~~ UTLS clouds at midlatitudes occur as frequently as over the tropics, but the spatial extents are smaller and the intensities are ~~stronger~~ weaker than in the tropics ~~than in midlatitudes~~.

As the lifetime of tropical tropopause layer (TTL) cirrus may be as long as 12-24 h (Jensen et al., 2011), we also analyzed the correlation with UTLS clouds observed by AIRS measurements 12 hours (-12 h LTD) and 24 hours (-24 h LTD) before the SIC detection (Appendix. C). The left column of Fig. C1 shows fractions of SICs related to UTLS clouds, which are detected at 0 LTD and -12 h LTD (UTLS clouds at -12 h \cup 0 h LTD) to SICs, and the right column (Fig. C1) are fractions of SICs related to UTLS clouds detected at 0 LTD, -12 h LTD and -24 h LTD (UTLS clouds at -24 h \cup -12 h \cup 0 LTD) in different seasons. We find that fractions of SICs related to UTLS clouds generally increase by 10 % when another 12 h time period is included. More SIC occurrences can be traced back to UTLS clouds if the lifetime of SICs is taken into account. However, the higher fractions could be simply be produced by only involving more time steps and data. Further analysis would require knowledge on the lifetime of SICs.

The sampling time of CALIOP may have an impact on the results presented here. While the diurnal cycle of high altitude reaching convection is well known (Hendon and Woodberry, 1993; Tian et al., 2006; Hohenegger and Stevens, 2013), little is known about the lifetime and diurnal cycle of SICs (Dauhut et al., 2020). At midlatitudes, over the central United States, the largest average fraction of overshoots was observed during the late afternoon to early evening local time (Cooney et al., 2018) (Solomon et al., 2016), whereas CALIOP samples this area during the local minimum. In the tropics, the maximum precipitation from large mesoscale convective systems occurred in the local afternoon over land (Nesbitt and Zipser, 2003), but CALIPSO passes by the tropics after midnight (around 01:30 LT). Stratospheric clouds in the tropics have two peaks at 19:00–20:00 LT and the 00:00–01:00 LT from Cloud-Aerosol Transport System (CATS) lidar measurements. The expansion of convective clouds, the spread of winds, and the propagation of convective-generated gravity waves can all play a role in the high percentages of stratospheric clouds observed later (Dauhut et al., 2020). Since only measurements at 01:30 LT were used in this study, it is important to keep in mind the possible limitations associated with the diurnal cycles of deep convection and SICs.

4.3 Stratospheric aerosols and SICs uncertainties

Stratospheric aerosols (dust, contaminated dust and volcanic ash) were extracted from CALIPSO measurements to investigate their correlation with SICs. High correlation coefficients of SICs and SAs (Fig. 10 d) and some high SIC frequencies co-occurring immediately with or with 1-2 month lag after large volcanic eruptions or wildfires (Fig. 12 and Fig. 8) indicate potential effects of volcanic aerosol and biomass burning on the observation of SICs with CALIPSO.

800 Despite the recent ~~improvement in the improvements in~~ CALIOP aerosol and cloud discrimination (Liu et al., 2019), we investigated potential aerosol cloud misclassifications further by comparing the SIC anomalies of CALIOP and ~~MIPAS measurements in the overlapping measurement period between~~ Michelson Interferometer for Passive Atmospheric Sounding (MIPAS) measurements from January 2007 ~~and to~~ April 2012 (Fig. 13). As MIPAS is an ~~IR-infrared~~ limb emission instrument and its algorithm for classification between ice, volcanic ash, and sulfate aerosol is entirely different to CALIPSO, as it relies
805 on spectral signatures (Griessbach et al., 2014, 2016), we assumed that it does not necessarily show the same anomalies. ~~In the southern hemisphere~~ At SH midlatitudes one (June 2011, $40^{\circ} - 65^{\circ}$ S) out of two positive SIC anomalies between 2007 and 2012 in the CALIOP data coincides with the volcanic plume after the eruption of Puyehue-Cordón Caulle in June 2011. In the MIPAS data, this anomaly is not visible. The eruption of Puyehue-Cordón Caulle is known to have injected significant amounts of volcanic ash (Klüser et al., 2013; Hoffmann et al., 2014a). Moreover, Klüser et al. (2013) show that "the ash plume
810 is transported very close to and potentially partly within or beneath ice clouds". In such a case the CALIOP "cloud fringe amelioration" algorithm might rather classify these detections as ice clouds instead of aerosol (Liu et al., 2019). Moreover, Liu et al. (2019) point out that the aerosol cloud classification for this volcanic plume was particularly challenging due to the dense and depolarizing aerosol.

~~In the northern hemisphere~~ At NH midlatitudes also one significant positive SIC anomaly (August to October 2008, $45^{\circ} -$
815 ~~80~~60 $^{\circ}$ N) in the CALIOP data coincides with the volcanic plume after the eruption of Kasatochi in June 2008. In ~~the~~ MIPAS, this anomaly is not visible, but starting from November 2008 a positive anomaly is visible. The Kasatochi eruption is known to have mainly injected SO_2 (1.21 Tg) and some ash (0.31 Tg) (e.g. Prata et al., 2010). However, the volcanic aerosol plume following the eruption of the Sarychev volcano in June 2009, which injected somewhat less SO_2 (1 Tg) (Clarisse et al., 2012) and a slightly smaller fraction of ash (Andersson et al., 2013), does not coincide with a positive SIC anomaly. The major
820 difference between both plumes is that the Kasatochi plume was distributed around the tropopause at altitudes between 9.1 - 13.7 km (Corradini et al., 2010), whereas the Sarychev plume was distributed over a larger altitude range and reached higher into the stratosphere with plume heights between 8.5 and 17.5 km (e.g. Doeringer et al., 2012). Especially the higher plume height makes it less likely to be interpreted as an ice cloud in the lowermost stratosphere.

In the tropics, the two strongest anomalies for CALIOP are correlated with the volcanic eruptions of Merapi in Novem-
825 ber 2010 (November 2010 to January 2011, SH tropics) and Nabro in June 2011 (May to July 2011, NH tropics) (Fig. 12 and Fig. 13). In both cases the MIPAS data also shows a positive, but weaker, anomaly. ~~Although~~ As volcanic aerosol is known to induce ice cloud formation and although the MIPAS data is more noisy and also shows some (not discussed) significant anomalies, which are not present in the CALIOP data, we consider the ~~positive event-related anomalies rather a misclassification analysis of positive correlations between SICs and aerosol requires a more in-depths investigation to separate~~
830 causal correlations from potential misclassifications in CALIPSO data.

4.4 ~~Correlations of SICs with related factors~~

~~Tropopause temperature, deep convection, stratospheric aerosol and gravity waves are important factors related to the occurrence of SICs over different regions. For example, the correlation coefficients between SIC and deep convection frequencies are up~~

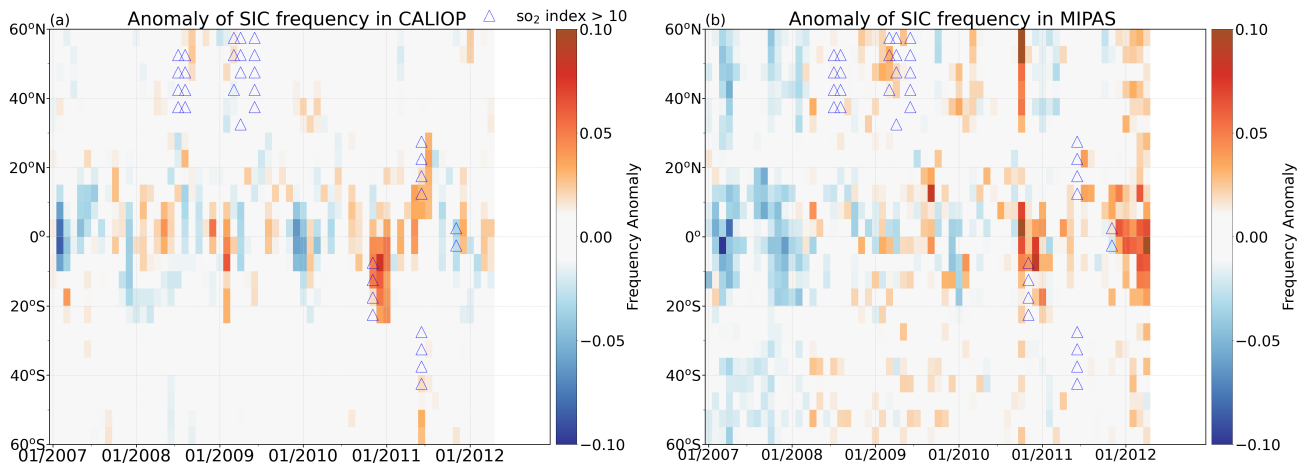


Figure 13. Monthly anomalies of SIC frequencies from CALIOP (a) and MIPAS (b) measurements. Blue triangles are data with SI > 10 K derived from AIRS observations.

to 0.92 over the Asian Monsoon and 0.89 over the North American Monsoon; correlation coefficients of SIC frequency and tropopause temperature are -0.78 and -0.67 over southern South Africa and the Indo-Pacific Warm Pool (Table ??). Long-term fluctuations of all parameters presented in Fig. ?? Fig. ?? greatly reveal their relations. However, correlation coefficients may be affected by linear trends of factors. Long-term trends for all parameters were calculated (Table ??) and detrending was processed for all phenomena. Re-calculated correlation coefficients after detrending are shown in Table ?. Detrended data was calculated as the difference between the observed data and predicted values from a regression model. A general decrease in tropopause temperature in all regions is in line with decreasing trend of tropical tropopause temperature reported by Randel et al. (2006) and Tegtmeier et al. (2020a). In contrast, a general increase in stratospheric aerosol frequencies is observed in all regions. After detrending, correlation coefficients of SIC with other factors changed slightly, but the correlation coefficients with SA frequencies generally increased. Correlation coefficients are up to 0.73 ± 0.05 , 0.79 ± 0.05 and 0.82 ± 0.05 over IPWP, TSA and EA, respectively, suggesting an enhanced correlation between stratospheric aerosol and the occurrence of SICs –

Slopes of monthly SIC frequency (pp/year), 1st-TPT (K/year), event frequencies of SICs (pp/year) and deep convection (eSICs, eDC) (pp/year), SAs (pp/year), GW ($0.01^{\circ}\text{K}^2/\text{year}$), QBO 70hPa (m/s/year), Niño3.4 SST (K/year) during 2007-2019 Regions SICs 1st-TPT eSICs eDC SAs GW QBO 70hPa Niño3.4 SST IPWP (15°S - 15°N) In this study, we conducted relationship analyses between stratospheric ice clouds and lapse rate tropopause temperature, UTLS clouds, gravity waves, 90°E - 180°E)

850 -0.21 -0.21 -0.07 -0.02 0.03^{**} 0.00 -0.08 0.09 TSA (20°S - 10°N , 40°W - 100°W) -0.32^{*} -0.19 -0.17 -0.04 0.04^{**} -0.01 EA (15°S - 15°N , 10°W - 40°E) -0.22 -0.23 -0.10 -0.09 0.03^{**} -0.01 AM (5°N - 35°N , 50°E - 120°E) -0.08 -0.24 -0.10 -0.04 0.00 0.00 NAM (0° - 30°N , 60°W - 120°W) -0.11 -0.17 -0.03 0.11 0.01^{**} 0.00 SSA (30°S - 60°S , 10°W - 80°W) 0.05 -0.31 0.07 -0.07 0.04^{**} 0.15 NA (40°N - 75°N , 50°W - 30°E) -0.08 -0.28 -0.09 0.03 0.00 0.09 and stratospheric aerosols based on 13 years (2007-2019) of satellite observations by CALIPSO and AIRS together with tropopause data from the ERA5 reanalyses.

855 Correlation coefficients and standard deviations after detrending Regions 1st-TPT eDC SAs GW QBO 70hPa Niño3.4 SST IPWP (SICs are mainly detected over the tropical continents. Spatial and temporal variations of SICs from 2007 to 2019 indicate that SICs in the tropics follow the ITCZ over time. Monthly time series in Fig. 2 show inter-annual variability of SICs at different latitudes, for example, pronounced high SICs at 15°S - 15°S - 5°N , 90°E - 180°E) -0.58 ± 0.05 -0.43 ± 0.07 0.73 ± 0.05 0.36 ± 0.09 -0.22 ± 0.06 -0.47 ± 0.06 TSA (N in November 2010 to January 2011, 20°S - 10°S - 40°N , 40°W - 100°W)

860 -0.74 ± 0.04 0.20 ± 0.09 0.79 ± 0.05 0.44 ± 0.06 -0.05 ± 0.09 -0.14 ± 0.08 EA (15°S - 15°N , 10°W - 40°E) -0.66 ± 0.05 0.23 ± 0.08 0.82 ± 0.05 0.04 ± 0.08 -0.08 ± 0.08 -0.10 ± 0.08 AM (5°N - 35°N , 50°E - 120°E) -0.56 ± 0.06 0.92 ± 0.01 0.57 ± 0.05 0.71 ± 0.04 -0.06 ± 0.07 -0.10 ± 0.07 NAM (0° - 30°N , 60°W - 120°W) 0.17 ± 0.09 0.89 ± 0.02 0.67 ± 0.07 0.52 ± 0.05 -0.01 ± 0.07 0.04 ± 0.08 SSA (30°S - 60°S , 10°W - 80°W) -0.72 ± 0.04 0.63 ± 0.05 -0.19 ± 0.08 0.71 ± 0.03 0.04 ± 0.08 0.07 ± 0.07 NA (40°N - 75°N , 50°W - 30°E)

865 -0.79 ± 0.04 0.61 ± 0.05 0.01 ± 0.08 0.64 ± 0.05 0.06 ± 0.08 -0.05 ± 0.09 S in May 2015 and low SIC frequencies over the tropics in 2015-2016. The highest frequencies of SICs at midlatitudes are more often observed in local winters.

Stratospheric ice clouds (SICs) have an important impact on the water vapor balance and radiative budget in the UTLS, but knowledge of their formation and variation is still limited. In this study, we analyzed 13 years (2007-2019) of satellite observations by CALIPSO and AIRS together with data from ERA5 reanalyses to investigate the long-term variability of SICs and potential effects of Several processes and parameters, i.e., double tropopauses, tropopause temperature, deep convection UTLS

870 clouds, gravity waves, and stratospheric aerosol on the occurrence of SICs.

A SIC is defined as an ice cloud with a cloud top height 0.25 km above the first thermal tropopause derived from ERA5 temperatures in this study. In agreement with results in Pan and Munchak (2011) and Zou et al. (2020), SICs are mainly detected over tropical continents and more SICs are observed in local winter in both hemispheres. The and stratospheric aerosols are investigated individually with respect to the occurrence of SICs between the first and second thermal tropopause suggests a

875 vertical instability of the UTLS, in the tropics and at midlatitudes. We found that SICs associated with the double tropopauses are mostly located at midlatitudes (between 25° - 60°) in winter time. Nearly During local winter and autumn, nearly 80-100 % of the SICs associated with double tropopauses are observed around 30°N /S during local winter and autumn, which is, which

are closely related to the polar-ward poleward isentropic transport and mixing of water vapor in the lowermost stratosphere (Randel et al., 2007; Peevey et al., 2012).

880 Monthly 5° latitudinal band mean SIC occurrence frequencies from 2007 to 2019 were analyzed to present the seasonal cycle and inter-annual variability of SICs. Lower tropopause temperatures are usually co-located with a higher frequency of SICs. A generally inverse correlation between tropopause temperature and SIC occurrence frequency is detected on the global scale (Fig. 10 a), especially in the tropics, where the largest negative coefficient is < -0.8 over tropical South America, equatorial Africa and northern Australia.

885 Hotspots of deep convection and gravity waves are similarly located (Randel et al., 2007; Peevey et al., 2012; Spang et al., 2015). SIC occurrences are inversely correlated with tropopause temperatures; the coldest LRT1 coincides with the highest frequencies of SICs over the tropical continents. Patterns of high frequencies of UTLS clouds, gravity waves and stratospheric aerosols all have high consistency with the SICs over the tropical continents, western and the northern Pacific, North America (Great Plains), northern Atlantic, Central America, Argentina and southern Brazil. Gravity waves have stronger signals at mid- and
890 high latitudes in local winter. The same patterns were found for the correlation between SICs and deep convection, SICs central North America, and gravity waves (Fig. 10 b, c). Positive high correlations (> 0.8) are found in Central America, tropical South America, southern Asian, maritime continent and northern Australia, southern Africa and Madagascar. However, the high correlation between deep convection southern South America in different seasons.

We found that over the tropical continents, the highest correlation coefficients of SICs are with tropopause temperature.
895 UTLS clouds have the highest correlations with SICs in the monsoon domains and over the central United States. At midlatitudes, in the latitude range between 45° and 60°, especially over Patagonia and the Drake Passage, tropopause temperature and gravity waves themselves (Hoffmann et al., 2013) leads to an overlap of their effects on SIC occurrence have the highest correlation with the occurrence of SICs. However, the second-highest correlation coefficients of SICs are mixed with all other processes. The overlapping high correlation coefficients and relatively close correlation coefficients ($0.6 < \text{absolute } r < 0.8$ or $0.8 < \text{absolute } r < 1.0$) of SICs with all processes indicate strong associations between the tropopause temperature, UTLS clouds,
900 gravity waves, and stratospheric aerosols (Gettelman et al., 2002; Bourassa et al., 2012; Hoffmann et al., 2013; Dinh et al., 2016), which increases the challenge of separating their effects on the occurrence of SICs. Therefore, the fractions of the SICs related to deep convection (Fig. 6) were calculated to quantify the impact of deep convection as much as possible. Our results show that more than half of the SICs are related to deep convection over the northern Pacific, maritime continent, Mediterranean and
905 Black Sea, Argentina and southern Brazil in DJF. In JJA, up to 80 % SICs are related to deep convection over the Great Plains and Central America.

The global relation between SICs and stratospheric aerosol was also analyzed as the coincidence of high SIC frequencies and volcanic eruptions and wildfires were detected in some cases (Fig. 8). Worldwide positive correlations between SICs and SAs are observed in this work. High correlation coefficients (> 0.6) are mostly detected over southern Asian, northern Australia,
910 southern Africa and Madagascar, the central Pacific Ocean and Central America. However, this positive correlation might be affected by the misclassification of aerosol and ice in CALIPSO (Reverdy et al., 2012).

Above we presented high correlation of SIC occurrence frequency with double tropauses, tropopause temperature, deep convection, gravity waves and stratospheric aerosol on a global scale. However, inherent correlations of the above listed factors Monthly anomaly analyses of SICs and all processes for 5° latitude bands reveal more explicit influences of processes on the occurrence and variability of SICs at various latitude bands and points in time. The anomalous SICs are mostly in line with the tropopause temperature. Volcanic eruptions that produce high stratospheric aerosol loads can largely influence the scale- and time- limited high SIC frequencies, such as high correlation between deep convection and gravity waves (Hoffmann et al., 2013), variation of temperature excited by deep convection and gravity waves (Gettelman et al., 2002) and sudden increase of stratospheric aerosol transported by vertical upwelling and wave propagation, make it difficult to clarify their impacts on SIC occurrence. Small regions were selected to specify the impacts of different factors. Results show that tropopause temperature and stratospheric aerosol show the highest correlation with the high frequency of SICs over the Indo-Pacific Warm Pool, tropical South America and equatorial Africa. Deep convection and some strong volcanoes like Merapi, Nabro and Puyehue-Cordón Caulle in 2011, Calbuco in 2015 and Raikoke in 2019. The possible misclassification of clouds and aerosols by CALIOP should be noted. The contributions of UTLS clouds and gravity waves are highly correlated with the occurrence of SICs in the Asian Monsoon and the North American Monsoon region. Gravity waves and tropopause temperature have high correlation coefficients with SIC occurrence frequency in southern South America and the northern Atlantic, also observed, i.e., in 40° N in January-March 2011 and from December 2012 to January 2013.

Based on satellite observations from CALIPSO and AIRS, we investigated the global distribution and long-term variability. We investigated the distribution and time series of stratospheric ice clouds and assessed its relations their relationships with tropopause temperature, deep convection UTLS clouds, gravity waves and stratospheric aerosol. Generally, positive correlations are observed between SICs and deep convection, gravity waves, stratospheric aerosol, and inverse correlations are detected between SICs and tropopause temperature aerosols. All processes have high correlations with the occurrence and variability of SICs. However, the specific role of different factors varies over regions high inherent correlations of all processes make it difficult to disentangle their contributions. The occurrence and variability of SICs show a substantial spatial and temporal dependency on different processes. To further explore the formation mechanisms and precisely elucidate the origin of SICs, specific regional analyses, Lagrangian modelling and microphysical simulations are required in future studies.

Data availability. Convection and gravity wave data from AIRS used in this study are available at <https://www.re3data.org/repository/r3d100012430> (last access: 3 December 2020) (Hoffmann, 2020). ERA5 tropopause data are available at <https://www.re3data.org/repository/r3d100013201> (last access: 25 November 2021) (Hoffmann, 2021a). The AIRS volcanic data are available at <https://datapub.fz-juelich.de/slcs/airs/volcanoes> (last access: 01 July 2021) (Hoffmann, 2021b). Monthly mean zonal wind over Singapore are obtained from <https://www.geo.fu-berlin.de/en/met/ag/strat/produkte/qbo/index.html> and SST data are obtained from <https://www.ncdc.noaa.gov/teleconnections/enso/indicators/sst/>. Cirrus cloud top heights from CALIPSO are available upon request from the contact author, Ling Zou (l.zou@fz-juelich.de; cheryl_zou@whu.edu.cn).

Appendix A: Event frequency of SICs

945 Figure. A1 shows the seasonal event frequencies of SICs, which is the ratio of number of days in which SICs (≥ 1 detection) occur to the total number of days in a given time period. Global features are similar to occurrence frequencies in Fig. 1 ~~that~~ hotspots. Hotspots of SICs are located ~~in-over the~~ tropical continents. However, event frequencies are lower than occurrence frequencies in the tropics but higher than occurrence frequencies ~~in-at~~ midlatitudes. High latitudes will not be discussed here in detail as high frequencies ~~over there~~ may relate to the occurrence of PSCs. From Fig. A1 and Fig. 1, we can find that

950 SICs are more ~~often~~ frequently detected over tropics than ~~in-midlatitudes on time-scale~~ at midlatitudes and the horizontal extent of SICs over tropics is much wider than that ~~in-at~~ midlatitudes.

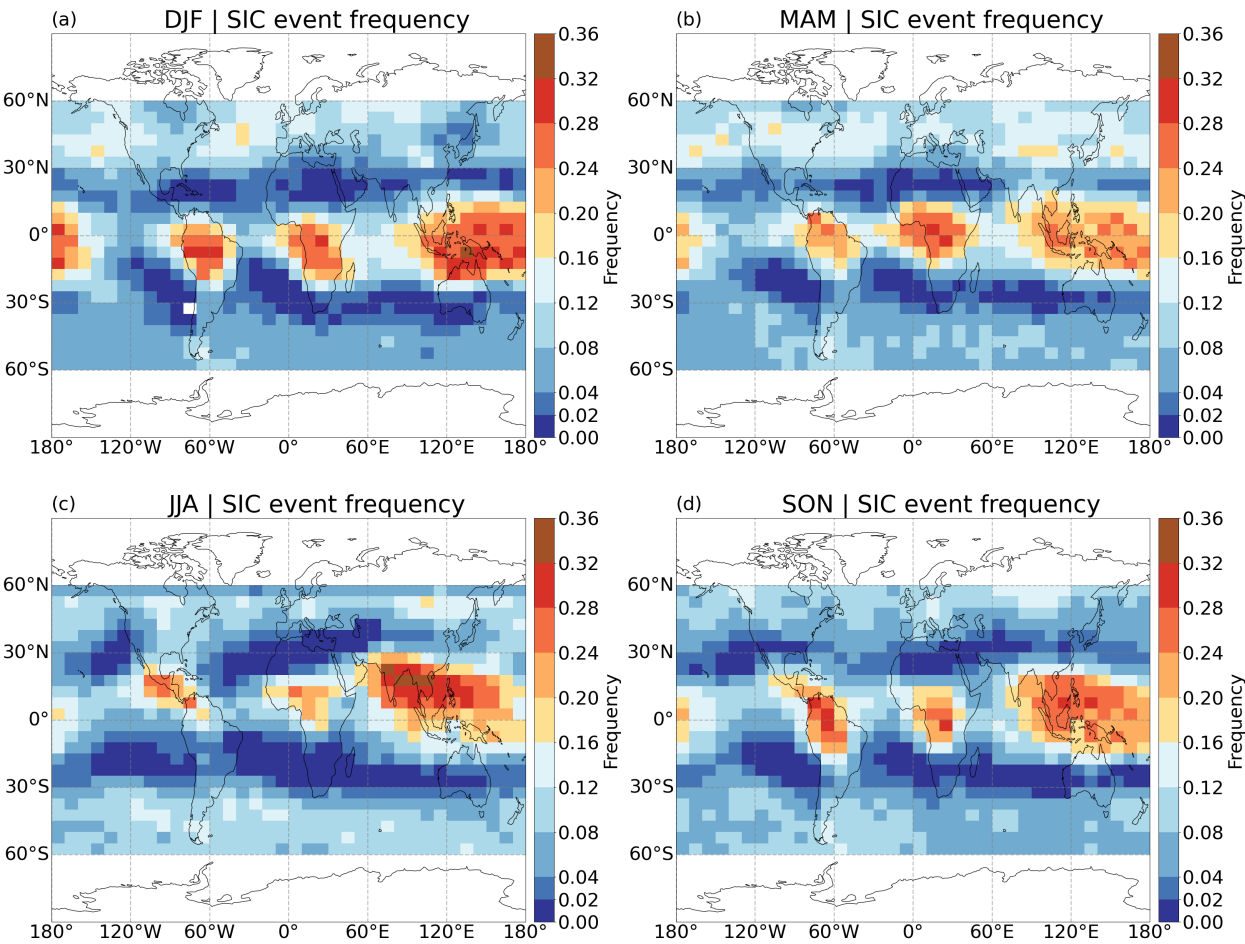


Figure A1. Event frequencies of SICs on a $5^{\circ} \times 10^{\circ}$ (latitude \times longitude) grid box from CALIPSO measurements during 2007-2019.

Appendix B: Occurrence frequency of ~~deep convection~~UTLS clouds

Occurrence frequency of ~~deep convection~~UTLS clouds in AIRS are presented in Fig. B1. In DJF, high frequencies of ~~deep convection are found in~~UTLS clouds are found over the northern Pacific, Alaska, western Canada, ~~the~~ northern Atlantic close to the United States, eastern and western ~~sided of~~side of the Tibetan plateau, Argentina and southern Brazil, northern Australia, ~~Mediterranean and black sea~~the Mediterranean and the Black Sea region. In JJA, hotspots of ~~deep convection are located at~~UTLS clouds are located over central North America (Great Plains), Central America, central Africa, southern Asia~~and~~, and ~~the~~ Western Pacific Ocean, ~~southern Brazil and latitudinal band in over southern Brazil, and the latitudinal band at~~ 30°S-45°S. MAM and SON are intermediate seasons which have similar regions of high ~~deep convection~~UTLS cloud frequency as DJF and JJA. The seasonal patterns and ~~values of deep convection amgnitudes of~~UTLS cloud frequency are overall similar to ~~the~~ results shown in Hoffmann et al. (2013). Similar patterns can be found both in event frequency and occurrence frequency of ~~deep convection~~UTLS clouds, but signals in Fig. 5 are much stronger than that in Fig. B1, ~~which indicates that high frequencies of deep convection on time scale but relatively small spatial extent of it on coverage.~~

Appendix C: Fraction of SICs related to ~~deep convection~~UTLS clouds

Considering possible effects of ~~deep convection occurred before detection of~~SICs, ~~deep convection~~UTLS clouds that occurred before the detection time of the SICs, we analyzed UTLS clouds from AIRS observations ~~detected at~~-12 hours (-12h LTD) and 24 hours (-24h LTD) before ~~are analyzed the~~ SIC detections in Fig. C1. Left column shows fractions of SICs related to ~~deep convection~~UTLS clouds, which are detected at 0 LTD and ~~-12h LTD (DC at -12h -12 h LTD (UTLS clouds at -12 h \cup 0h 0 h LTD)~~ to SICs, and right column (Fig. C1) are fractions of SICs related to ~~deep convection~~UTLS clouds detected at both 0 LTD, ~~-12h LTD and -24h LTD (DC at -24h -12 h LTD and -24 h LTD (UTLS clouds at -24 h \cup -12h -12 h \cup 0 LTD)~~ in difference seasons. By comparing ~~the~~ results in Fig. 6 and Fig. C1, we find that about 10 % more SICs are related to the ~~deep convection when one more time detection~~UTLS clouds when aother 12 h time period is included. It ~~means more SIC occurrence is found that more SIC occurrences~~ can be traced back to ~~deep convection if the lifetime of SICs would be considered.~~UTLS clouds if the longer lifetimes of SICs are considered. However, the higher fractions could also be produced by only involving more time steps and data in the analysis.

Appendix D: ~~Other four regions~~The regional averaged monthly anomalies.

Over tropical South America, strong correlations of SIC frequencies are found with the tropopause temperature and SAs (~~Anomalies for regional means over the tropics (20° S-20° N), northern midlatitudes (40° N-60° N) and southern midlatitudes (40° S-60° S) are shown in lines in Fig. ??~~). High SIC frequencies in 2008-2011 are co-located with cold tropopause temperature, positive SA frequency anomalies and high brightness temperature variances. However, the relation of SICs and deep convection is low with the correlation coefficient only of 0.18 ± 0.09 .

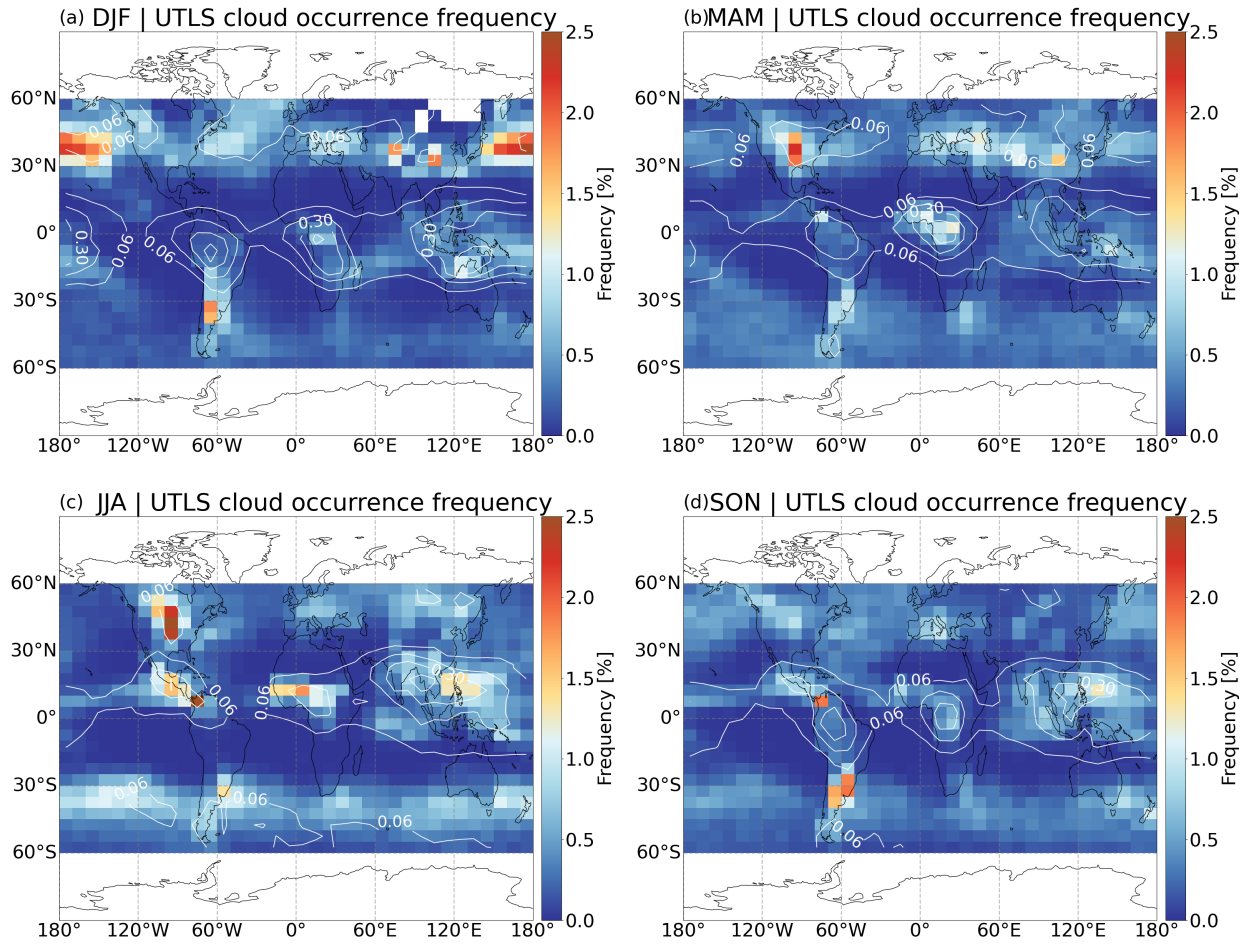


Figure B1. Seasonal mean occurrence frequency of ~~deep-convection~~-UTLS clouds derived from AIRS measurements during 2007-2019.

Over equatorial Africa, the strongest correlation of SIC frequencies is detected with the tropopause temperature with a correlation coefficient of -0.71 ± 0.05 (Fig. ??). The correlation coefficient between SIC frequencies and SA frequencies is also high, and we can find an increasing trend of SA frequencies from 2007 to 2019. The increased stratospheric aerosols in 2011, 2012, 2013, D1, which are differences between the monthly mean and all year mean values. Seasonal cycles of parameters are included in the linear anomalies over three latitude bands. For the linear mean anomalies, SICs, LRT1-T, UTLS clouds, and gravity waves show seasonal cycles in the tropics and at midlatitudes. In the tropics and at NH midlatitudes, high SIC frequencies are detected during the boreal winter and low frequencies are seen during the boreal summer, in contrast to the situation at SH midlatitudes. Seasonal cycles of SIC frequencies are generally consistent with UTLS clouds and gravity waves but opposite to tropopause temperatures. No obvious seasonal cycles can be found in stratospheric aerosols over all regions. However, the regional mean abnormal high SAs influence the variability of SICs, i.e., September 2008 and August 2017 in NH midlatitudes, April 2018 and January 2019 are consistent with the high SIC frequencies. The large amplitudes of gravity waves

Fraction of SICs related to UTLS clouds [%]

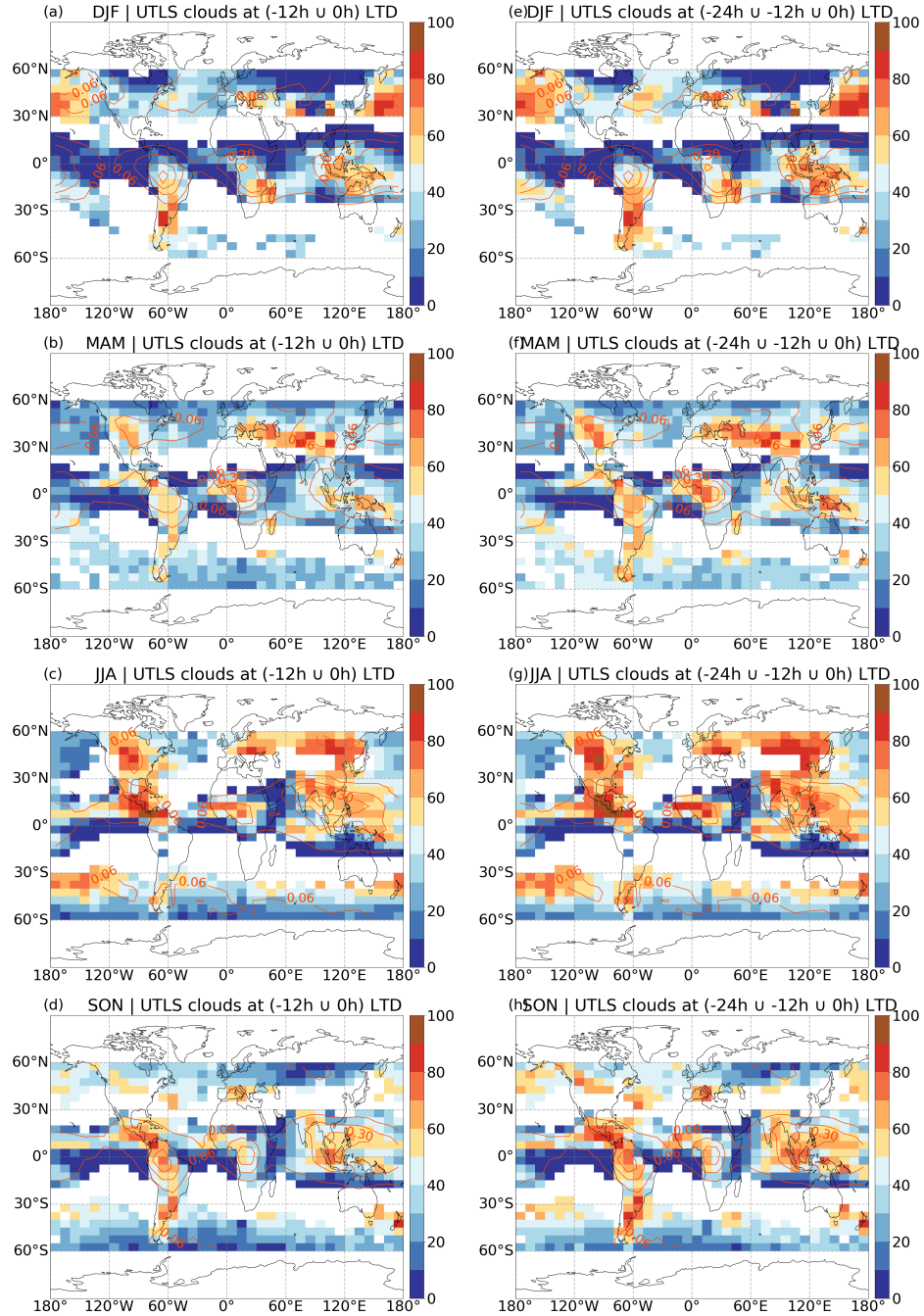


Figure C1. The fraction of SICs related to deep-convection UTLS clouds with deep-convection UTLS clouds observed by AIRS measurements at 12 hours (-12h -12 h LTD) and 24 hours (-24h -24 h LTD) before the SIC detection. The occurrence frequency of SICs are is shown in red contours with an interval of 0.12.

in 2011–2013 show high correlations with the high frequencies of SICs. Like the other two tropical regions (IPWP and TSA), event frequencies of deep convection over EA present low correlations with SIC occurrence.

995 Over the North American Monsoon region (Fig. ??), seasonal fluctuations of deep convection are highly consistent with SIC frequency with a correlation of 0.89 ± 0.02 . Gravity waves are generally in line with SIC frequencies with a correlation of 0.54 ± 0.05 . High SIC frequency from June to September 2015 is strongly dependent on stratospheric aerosols, which may be produced by a volcanic eruption (Wolf (0°) in May 2015). Deep convection is highly associated with the occurrence and variability of SICs over the North American Monsoon region.

1000 Over the North Atlantic (Fig. ??), tropopause temperature and gravity waves have the strongest correlations with the occurrence of SICs in the tropics and June 2011 at SH midlatitudes. The low tropopause temperature and high brightness temperature variance align with high SIC frequency anomalies in winter. The event frequencies of deep convection and SICs are also positively correlated over this region. The relation of SICs and SAs is relatively small, and the high SA frequencies may be due to misclassified PSCs over high latitudes.

1005 *Author contributions.* LZ, LH, SG and RS conceived the study design. LH provided the AIRS data and the ERA5 tropopause data. SG provided the MIPAS data. LZ processed the CALIPSO data and compiled all results. LZ wrote the manuscript with contributions from all authors.

Competing interests. The authors declare that they have no conflict of interest.

Acknowledgements. This work was supported by the German Research Foundation (DFG) through the AeroTrac project under the grant ID: 1010 DFG HO5102/1-1. We gratefully acknowledge the computing time granted on the supercomputers JURECA and JUWELS at Forschungszentrum Jülich. CALIPSO data are obtained from the NASA Langley Research Center Atmospheric Science Data Center. The AIRS data were distributed by the NASA Goddard Earth Sciences Data Information and Services Center. The ERA5 data were obtained from the European Centre for Medium-Range Weather Forecasts. The MIPAS data were provided by the European Space Agency.

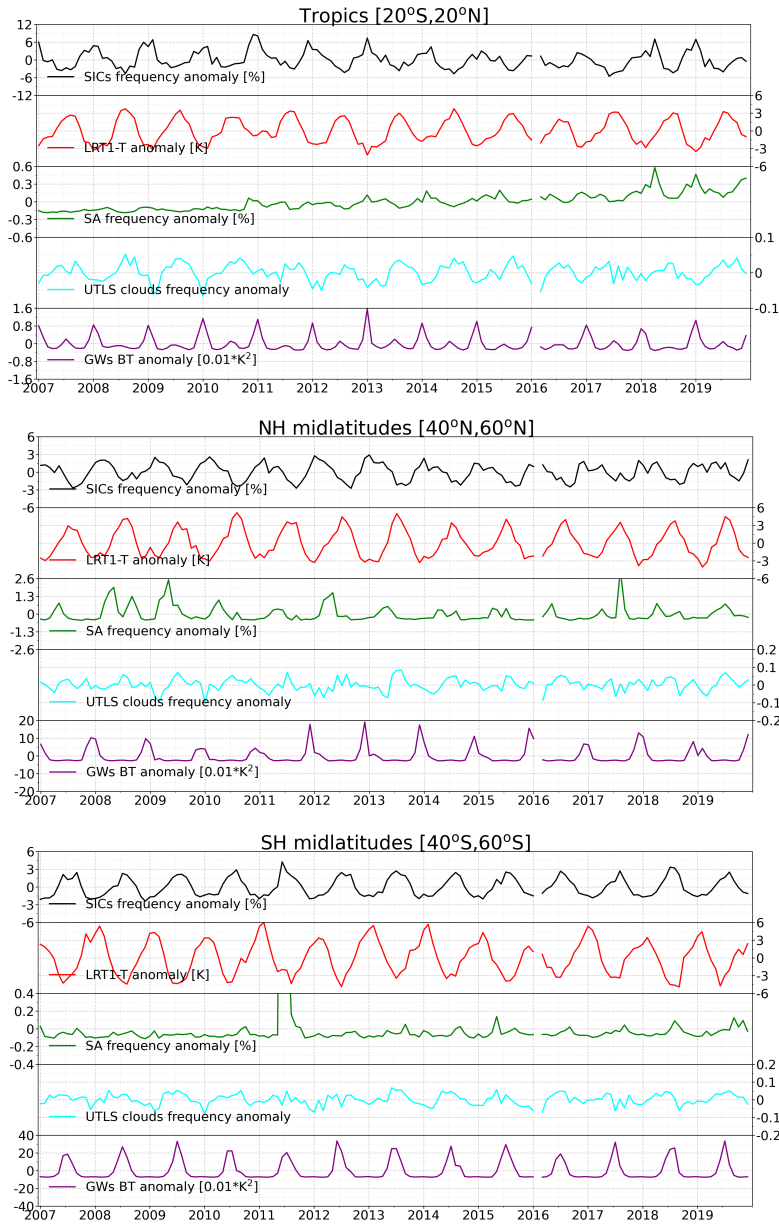


Figure D1. Monthly-Regional averaged monthly anomalies of SIC frequency, tropopause-LRT1 temperature(1st-TPT), event-frequencies of SIC and deep convection, stratospheric aerosol frequency, UTLS clouds and gravity waves from 2007 to 2019 over Tropical South America the tropics (20° S-10S-20° N), northern midlatitudes (40° W-100N-60° W) , from 2007 to 2019 and southern midlatitudes (40° S-60° S).

Monthly anomalies of SIC frequency, tropopause temperature(1st-TPT), event-frequencies of SIC and deep convection, stratospheric aerosol frequency, and gravity waves over equatorial Africa (15° S-15° N, 10° W-40° E), from 2007 to 2019.

Monthly anomalies of SIC frequency, tropopause temperature(1st-TPT), event-frequencies of SIC and deep convection, stratospheric aerosol frequency, and gravity waves over North American Monsoon (0° -30° N, 60° W-120° W), from 2007 to 2019.

Monthly anomalies of SIC frequency, tropopause temperature(1st-TPT), event-frequencies of SIC and deep convection, stratospheric aerosol frequency, and gravity waves over North Atlantic (40° N-75° N, 50° W-30° E), from 2007 to 2019.

References

- 1015 Abhik, S., Hendon, H. H., and Wheeler, M. C.: On the Sensitivity of Convectively Coupled Equatorial Waves to the Quasi-Biennial Oscillation, *Journal of Climate*, 32, 5833 – 5847, <https://doi.org/10.1175/JCLI-D-19-0010.1>, 2019.
- Andersson, S. M., Martinsson, B. G., Friberg, J., Brenninkmeijer, C. A. M., Rauthe-Schöch, A., Hermann, M., van Velthoven, P. F. J., and Zahn, A.: Composition and evolution of volcanic aerosol from eruptions of Kasatochi, Sarychev and Eyjafjallajökull in 2008–2010 based on CARIBIC observations, *Atmospheric Chemistry and Physics*, 13, 1781–1796, <https://doi.org/10.5194/acp-13-1781-2013>, 2013.
- 1020 Ansmann, A., Baars, H., Chudnovsky, A., Mattis, I., Veselovskii, I., Haarig, M., Seifert, P., Engelmann, R., and Wandinger, U.: Extreme levels of Canadian wildfire smoke in the stratosphere over central Europe on 21–22 August 2017, *Atmospheric Chemistry and Physics*, 18, 11 831–11 845, <https://doi.org/10.5194/acp-18-11831-2018>, 2018.
- Aumann, H. H., Gregorich, D., Gaiser, S., Hagan, D., Pagano, T., Strow, L., and Ting, D.: AIRS Algorithm Theoretical Basis Document Level 1B Part 1: Infrared Spectrometer, Tech. rep., NASA, 2000.
- 1025 Aumann, H. H., Chahine, M. T., Gautier, C., Goldberg, M. D., Kalnay, E., McMillin, L. M., Revercomb, H., Rosenkranz, P. W., Smith, W. L., Staelin, D. H., Strow, L. L., and Susskind, J.: AIRS/AMSU/HSB on the aqua mission: Design, science objectives, data products, and processing systems, *IEEE Transactions on Geoscience and Remote Sensing*, 41, 253–263, <https://doi.org/10.1109/TGRS.2002.808356>, 2003.
- Aumann, H. H., Gregorich, D., and De Souza-Machado, S. M.: AIRS observations of deep convective clouds, in: *Atmospheric and Environmental Remote Sensing Data Processing and Utilization II: Perspective on Calibration/Validation Initiatives and Strategies*, vol. 6301, p. 63010J, SPIE, <https://doi.org/10.1117/12.681201>, 2006.
- 1030 Aumann, H. H., DeSouza-Machado, S. G., and Behrangi, A.: Deep convective clouds at the tropopause, *Atmospheric Chemistry and Physics*, 11, 1167–1176, <https://doi.org/10.5194/acp-11-1167-2011>, <https://acp.copernicus.org/articles/11/1167/2011/>, 2011.
- Avery, M. A., Davis, S. M., Rosenlof, K. H., Ye, H., and Dessler, A. E.: Large anomalies in lower stratospheric water vapour and ice during the 2015–2016 El Niño, 10, 405–409, <https://doi.org/10.1038/ngeo2961>, 2017.
- 1035 Barahona, D., Molod, A., and Kalesse, H.: Direct estimation of the global distribution of vertical velocity within cirrus clouds, *Scientific Reports*, 7, 1–11, <https://doi.org/10.1038/s41598-017-07038-6>, 2017.
- Bartolome Garcia, I., Spang, R., Ungermann, J., Griessbach, S., Krämer, M., Höpfner, M., and Riese, M.: Observation of cirrus clouds with GLORIA during the WISE campaign: detection methods and cirrus characterization, *Atmospheric Measurement Techniques*, 14, 3153–3168, <https://doi.org/10.5194/amt-14-3153-2021>, 2021.
- 1040 Boehm, M. T. and Verlinde, J.: Stratospheric influence on upper tropospheric tropical cirrus, *Geophysical Research Letters*, 27, 3209–3212, <https://doi.org/10.1029/2000GL011678>, 2000.
- Bourassa, A. E., Robock, A., Randel, W. J., Deshler, T., Rieger, L. A., Lloyd, N. D., Llewellyn, E. J. T., and Degenstein, D. A.: Large Volcanic Aerosol Load in the Stratosphere Linked to Asian Monsoon Transport, *Science*, 337, 78–81, <https://doi.org/10.1126/science.1219371>, 2012.
- 1045 Brewer, A. W.: Evidence for a world circulation provided by the measurements of helium and water vapour distribution in the stratosphere, *Quarterly Journal of the Royal Meteorological Society*, 75, 351–363, <https://doi.org/10.1002/qj.49707532603>, 1949.
- Campbell, J. R., Welton, E. J., Krotkov, N. A., Yang, K., Stewart, S. A., and Fromm, M. D.: Likely seeding of cirrus clouds by stratospheric Kasatochi volcanic aerosol particles near a mid-latitude tropopause fold, *Atmospheric Environment*, 46, 441–448, <https://doi.org/10.1016/j.atmosenv.2011.09.027>, 2012.
- 1050

- Chae, J. H. and Sherwood, S. C.: Annual temperature cycle of the tropical tropopause: A simple model study, *Journal of Geophysical Research: Atmospheres*, 112, <https://doi.org/10.1029/2006JD007956>, 2007.
- Chahine, M. T., Pagano, T. S., Aumann, H. H., Atlas, R., Barnet, C., Blaisdell, J., Chen, L., Divakarla, M., Fetzer, E. J., Goldberg, M., Gautier, C., Granger, S., Hannon, S., Irion, F. W., Kakar, R., Kalnay, E., Lambrigtsen, B. H., Lee, S. Y., Le Marshall, J., Mcmillan, W. W.,
1055 Mcmillin, L., Olsen, E. T., Revercomb, H., Rosenkranz, P., Smith, W. L., Staelin, D., Strow, L. L., Susskind, J., Tobin, D., Wolf, W., and Zhou, L.: Improving weather forecasting and providing new data on greenhouse gases, *Bulletin of the American Meteorological Society*, 87, 911–926, <https://doi.org/10.1175/BAMS-87-7-911>, 2006.
- Chang, K.-W. and L'Ecuyer, T.: Influence of gravity wave temperature anomalies and their vertical gradients on cirrus clouds in the tropical tropopause layer – a satellite-based view, *Atmospheric Chemistry and Physics*, 20, 12 499–12 514, [https://doi.org/10.5194/acp-20-12499-](https://doi.org/10.5194/acp-20-12499-2020)
1060 2020, 2020.
- Chouza, F., Leblanc, T., Barnes, J., Brewer, M., Wang, P., and Koon, D.: Long-term (1999–2019) variability of stratospheric aerosol over Mauna Loa, Hawaii, as seen by two co-located lidars and satellite measurements, *Atmospheric Chemistry and Physics*, 20, 6821–6839, <https://doi.org/10.5194/acp-20-6821-2020>, 2020.
- Clarisse, L., Hurtmans, D., Clerbaux, C., Hadji-Lazaro, J., Ngadi, Y., and Coheur, P.-F.: Retrieval of sulphur dioxide from the infrared atmospheric sounding interferometer (IASI), *Atmospheric Measurement Techniques*, 5, 581–594, <https://doi.org/10.5194/amt-5-581-2012>,
1065 2012.
- Clodman, J.: Some statistical aspects of cirrus cloud, *Monthly Weather Review*, 85, 37–41, [https://doi.org/10.1175/1520-0493\(1957\)085<0037:SSAOCC>2.0.CO;2](https://doi.org/10.1175/1520-0493(1957)085<0037:SSAOCC>2.0.CO;2), 1957.
- Collimore, C. C., Martin, D. W., Hitchman, M. H., Huesmann, A., and Waliser, D. E.: On The Relationship between the QBO and Tropical
1070 Deep Convection, *Journal of Climate*, 16, 2552–2568, [https://doi.org/10.1175/1520-0442\(2003\)016<2552:OTRBTQ>2.0.CO;2](https://doi.org/10.1175/1520-0442(2003)016<2552:OTRBTQ>2.0.CO;2), 2003.
- Cooney, J. W., Bowman, K. P., Homeyer, C. R., and Fenske, T. M.: Ten Year Analysis of Tropopause-Overshooting Convection Using GridRad Data, *Journal of Geophysical Research: Atmospheres*, 123, 329–343, <https://doi.org/10.1002/2017JD027718>, 2018.
- Corradini, S., Merucci, L., Prata, A. J., and Piscini, A.: Volcanic ash and SO₂ in the 2008 Kasatochi eruption: Retrievals comparison from different IR satellite sensors, *Journal of Geophysical Research: Atmospheres*, 115, D00L21, <https://doi.org/10.1029/2009JD013634>, 2010.
- Corti, T., Luo, B. P., Fu, Q., Vömel, H., and Peter, T.: The impact of cirrus clouds on tropical troposphere-to-stratosphere transport, *Atmospheric Chemistry and Physics*, 6, 2539–2547, <https://doi.org/10.5194/acp-6-2539-2006>, 2006.
1075
- Cziczo, D. J., Froyd, K. D., Hoose, C., Jensen, E. J., Diao, M., Zondlo, M. A., Smith, J. B., Twohy, C. H., and Murphy, D. M.: Clarifying the Dominant Sources and Mechanisms of Cirrus Cloud Formation, *Science*, 340, 1320–1324, <https://doi.org/10.1126/science.1234145>, 2013.
- Dauhut, T., Noel, V., and Dion, I.-A.: The diurnal cycle of the clouds extending above the tropical tropopause observed by spaceborne lidar, *Atmospheric Chemistry and Physics*, 20, 3921–3929, <https://doi.org/10.5194/acp-20-3921-2020>, 2020.
1080
- de la TORRE, A., TSUDA, T., HAJJ, G., and WICKERT, J.: A Global Distribution of the Stratospheric Gravity Wave Activity from GPS Occultation Profiles with SAC-C and CHAMP, *Journal of the Meteorological Society of Japan. Ser. II*, 82, 407–417, <https://doi.org/10.2151/jmsj.2004.407>, 2004.
- De Reus, M., Borrmann, S., Bansemer, A., Heymsfield, A. J., Weigel, R., Schiller, C., Mitev, V., Frey, W., Kunkel, D., Kürten, A., Curtius, J., Sitnikov, N. M., Ulanovsky, A., and Ravegnani, F.: Evidence for ice particles in the tropical stratosphere from in-situ measurements, *Atmospheric Chemistry and Physics*, 9, 6775–6792, <https://doi.org/10.5194/acp-9-6775-2009>, 2009.
1085

- Dessler, A. E.: Clouds and water vapor in the Northern Hemisphere summertime stratosphere, *Journal of Geophysical Research: Atmospheres*, 114, <https://doi.org/10.1029/2009JD012075>, 2009.
- 1090 Dinh, T., Durran, D. R., and Ackerman, T.: Cirrus and water vapor transport in the tropical tropopause layer – Part 1: A specific case modeling study, *Atmospheric Chemistry and Physics*, 12, 9799–9815, <https://doi.org/10.5194/acp-12-9799-2012>, 2012.
- Dinh, T., Podglajen, A., Hertzog, A., Legras, B., and Plougonven, R.: Effect of gravity wave temperature fluctuations on homogeneous ice nucleation in the tropical tropopause layer, *Atmospheric Chemistry and Physics*, 16, 35–46, <https://doi.org/10.5194/acp-16-35-2016>, 2016.
- 1095 Doeringer, D., Eldering, A., Boone, C. D., González Abad, G., and Bernath, P. F.: Observation of sulfate aerosols and SO₂ from the Sarychev volcanic eruption using data from the Atmospheric Chemistry Experiment (ACE), *Journal of Geophysical Research: Atmospheres*, 117, D03 203, <https://doi.org/10.1029/2011JD016556>, 2012.
- Efron, B. and Tibshirani, R.: The Bootstrap Method for Assessing Statistical Accuracy, *Behaviormetrika*, 12, 1–35, https://doi.org/10.2333/bhmk.12.17_1, 1985.
- Eguchi, N. and Shiotani, M.: Intraseasonal variations of water vapor and cirrus clouds in the tropical upper troposphere, *Journal of Geophysical Research: Atmospheres*, 109, D12 106, <https://doi.org/10.1029/2003JD004314>, 2004.
- 1100 Eleftheratos, K., Zerefos, C. S., Zanis, P., Balis, D. S., Tselioudis, G., Gierens, K., and Sausen, R.: A study on natural and manmade global interannual fluctuations of cirrus cloud cover for the period 1984–2004, *Atmospheric Chemistry and Physics*, 7, 2631–2642, <https://doi.org/10.5194/acp-7-2631-2007>, 2007.
- Eleftheratos, K., Zerefos, C. S., Varotsos, C., and Kapsomenakis, I.: Interannual variability of cirrus clouds in the tropics in El Niño Southern Oscillation (ENSO) regions based on International Satellite Cloud Climatology Project (ISCCP) satellite data, *International Journal of Remote Sensing*, 32, 6395–6405, <https://doi.org/10.1080/01431161.2010.510491>, 2011.
- 1105 Ern, M., Hoffmann, L., and Preusse, P.: Directional gravity wave momentum fluxes in the stratosphere derived from high-resolution AIRS temperature data, *Geophysical Research Letters*, 44, 475–485, <https://doi.org/10.1002/2016GL072007>, 2017.
- Feng, P.-N. and Lin, H.: Modulation of the MJO-Related Teleconnections by the QBO, *Journal of Geophysical Research: Atmospheres*, 124, 12 022–12 033, <https://doi.org/10.1029/2019JD030878>, 2019.
- 1110 Field, P. R. and Wood, R.: Precipitation and Cloud Structure in Midlatitude Cyclones, *Journal of Climate*, 20, 233 – 254, <https://doi.org/10.1175/JCLI3998.1>, 2007.
- Friberg, J., Martinsson, B. G., Sporre, M. K., Andersson, S. M., Brenninkmeijer, C. A. M., Hermann, M., van Velthoven, P. F. J., and Zahn, A.: Influence of volcanic eruptions on midlatitude upper tropospheric aerosol and consequences for cirrus clouds, *Earth and Space Science*, 2, 285–300, <https://doi.org/10.1002/2015EA000110>, 2015.
- 1115 Froyd, K. D., Murphy, D. M., Lawson, P., Baumgardner, D., and Herman, R. L.: Aerosols that form subvisible cirrus at the tropical tropopause, *Atmospheric Chemistry and Physics*, 10, 209–218, <https://doi.org/10.5194/acp-10-209-2010>, 2010.
- Fu, R., Hu, Y., Wright, J. S., Jiang, J. H., Dickinson, R. E., Chen, M., Filipiak, M., Read, W. G., Waters, J. W., and Wu, D. L.: Short circuit of water vapor and polluted air to the global stratosphere by convective transport over the Tibetan Plateau, *Proceedings of the National Academy of Sciences*, 103, 5664–5669, <https://doi.org/10.1073/pnas.0601584103>, 2006.
- 1120 Gasparini, B., Meyer, A., Neubauer, D., Münch, S., and Lohmann, U.: Cirrus Cloud Properties as Seen by the CALIPSO Satellite and ECHAM-HAM Global Climate Model, *Journal of Climate*, 31, 1983 – 2003, <https://doi.org/10.1175/JCLI-D-16-0608.1>, 2018.
- Gettelman, A., Salby, M. L., and Sassi, F.: Distribution and influence of convection in the tropical tropopause region, *Journal of Geophysical Research: Atmospheres*, 107, D10, <https://doi.org/10.1029/2001JD001048>, 2002.

- 1125 Getzewich, B. J., Vaughan, M. A., Hunt, W. H., Avery, M. A., Powell, K. A., Tackett, J. L., Winker, D. M., Kar, J., Lee, K.-P., and Toth, T. D.: CALIPSO lidar calibration at 532 nm: version 4 daytime algorithm, *Atmospheric Measurement Techniques*, 11, 6309–6326, <https://doi.org/10.5194/amt-11-6309-2018>, 2018.
Global Volcanism Program: Volcanoes of the World, v. 4.10.0 (14 May 2021)., <https://doi.org/10.5479/si.GVP.VOTW4-2013>, last accessed: 2021-06-25, 2013.
- 1130 Griessbach, S., Hoffmann, L., Spang, R., and Riese, M.: Volcanic ash detection with infrared limb sounding: MIPAS observations and radiative transfer simulations, *Atmospheric Measurement Techniques*, 7, 1487–1507, <https://doi.org/10.5194/amt-7-1487-2014>, 2014.
Griessbach, S., Hoffmann, L., Spang, R., Von Hobe, M., Müller, R., and Riese, M.: Infrared limb emission measurements of aerosol in the troposphere and stratosphere, *Atmospheric Measurement Techniques*, 9, 4399–4423, <https://doi.org/10.5194/amt-9-4399-2016>, 2016.
Haag, W. and Kärcher, B.: The impact of aerosols and gravity waves on cirrus clouds at midlatitudes, *Journal of Geophysical Research: Atmospheres*, 109, D12 202, <https://doi.org/10.1029/2004JD004579>, 2004.
- 1135 Hendon, H. H. and Woodberry, K.: The diurnal cycle of tropical convection, *Journal of Geophysical Research: Atmospheres*, 98, 16 623–16 637, <https://doi.org/10.1029/93JD00525>, 1993.
Hersbach, H., Bell, B., Berrisford, P., Hirahara, S., Horányi, A., Muñoz-Sabater, J., Nicolas, J., Peubey, C., Radu, R., Schepers, D., Simmons, A., Soci, C., Abdalla, S., Abellan, X., Balsamo, G., Bechtold, P., Biavati, G., Bidlot, J., Bonavita, M., De Chiara, G., Dahlgren, P., Dee, D., Diamantakis, M., Dragani, R., Flemming, J., Forbes, R., Fuentes, M., Geer, A., Haimberger, L., Healy, S., Hogan, R. J., Hólm, E., Janisková, M., Keeley, S., Laloyaux, P., Lopez, P., Lupu, C., Radnoti, G., de Rosnay, P., Rozum, I., Vamborg, F., Villaume, S., and Thépaut, J.-N.: The ERA5 global reanalysis, *Quarterly Journal of the Royal Meteorological Society*, 146, 1999–2049, <https://doi.org/10.1002/qj.3803>, 2020.
- 1140 Highwood, E. J. and Hoskins, B. J.: The tropical tropopause, *Quarterly Journal of the Royal Meteorological Society*, 124, 1579–1604, <https://doi.org/10.1002/qj.49712454911>, 1998.
- 1145 Hoffmann, L.: AIRS/Aqua Observations of Gravity Waves; re3data.org - Registry of Research Data Repositories., <https://doi.org/10.17616/R34J42>, last accessed: 2020-12-03, 2020.
Hoffmann, L.: Reanalysis Tropopause Data Repository; re3data.org - Registry of Research Data Repositories., <https://doi.org/10.17616/R31NJMOH>, last accessed: 2021-11-25, 2021a.
- 1150 Hoffmann, L.: AIRS/Aqua Observations of Volcanic Emissions, <https://doi.org/10.26165/JUELICH-DATA/VPHA3R>, last accessed: 2021-07-01, 2021b.
Hoffmann, L. and Alexander, M. J.: Occurrence frequency of convective gravity waves during the North American thunderstorm season, *Journal of Geophysical Research Atmospheres*, 115, 20 111, <https://doi.org/10.1029/2010JD014401>, 2010.
Hoffmann, L. and Spang, R.: An assessment of tropopause characteristics of the ERA5 and ERA-Interim meteorological reanalyses, *Atmospheric Chemistry and Physics Discussions*, 2021, 1–44, <https://doi.org/10.5194/acp-2021-961>, <https://acp.copernicus.org/preprints/acp-2021-961/>, 2021.
- 1155 Hoffmann, L. and Spang, R.: An assessment of tropopause characteristics of the ERA5 and ERA-Interim meteorological reanalyses, *Atmospheric Chemistry and Physics*, 22, 4019–4046, <https://doi.org/10.5194/acp-22-4019-2022>, <https://acp.copernicus.org/articles/22/4019/2022/>, 2022.
- 1160 Hoffmann, L., Xue, X., and Alexander, M. J.: A global view of stratospheric gravity wave hotspots located with Atmospheric Infrared Sounder observations, *Journal of Geophysical Research: Atmospheres*, 118, 416–434, <https://doi.org/10.1029/2012JD018658>, 2013.

- Hoffmann, L., Alexander, M. J., Clerbaux, C., Grimsdell, A. W., Meyer, C. I., Rößler, T., and Tournier, B.: Intercomparison of stratospheric gravity wave observations with AIRS and IASI, *Atmos. Meas. Tech.*, 7, 4517–4537, <https://doi.org/10.5194/amt-7-4517-2014>, 2014a.
- Hoffmann, L., Griessbach, S., and Meyer, C. I.: Volcanic emissions from AIRS observations: detection methods, case study, and statistical analysis, in: *Remote Sensing of Clouds and the Atmosphere XIX; and Optics in Atmospheric Propagation and Adaptive Systems XVII*, vol. 9242, p. 924214, SPIE, <https://doi.org/10.1117/12.2066326>, 2014b.
- Hoffmann, L., Rößler, T., Griessbach, S., Heng, Y., and Stein, O.: Lagrangian transport simulations of volcanic sulfur dioxide emissions: Impact of meteorological data products, *Journal of Geophysical Research*, 121, 4651–4673, <https://doi.org/10.1002/2015JD023749>, 2016.
- Hoffmann, L., Wu, X., and Alexander, M. J.: Satellite Observations of Stratospheric Gravity Waves Associated With the Intensification of Tropical Cyclones, *Geophysical Research Letters*, 45, 1692–1700, <https://doi.org/10.1002/2017GL076123>, 2018.
- Hohenegger, C. and Stevens, B.: Controls on and impacts of the diurnal cycle of deep convective precipitation, *Journal of Advances in Modeling Earth Systems*, 5, 801–815, <https://doi.org/10.1002/2012MS000216>, 2013.
- Holton, J. R. and Gettelman, A.: Horizontal transport and the dehydration of the stratosphere, *Geophysical Research Letters*, 28, 2799–2802, <https://doi.org/10.1029/2001GL013148>, 2001.
- Homeyer, C. R., Bowman, K. P., and Pan, L. L.: Extratropical tropopause transition layer characteristics from high-resolution sounding data, *Journal of Geophysical Research Atmospheres*, 115, D13 108, <https://doi.org/10.1029/2009JD013664>, 2010.
- Homeyer, C. R., Pan, L. L., and Barth, M. C.: Transport from convective overshooting of the extratropical tropopause and the role of large-scale lower stratosphere stability, *Journal of Geophysical Research: Atmospheres*, 119, 2220–2240, <https://doi.org/10.1002/2013JD020931>, 2014.
- Homeyer, C. R., McAuliffe, J. D., and Bedka, K. M.: On the Development of Above-Anvil Cirrus Plumes in Extratropical Convection, *Journal of the Atmospheric Sciences*, 74, 1617–1633, <https://doi.org/10.1175/JAS-D-16-0269.1>, 2017.
- Inai, Y., Shibata, T., Fujiwara, M., Hasebe, F., and Vömel, H.: High supersaturation inside cirrus in well-developed tropical tropopause layer over Indonesia, *Geophysical Research Letters*, 39, <https://doi.org/10.1029/2012GL053638>, 2012.
- Jain, S., Jain, A. R., and Mandal, T. K.: Role of convection in hydration of tropical UTLS: implication of AURA MLS long-term observations, *Annales Geophysicae*, 31, 967–981, <https://doi.org/10.5194/angeo-31-967-2013>, 2013.
- Jensen, E. and Pfister, L.: Transport and freeze-drying in the tropical tropopause layer, *Journal of Geophysical Research: Atmospheres*, 109, D02 207, <https://doi.org/10.1029/2003JD004022>, 2004.
- Jensen, E. J. and Toon, O. B.: The potential effects of volcanic aerosols on cirrus cloud microphysics, *Geophysical Research Letters*, 19, 1759–1762, <https://doi.org/10.1029/92GL01936>, 1992.
- Jensen, E. J., Toon, O. B., Selkirk, H. B., Spinhirne, J. D., and Schoeberl, M. R.: On the formation and persistence of subvisible cirrus clouds near the tropical tropopause, *Journal of Geophysical Research: Atmospheres*, 101, 21 361–21 375, <https://doi.org/10.1029/95JD03575>, 1996.
- Jensen, E. J., Pfister, L., Bui, T.-P., Lawson, P., and Baumgardner, D.: Ice nucleation and cloud microphysical properties in tropical tropopause layer cirrus, *Atmospheric Chemistry and Physics*, 10, 1369–1384, <https://doi.org/10.5194/acp-10-1369-2010>, 2010.
- Jensen, E. J., Pfister, L., and Toon, O. B.: Impact of radiative heating, wind shear, temperature variability, and microphysical processes on the structure and evolution of thin cirrus in the tropical tropopause layer, *Journal of Geophysical Research: Atmospheres*, 116, D12 209, <https://doi.org/10.1029/2010JD015417>, 2011.

- Jensen, E. J., Ueyama, R., Pfister, L., Bui, T. V., Alexander, M. J., Podglajen, A., Hertzog, A., Woods, S., Lawson, R. P., Kim, J.-E., and Schoeberl, M. R.: High-frequency gravity waves and homogeneous ice nucleation in tropical tropopause layer cirrus, *Geophysical Research Letters*, 43, 6629–6635, <https://doi.org/10.1002/2016GL069426>, 2016.
- Kärcher, B. and Ström, J.: The roles of dynamical variability and aerosols in cirrus cloud formation, *Atmospheric Chemistry and Physics*, 3, 823–838, <https://doi.org/10.5194/acp-3-823-2003>, 2003.
- Keckhut, P., Hauchecorne, A., Bekki, S., Colette, A., David, C., and Jumelet, J.: Indications of thin cirrus clouds in the stratosphere at mid-latitudes, *Atmospheric Chemistry and Physics*, 5, 3407–3414, <https://doi.org/10.5194/acp-5-3407-2005>, 2005.
- Kim, J.-E., Alexander, M. J., Bui, T. P., Dean-Day, J. M., Lawson, R. P., Woods, S., Hlavka, D., Pfister, L., and Jensen, E. J.: Ubiquitous influence of waves on tropical high cirrus clouds, *Geophysical Research Letters*, 43, 5895–5901, <https://doi.org/10.1002/2016GL069293>, 2016.
- Kloss, C., Berthet, G., Sellitto, P., Ploeger, F., Taha, G., Tidiga, M., Eremenko, M., Bossolasco, A., Jégou, F., Renard, J.-B., and Legras, B.: Stratospheric aerosol layer perturbation caused by the 2019 Raikoke and Ulawun eruptions and their radiative forcing, *Atmospheric Chemistry and Physics*, 21, 535–560, <https://doi.org/10.5194/acp-21-535-2021>, 2021.
- Klüser, L., Erbertseder, T., and Meyer-Arnek, J.: Observation of volcanic ash from Puyehue–Cordón Caulle with IASI, *Atmospheric Measurement Techniques*, 6, 35–46, <https://doi.org/10.5194/amt-6-35-2013>, 2013.
- Kärcher, B.: Cirrus Clouds and Their Response to Anthropogenic Activities, 3, 45–57, <https://doi.org/10.1007/s40641-017-0060-3>, 2017.
- Lee, S. S. and Penner, J. E.: Aerosol effects on ice clouds: can the traditional concept of aerosol indirect effects be applied to aerosol-cloud interactions in cirrus clouds?, *Atmospheric Chemistry and Physics*, 10, 10 345–10 358, <https://doi.org/10.5194/acp-10-10345-2010>, 2010.
- Liess, S. and Geller, M. A.: On the relationship between QBO and distribution of tropical deep convection, *Journal of Geophysical Research: Atmospheres*, 117, D03 108, <https://doi.org/10.1029/2011JD016317>, 2012.
- Liou, K.-N.: Influence of Cirrus Clouds on Weather and Climate Processes: A Global Perspective, *Monthly Weather Review*, 114, 1167–1199, [https://doi.org/10.1175/1520-0493\(1986\)114<1167:iocow>2.0.co;2](https://doi.org/10.1175/1520-0493(1986)114<1167:iocow>2.0.co;2), 1986.
- Liu, Z., Kar, J., Zeng, S., Tackett, J., Vaughan, M., Avery, M., Pelon, J., Getzewich, B., Lee, K.-P., Magill, B., Omar, A., Lucker, P., Trepte, C., and Winker, D.: Discriminating between clouds and aerosols in the CALIOP version 4.1 data products, *Atmospheric Measurement Techniques*, 12, 703–734, <https://doi.org/10.5194/amt-12-703-2019>, 2019.
- Lohmann, U. and Feichter, J.: Global indirect aerosol effects: a review, *Atmospheric Chemistry and Physics*, 5, 715–737, <https://doi.org/10.5194/acp-5-715-2005>, <https://acp.copernicus.org/articles/5/715/2005/>, 2005.
- Lohmann, U., Kärcher, B., and Timmreck, C.: Impact of the Mount Pinatubo eruption on cirrus clouds formed by homogeneous freezing in the ECHAM4 GCM, *Journal of Geophysical Research: Atmospheres*, 108, <https://doi.org/10.1029/2002JD003185>, 2003.
- Lolli, S., Madonna, F., Rosoldi, M., Campbell, J. R., Welton, E. J., Lewis, J. R., Gu, Y., and Pappalardo, G.: Impact of varying lidar measurement and data processing techniques in evaluating cirrus cloud and aerosol direct radiative effects, *Atmospheric Measurement Techniques*, 11, 1639–1651, <https://doi.org/10.5194/amt-11-1639-2018>, 2018.
- Mace, G. G., Deng, M., Soden, B., and Zipser, E.: Association of Tropical Cirrus in the 10–15-Km Layer with Deep Convective Sources: An Observational Study Combining Millimeter Radar Data and Satellite-Derived Trajectories, *Journal of the Atmospheric Sciences*, 63, 480–503, <https://doi.org/10.1175/JAS3627.1>, 2006.
- Malinina, E., Rozanov, A., Niemeier, U., Wallis, S., Arosio, C., Wrana, F., Timmreck, C., von Savigny, C., and Burrows, J. P.: Changes in stratospheric aerosol extinction coefficient after the 2018 Ambae eruption as seen by OMPS-LP and MAECHAM5-HAM, *Atmospheric Chemistry and Physics*, 21, 14 871–14 891, <https://doi.org/10.5194/acp-21-14871-2021>, 2021.

- Massie, S., Lowe, P., Tie, X., Hervig, M., Thomas, G., and Russell III, J.: Effect of the 1997 El Niño on the distribution of upper tropospheric cirrus, *Journal of Geophysical Research: Atmospheres*, 105, 22 725–22 741, <https://doi.org/10.1029/2000JD900322>, 2000.
- Massie, S., Gettelman, A., Randel, W., and Baumgardner, D.: Distribution of tropical cirrus in relation to convection, *Journal of Geophysical Research: Atmospheres*, 107, 4591, <https://doi.org/10.1029/2001JD001293>, 2002.
- 1240 Meyer, C. I., Ern, M., Hoffmann, L., Trinh, Q. T., and Alexander, M. J.: Intercomparison of AIRS and HIRDLS stratospheric gravity wave observations, *Atmospheric Measurement Techniques*, 11, 215–232, <https://doi.org/10.5194/amt-11-215-2018>, 2018.
- Munchak, L. A. and Pan, L. L.: Separation of the lapse rate and the cold point tropopauses in the tropics and the resulting impact on cloud top-tropopause relationships, *Journal of Geophysical Research: Atmospheres*, 119, 7963–7978, <https://doi.org/10.1002/2013JD021189>, 2014.
- 1245 Murgatroyd, R. J. and Goldsmith, P.: High cloud over southern England, *Nature*, 178, 788, <https://doi.org/10.1038/178788a0>, 1956.
- Nesbitt, S. W. and Zipser, E. J.: The Diurnal Cycle of Rainfall and Convective Intensity according to Three Years of TRMM Measurements, *Journal of Climate*, 16, 1456 – 1475, [https://doi.org/10.1175/1520-0442\(2003\)016<1456:TDCORA>2.0.CO;2](https://doi.org/10.1175/1520-0442(2003)016<1456:TDCORA>2.0.CO;2), 2003.
- Noël, V. and Haeffelin, M.: Midlatitude cirrus clouds and multiple tropopauses from a 2002–2006 climatology over the SIRTa observatory, *Journal of Geophysical Research Atmospheres*, 112, D13206, <https://doi.org/10.1029/2006JD007753>, 2007.
- 1250 Noel, V., Chepfer, H., Hoareau, C., Reverdy, M., and Cesana, G.: Effects of solar activity on noise in CALIOP profiles above the South Atlantic Anomaly, *Atmospheric Measurement Techniques*, 7, 1597–1603, <https://doi.org/10.5194/amt-7-1597-2014>, <https://amt.copernicus.org/articles/7/1597/2014/>, 2014.
- Noh, Y. M., Shin, D. H., and Müller, D.: Variation of the vertical distribution of Nabro volcano aerosol layers in the stratosphere observed by LIDAR, *Atmospheric Environment*, 154, 1–8, <https://doi.org/10.1016/j.atmosenv.2017.01.033>, 2017.
- 1255 Ohneiser, K., Ansmann, A., Engelmann, R., Ritter, C., Chudnovsky, A., Veselovskii, I., Baars, H., Gebauer, H., Griesche, H., Radenz, M., Hofer, J., Althausen, D., Dahlke, S., and Maturilli, M.: Siberian fire smoke in the High-Arctic winter stratosphere observed during MOSAiC 2019–2020, *Atmospheric Chemistry and Physics Discussions*, 2021, 1–36, <https://doi.org/10.5194/acp-2021-117>, 2021.
- Pan, L. L. and Munchak, L. A.: Relationship of cloud top to the tropopause and jet structure from CALIPSO data, *Journal of Geophysical Research Atmospheres*, 116, 1–17, <https://doi.org/10.1029/2010JD015462>, 2011.
- 1260 Pan, L. L., Honomichl, S. B., Bui, T. V., Thornberry, T., Rollins, A., Hintsä, E., and Jensen, E. J.: Lapse Rate or Cold Point: The Tropical Tropopause Identified by In Situ Trace Gas Measurements, *Geophysical Research Letters*, 45, 10,756–10,763, <https://doi.org/10.1029/2018GL079573>, 2018.
- Peevey, T. R., Gille, J. C., Randall, C. E., and Kunz, A.: Investigation of double tropopause spatial and temporal global variability utilizing High Resolution Dynamics Limb Sounder temperature observations, *Journal of Geophysical Research: Atmospheres*, 117, <https://doi.org/10.1029/2011JD016443>, 2012.
- 1265 Peevey, T. R., Gille, J. C., Homeyer, C. R., and Manney, G. L.: The double tropopause and its dynamical relationship to the tropopause inversion layer in storm track regions, *Journal of Geophysical Research: Atmospheres*, 119, 10,194–10,212, <https://doi.org/10.1002/2014JD021808>, 2014.
- Pfister, L., Selkirk, H. B., Jensen, E. J., Schoeberl, M. R., Toon, O. B., Browell, E. V., Grant, W. B., Gary, B., Mahoney, M. J., Bui, T. V., and Hintsä, E.: Aircraft observations of thin cirrus clouds near the tropical tropopause, *Journal of Geophysical Research: Atmospheres*, 106, 9765–9786, <https://doi.org/10.1029/2000JD900648>, 2001.
- 1270 Podglajen, A., Plougonven, R., Hertzog, A., and Jensen, E.: Impact of gravity waves on the motion and distribution of atmospheric ice particles, *Atmospheric Chemistry and Physics*, 18, 10 799–10 823, <https://doi.org/10.5194/acp-18-10799-2018>, 2018.

- Prata, A. J., Gangale, G., Clarisse, L., and Karagulian, F.: Ash and sulfur dioxide in the 2008 eruptions of Okmok and Kasatochi: Insights from high spectral resolution satellite measurements, *Journal of Geophysical Research: Atmospheres*, 115, D00L18, <https://doi.org/10.1029/2009JD013556>, 2010.
- Pruppacher, H. R. and Klett, J. D.: *Microphysics of Clouds and Precipitation*: Reprinted 1980, Springer Science & Business Media.
- Randel, W. J., Wu, F., Vömel, H., Nedoluha, G. E., and Forster, P.: Decreases in stratospheric water vapor after 2001: Links to changes in the tropical tropopause and the Brewer-Dobson circulation, *Journal of Geophysical Research: Atmospheres*, 111, D12 312, <https://doi.org/10.1029/2005JD006744>, 2006.
- Randel, W. J., Seidel, D. J., and Pan, L. L.: Observational characteristics of double tropopauses, *Journal of Geophysical Research: Atmospheres*, 112, D07 309, <https://doi.org/10.1029/2006JD007904>, 2007.
- Reverdy, M., Noel, V., Chepfer, H., and Legras, B.: On the origin of subvisible cirrus clouds in the tropical upper troposphere, *Atmospheric Chemistry and Physics*, 12, 12 081–12 101, <https://doi.org/10.5194/acp-12-12081-2012>, 2012.
- Sandhya, M., Sridharan, S., Devi, M. I., Niranjan, K., and Jayaraman, A.: A case study of formation and maintenance of a lower stratospheric cirrus cloud over the tropics, *Annales Geophysicae*, 33, 599–608, <https://doi.org/10.5194/angeo-33-599-2015>, 2015.
- Sassen, K., Wang, Z., and Liu, D.: Global distribution of cirrus clouds from CloudSat/cloud-aerosol lidar and infrared pathfinder satellite observations (CALIPSO) measurements, *Journal of Geophysical Research Atmospheres*, 113, <https://doi.org/10.1029/2008JD009972>, 2008.
- Sassen, K., Wang, Z., and Liu, D.: Cirrus clouds and deep convection in the tropics: Insights from CALIPSO and CloudSat, *Journal of Geophysical Research: Atmospheres*, 114, <https://doi.org/10.1029/2009JD011916>, 2009.
- Schoeberl, M. R. and Dessler, A. E.: Dehydration of the stratosphere, *Atmospheric Chemistry and Physics*, 11, 8433–8446, <https://doi.org/10.5194/acp-11-8433-2011>, 2011.
- Schoeberl, M. R., Jensen, E. J., and Woods, S.: Gravity waves amplify upper tropospheric dehydration by clouds, *Earth and Space Science*, 2, 485–500, <https://doi.org/10.1002/2015EA000127>, 2015.
- Schoeberl, M. R., Jensen, E. J., Pfister, L., Ueyama, R., Wang, T., Selkirk, H., Avery, M., Thornberry, T., and Dessler, A. E.: Water Vapor, Clouds, and Saturation in the Tropical Tropopause Layer, *Journal of Geophysical Research: Atmospheres*, 124, 3984–4003, <https://doi.org/10.1029/2018JD029849>, 2019.
- Schwartz, M. J., Manney, G. L., Hegglin, M. I., Livesey, N. J., Santee, M. L., and Daffer, W. H.: Climatology and variability of trace gases in extratropical double-tropopause regions from MLS, HIRDLS, and ACE-FTS measurements, *Journal of Geophysical Research: Atmospheres*, 120, 843–867, <https://doi.org/10.1002/2014JD021964>, 2015.
- Selimovic, V., Yokelson, R. J., McMeeking, G. R., and Cofield, S.: In situ measurements of trace gases, PM, and aerosol optical properties during the 2017 NW US wildfire smoke event, *Atmospheric Chemistry and Physics*, 19, 3905–3926, <https://doi.org/10.5194/acp-19-3905-2019>, 2019.
- Sherwood, S. C., Horinouchi, T., and Zeleznik, H. A.: Convective Impact on Temperatures Observed near the Tropical Tropopause, *Journal of the Atmospheric Sciences*, 60, 1847 – 1856, [https://doi.org/10.1175/1520-0469\(2003\)060<1847:CIOTON>2.0.CO;2](https://doi.org/10.1175/1520-0469(2003)060<1847:CIOTON>2.0.CO;2), 2003.
- Solomon, D. L., Bowman, K. P., and Homeyer, C. R.: Tropopause-Penetrating Convection from Three-Dimensional Gridded NEXRAD Data, *Journal of Applied Meteorology and Climatology*, 55, 465 – 478, <https://doi.org/10.1175/JAMC-D-15-0190.1>, 2016.
- Spang, R., Günther, G., Riese, M., Hoffmann, L., Müller, R., and Griessbach, S.: Satellite observations of cirrus clouds in the Northern Hemisphere lowermost stratosphere, *Atmospheric Chemistry and Physics*, 15, 927–950, <https://doi.org/10.5194/acp-15-927-2015>, 2015.

- Taylor, J. R., Randel, W. J., and Jensen, E. J.: Cirrus cloud-temperature interactions in the tropical tropopause layer: a case study, *Atmospheric Chemistry and Physics*, 11, 10085–10095, <https://doi.org/10.5194/acp-11-10085-2011>, 2011.
- 1315 Tegtmeier, S., Anstey, J., Davis, S., Dragani, R., Harada, Y., Ivanciu, I., Pilch Kedzierski, R., Krüger, K., Legras, B., Long, C., Wang, J. S., Wargan, K., and Wright, J. S.: Temperature and tropopause characteristics from reanalyses data in the tropical tropopause layer, *Atmospheric Chemistry and Physics*, 20, 753–770, <https://doi.org/10.5194/acp-20-753-2020>, 2020a.
- Tegtmeier, S., Anstey, J., Davis, S., Ivanciu, I., Jia, Y., McPhee, D., and Pilch Kedzierski, R.: Zonal Asymmetry of the QBO Temperature Signal in the Tropical Tropopause Region, *Geophysical Research Letters*, 47, e2020GL089533, <https://doi.org/10.1029/2020GL089533>, 2020b.
- 1320 Tian, B., Waliser, D. E., and Fetzer, E. J.: Modulation of the diurnal cycle of tropical deep convective clouds by the MJO, *Geophysical Research Letters*, 33, L20704, <https://doi.org/10.1029/2006GL027752>, 2006.
- Trier, S. B. and Sharman, R. D.: Mechanisms Influencing Cirrus Banding and Aviation Turbulence near a Convectively Enhanced Upper-Level Jet Stream, *Monthly Weather Review*, 144, 3003 – 3027, <https://doi.org/10.1175/MWR-D-16-0094.1>, 2016.
- Trier, S. B., Sharman, R. D., Muñoz-Esparza, D., and Lane, T. P.: Environment and Mechanisms of Severe Turbulence in a Midlatitude Cyclone, *Journal of the Atmospheric Sciences*, 77, 3869 – 3889, <https://doi.org/10.1175/JAS-D-20-0095.1>, 2020.
- 1325 Tseng, H.-H. and Fu, Q.: Temperature Control of the Variability of Tropical Tropopause Layer Cirrus Clouds, *Journal of Geophysical Research: Atmospheres*, 122, 11,062–11,075, <https://doi.org/10.1002/2017JD027093>, 2017.
- Tzella, A. and Legras, B.: A Lagrangian view of convective sources for transport of air across the Tropical Tropopause Layer: distribution, times and the radiative influence of clouds, *Atmospheric Chemistry and Physics*, 11, 12517–12534, <https://doi.org/10.5194/acp-11-12517-2011>, 2011.
- 1330 Virts, K. S. and Wallace, J. M.: Annual, interannual, and intraseasonal variability of tropical tropopause transition layer cirrus, *Journal of the Atmospheric Sciences*, 67, 3097–3112, <https://doi.org/10.1175/2010JAS3413.1>, 2010.
- Wang, P. H., Minnis, P., McCormick, M. P., Kent, G. S., and Skeens, K. M.: A 6-year climatology of cloud occurrence frequency from Stratospheric Aerosol and Gas Experiment II observations (1985-1990), *Journal of Geophysical Research Atmospheres*, 101, 29407–29429, <https://doi.org/10.1029/96jd01780>, 1996.
- 1335 Wang, P. K., Cheng, K.-Y., Setvak, M., and Wang, C.-K.: The origin of the gullwing-shaped cirrus above an Argentinian thunderstorm as seen in CALIPSO images, *Journal of Geophysical Research: Atmospheres*, 121, 3729–3738, <https://doi.org/10.1002/2015JD024111>, 2016.
- Winker, D. M., Hunt, W. H., and McGill, M. J.: Initial performance assessment of CALIOP, *Geophysical Research Letters*, 34, L19803, <https://doi.org/10.1029/2007GL030135>, 2007.
- 1340 Winker, D. M., Vaughan, M. A., Omar, A., Hu, Y., Powell, K. A., Liu, Z., Hunt, W. H., and Young, S. A.: Overview of the CALIPSO mission and CALIOP data processing algorithms, *Journal of Atmospheric and Oceanic Technology*, 26, 2310–2323, <https://doi.org/10.1175/2009JTECHA1281.1>, 2009.
- WMO: Meteorology-a three-dimensional science:Second session for the commission for aerology, *WMO Bulletin*, 6, 134–138, 1957.
- Wylie, D., Jackson, D. L., Menzel, W. P., and Bates, J. J.: Trends in global cloud cover in two decades of HIRS observations, *Journal of Climate*, 18, 3021–3031, <https://doi.org/10.1175/JCLI3461.1>, 2005.
- 1345 Wylie, D. P., Menzel, W. P., Woolf, H. M., and Strabala, K. I.: Four years of global cirrus cloud statistics using HIRS, *Journal of Climate*, 7, 1972–1986, [https://doi.org/10.1175/1520-0442\(1994\)007<1972:FYOGCC>2.0.CO;2](https://doi.org/10.1175/1520-0442(1994)007<1972:FYOGCC>2.0.CO;2), 1994.
- Xian, T. and Homeyer, C. R.: Global tropopause altitudes in radiosondes and reanalyses, *Atmospheric Chemistry and Physics*, 19, 5661–5678, <https://doi.org/10.5194/acp-19-5661-2019>, 2019.

- 1350 Zhou, C., Dessler, A. E., Zelinka, M. D., Yang, P., and Wang, T.: Cirrus feedback on interannual climate fluctuations, *Geophysical Research Letters*, 41, 9166–9173, <https://doi.org/10.1002/2014GL062095>, 2014.
- Zou, L., Griessbach, S., Hoffmann, L., Gong, B., and Wang, L.: Revisiting global satellite observations of stratospheric cirrus clouds, *Atmospheric Chemistry and Physics*, 20, 9939–9959, <https://doi.org/10.5194/acp-20-9939-2020>, 2020.
- Zou, L., Hoffmann, L., Griessbach, S., Spang, R., and Wang, L.: Empirical evidence for deep convection being a major source of stratospheric ice clouds over North America, *Atmospheric Chemistry and Physics*, 21, 10 457–10 475, <https://doi.org/10.5194/acp-21-10457-2021>, 1355 2021.